Effect of Nano-Scale Twinning on the Fracture, Fatigue and Wear Properties of Copper.

by

Aparna Singh

Bachelor of Technology (2007)
Materials and Metallurgical Engineering
Indian Institute of Technology, Kanpur, India

Submitted to the Department of Materials Science and Engineering in partial fulfillment of the requirements for the degree of

Doctor of Philosophy in Materials Science and Engineering at the

MASSACHUSETTS INSTITUTE OF TECHNOLOGY

JUNE 2011

Author……

Department of Materials Science and Engineering
May 16, 2011

Certified by……

Christopher A. Schuh
Danae and Vasilios Salapatas Professor of Metallurgy
Thesis Supervisor

Accepted by……

Christopher A. Schuh
Danae and Vasilios Salapatas Professor of Metallurgy
Chair, Departmental Committee on Graduate Students

Effect of Nano-Scale Twinning on the Fracture, Fatigue and Wear Properties of Copper.

by

Aparna Singh

Submitted to the Department of Materials Science and Engineering on May 12, 2011 in partial fulfillment of the requirements for the degree of Doctor of Philosophy in Materials Science and Engineering

Abstract

Grain refinement in materials has been one of the most common strategies for improving the strength of materials. However this comes at the price of reduced ductility, fracture toughness and stable fatigue crack propagation life. It has been shown that controlled introduction of nano scale growth twins in ultra fined grained (UFG) Cu through pulsed electro deposition leads to an increase in strength while maintaining a significant amount of ductility. Besides, introduction of deformation twins by the process of dynamic plastic deformation (DPD) involving repeated compaction of coarse-grained (CG) copper at high strain rates and cryogenic temperatures have also shown similar trends in terms of improved strength and considerable strain before failure. Unlike grain boundaries, twin boundaries do not adversely affect the electrical conductivity and resistance towards electro migration of copper. However there have been no studies done to elucidate the role of nano-scale twins in affecting the fracture toughness, stable crack propagation and response under contact fatigue. The aim of the current work was to gain an understanding of the role of microstructural length scale and design in terms of the introduction of twin boundaries vs. grain refinement in influencing the above-mentioned properties.

With this aim stable crack propagation and fracture toughness studies were done on UFG copper specimens produced by pulsed electro deposition with an average grain size of 400-500nm but different twin densities to elucidate the effect of twin density on the damage tolerance of Cu. It was found that unlike grain refinement, twin lamellae refinement leads to an improvement in fracture toughness and stable fatigue crack growth life. In order to characterize the contact fatigue response of nano twinned copper, frictional sliding experiments were performed with a conical diamond indenter. The effects of twin density and number of repetitions of sliding cycles on the evolution of frictional coefficient and material pile up around the diamond indenter were studied quantitatively using depth-sensing instrumented sliding indentation. Cross-sectional focused ion beam (FIB) and scanning electron microscopy (SEM) observations were used to systematically monitor deformation-induced structural changes as a function of the number of frictional sliding passes. Nano indentation tests on the sliding tracks coupled with large-deformation finite element modeling (FEM) simulations were used to assess local gradients in

mechanical properties and deformation around the indenter track. The results indicate that friction evolution as well as local mechanical response is more strongly influenced by local structure evolution during repeated sliding than by the initial microstructure. The frictional sliding experiments also lead to the striking result that Cu specimens with both high and low density of nano twins eventually converge to a similar microstructure underneath the indenter after repeated tribological deformation. Similar trend of convergence of microstructure and hardness in the vicinity of the scratch was also observed for DPD and CG Cu. This trend strongly mirrors the well-known steady-state response of microcrystalline copper to cyclic loading. General perspectives on contact fatigue response of nano-twinned copper are developed on the basis of these new findings.

Thesis Supervisors: Professor Christopher A. Schuh

Title: Danae and Vasilios Salapatas Professor of Metallurgy.

Professor Subra Suresh

Title: Director of the National Science Foundation (NSF).

Acknowledgements

I am very grateful to MIT for giving me the opportunity of pursuing my graduate studies here. MIT is a place that has an abundance of extraordinary people whose attitude towards research makes one appreciate knowledge as an end in itself. My journey at MIT has been of continuous learning and it has been the support and guidance of the people mentioned below that has helped me climb this steep slope of learning at MIT.

I am very thankful to my Ph.D. advisors Professor Christopher Schuh and Professor Subra Suresh. Professor Suresh is a wonderful scientist, teacher and presenter. The topic of "Fracture and Fatigue" had appeared very esoteric to me before I was taught a course on this subject by him. He gives a lot of freedom to his students in terms of defining the breadth and depth of the project and that helped me feel self-motivated and responsible for the project and enjoy my research journey. His calmness and broad perceptions have contributed greatly to my PhD work. Professor Chris Schuh is an immensely kind and patient person and goes out of his way to help people. I cannot find enough words to thank him for his help and support during my stay at MIT. In addition, he is a terrific researcher, great advisor and wonderful teacher. He has a very logical, rational and holistic way of approaching any scientific issue and goes to the depth of every research problem. He was available at any time for discussing any research query or any other problem that I had. He has an expertise in presenting scientific work and helped me greatly with my presentations. He has provided me with valuable insights on wear of materials. He has a vibrant research group and attending his group meetings helped me a lot especially for the tribology part of my project.

I am also very grateful to Dr. Ming Dao who has been very kind to me throughout my stay at MIT and has shared his skills and experience in FEM modeling with me whether it had been for a class project for the FEM class that I took or for my research. He has been very close to the students in the group and was just one door knock away in terms of providing any help or suggestion.

I am also very thankful to Professor Lei Lu and Professor Nairong Tao for supplying the specimens and for the very interesting research project that they asked us to participate in. It has been a very nice and fruitful collaboration. I have been to China twice for experimental work and Professor Lu, Professor Tao, their students and their research staff has been immensely supportive and hospitable to me.

I would also like to thank my committee members Professor Samuel Allen and Professor Caroline Ross for taking out their valuable time to discuss my PhD work. I learnt a lot from the questions they asked and the concerns they raised regarding the content of my work and the way I presented it. It taught me a lot in terms of what are the relevant issues and key concerns that need to be addressed and emphasized for any scientific work.

I am also extremely grateful to the Office of Naval Research ONR (Grant N00014-08-1-0510) and Singapore MIT Alliance (SMA) for supporting this work.

I am grateful to Dr. Alan Schwartzman for teaching me how to use Micromaterials and Ms Yin-Lin Xie for teaching me polishing. I am also grateful to Mr. Tan at IMR, China for help in the FIB cutting and Dr. E.W. Qin and Mr. Tang for help in experiments. I would also like to thank my other teachers like Professor Bathe for teaching FEM superbly well. In addition Prof. Wuensch, Prof. Van Vliet and Prof. Marzari contributed greatly to my knowledge in fields about which I knew little to start with. I would also like to thank Prof. Rae Langton, Prof. Sally Haslanger, Prof. Suzanne Berger, Prof. Michael Piore, Prof. Margarita Groeger and Prof. Ceser Perez for being great teachers and unraveling the field and research methods of humanities and social sciences to me. I wish to thank my professors at IIT Kanpur for their continual inspiration.

I wish to acknowledge also the current and past members of Professor Suresh's group for their direct and indirect contributions to my thesis work. I sincerely appreciate the helpful demeanor of Mr. George Labonte and Mr. Ken Greene and their leadership on organizing and maintaining the laboratory. I am also thankful to Prof. Schuh's group members for being extremely welcoming and friendly.

I have been gifted with friends like Reetu Raj, Neha Tomar, Urvashi Srivastava, Siddarth Kumar, Suman Bose, Hyunjung Yi, Shin Young Kang, Yi Chun Lu, Zenith Zhang, Irene Chang, Manvendra Singh, Amit Singh, Atul Dhar, Rahul Kumar, Vivek Srivastava, Jagdeep Kaur, Biraja Kanungo, Arvind Kumar, Umesh Kumar, Babloo Kumar, Abhishek Tiwari, Naveen Kumar Gupta, K.Vikram, Mukul Kabir, Kedarnath Kolluri, Gagan Saini, Monica Diez and Brijendra Srivastava who have not only supported me in times thick and thin but have also made the journey of life extremely interesting, meaningful and fun.

I cannot express enough gratitude to my family. My mother Dr. S. Singh has always been a tower of strength for me. She is an extremely intelligent and wise lady. Her unconditional love, supportive nature and calm disposition have been conducive in channeling my energies to meaningful pursuits in life. My father Dr. B. Singh is an amazing person and lives up to the ideal of simple living and high thinking. He is an expert in Mathematics and Statistics with a very logical and rational thinking coupled with a great sense of humor. I would like to greatly thank my elder brother Mr. Mayank Kumar (PhD Candidate June 2011, Department of Mechanical Engineering, MIT). He has been a constant companion to me ever since I was born and we have spent wonderful times together. The serenity of his company and his cheerful smile are able to dissolve the biggest tensions in the mind in minutes. I still remember our childhood days when I would bombard him with questions ranging from extinction of dinosaurs to Ampere's swim rule in electromagnetism and he would answer them patiently as no one has ever done for me. I would always cherish him as life's greatest gift to me.

Contents

List of Figures and Captions

List of Tables and Captions

Chapter 1

Introduction

Reducing the grain size of a material to enhance its strength has long been a strategy used in microstructure design [1-6]. Marked improvement in properties like hardness, wear and corrosion resistance and diffusivity can be achieved by resorting to grain refinement in metals [1, 2, 4, 5, 7-9]. Some of the most common methods of producing nano grained metals include gas phase condensation of metals [10] or production of nano sized powders in bulk form and subsequent consolidation using hot isostatic pressing, shock consolidation or field activated sintering [11]. Others techniques that have been successfully used to produce nano grained (NG) materials include electro deposition [12] and crystallization of amorphous solids [13] . A number of Severe Plastic Deformation techniques (SPD) techniques [14] like equal channel angular pressing ECAP [15], high pressure torsion HPT [16] and cold rolling [17, 18] are frequently used to refine grain size of coarse grained (CG) metals and produce samples in bulk form without incorporating porosity but they have been successful in attaining grain sizes only in the ultra fine (UFG) regime. Dislocation manipulation, rearrangement and formation of various dislocation configurations are the primary mechanisms leading to grain refinement [19] in severe plastic deformation processes.

The strength of nano-grained materials has been found to increase with grain refinement down to at least 15 nm in most metals. The mechanisms leading to this strength enhancement at such small grain sizes is unclear as it is not expected that dislocation sources inside grains would be

operative at such grain sizes. There has been no experimental evidence of dislocation pile-ups in deformed specimens although computer simulations show dislocation partial dislocation emission from grain boundaries in nanograined metals [20, 21]. A lot of prior experimental studies [5, 7, 22-25] report that strength decreases with grain refinement below ~10nm (inverse Hall-Petch effect). Grain boundary sliding and Coble Creep are the expected deformation mechanisms taking place at such small grain sizes [23-25] although there is no direct experimental evidence of such processes reported.

In conventional microcrystalline metals and alloys (average grain dimensions typically bigger than 1 μm), grain refinement generally results in an increase in the resistance to fatigue crack initiation. In high cycle fatigue, this trend is reflected as higher fatigue endurance limit (which is elevated with higher strength); the endurance limit is typically measured through cyclic-stress-controlled experiments on initially-smooth laboratory specimens [26]. When the average grain size is refined to values typically below 100 nm, the resulting nanostructured metals exhibit significantly elevated strength and strain rate sensitivity and much lower activation volume, as well as improved resistance to corrosion, fatigue crack initiation for long-life as seen in the fatigue endurance limit, and monotonic and cyclic wear [7-9, 27-29] in comparison to microcrystalline metals and alloys [3, 5, 6]. However, such beneficial effects of grain size reduction are also commonly accompanied by reductions in ductility (Fig 1-1). The drop in ductility is ascribed to significant constraints encountered in accommodating plastic strain through the generation and accumulation of dislocations in the nano-grained (NG) metals [3, 5, 6, 30]. Furthermore, grain refinement into the nanocrystalline regime is known to degrade different metrics of damage tolerance including fracture toughness and the resistance to stable sub-critical crack growth under monotonic and cyclic loading, especially at lower values of stress

intensity factor range (the so-called near-threshold regime with crack growth rates typically smaller than 10^{-6} mm/cycle) where most of the fatigue fracture life is expended [26-28, 31]. The application of NG materials in high strength applications at elevated temperatures is also severely limited because of the unstable nature of the high grain boundaries for instance grain growth in NG Cu has been observed even at room temperature [32].

Moreover, the nanocrystalline microstructure has been shown to be unstable under high stresses for instance under indentation creep, the hardness has been reported to continue to decline due to grain growth because of the large excess energy of the grain boundaries [33, 34]. Stress assisted grain growth incurred by indentation has also been observed in NG Al [35]. Grain growth has also been shown to be promoted by tensile deformation [36], compression [37] and HPT [38]. In addition to these effects on mechanical properties, grain refinement, especially in the nanocrystalline regime, is also known to have a deleterious effect on electrical conductivity [39-42] and resistance to electromigration [43].

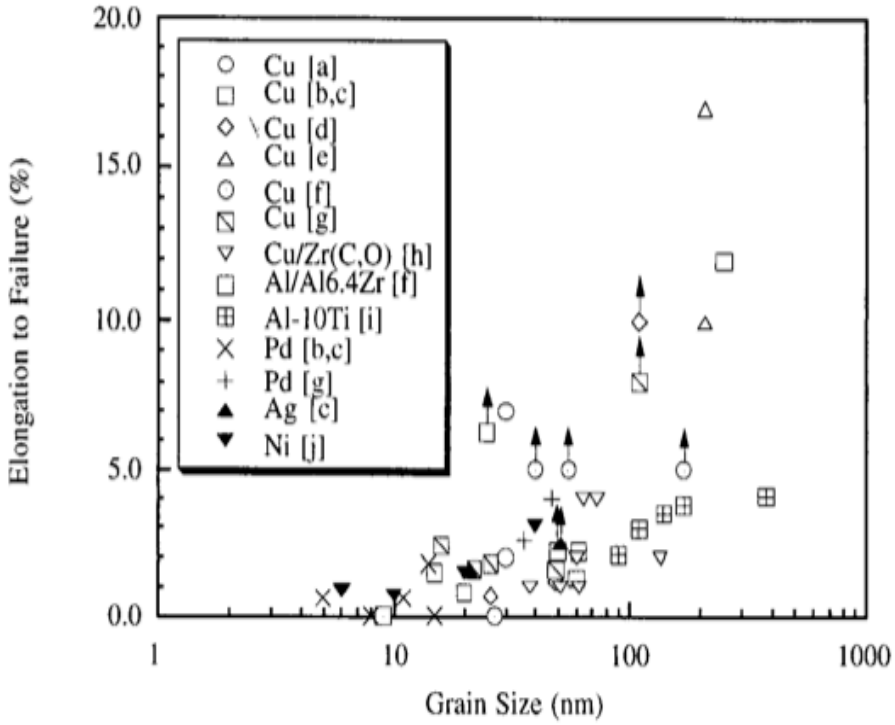

a. B. Günther, A. Baalmann, and H. Weiss, *Mater. Res. Soc. Symp. Proc.* **195**(1990)611.
b. G.W. Nieman, J.R. Weertman, and R.W. Siegel, ibid. **206**(1991)581.
c. G.W. Nieman, J.R. Weertman, and R.W. Siegel, *J. Mater. Res.* **6**(1991)1012.
d. P.G. Sanders, J.A. Eastman, and J.R. Weertman, in *Processing and Properties of Nanocrystalline Materials* (ed. C. Suryanarayana et al.), p.379. TMS, Warrendale, PA (1996).
e. V. Y. Gertsman, M. Hoffmann, H. Gleiter, and R. Birringer, *Acta Metall. Mater.* **42**(1994)3539.
f. J. A. Eastman, M. Choudry, M. N. Rittner, C. J. Youngdahl, M. Dollar, J. R. Weertman, R. J. DiMelfi, and L. J. Thompson, in *Chemistry and Physics of Nanostructures and Related Non-Equilibrium Materials* (edited by E. Ma *et al.*), p.173. TMS, Warrendale, PA (1997).
g. P. G. Sanders, J. A. Eastman, and J. R. Weertman, Acta Mater. **45**(1997)4019.
h. D. G. Morris and M. A. Morris, *Acta Metall. Mater.* **39**(1991)1763.
i. G. Liang, Z. Li, and E. Wang, *J. Mater. Sci.* , **31**(1996)901.
j. N. Wang, Z. Wang, K. T. Aust, and U. Erb, Mater. Sci. Eng. **A237**(1997)150

Fig 1-1 Tensile ductility of nanocrystalline metals and alloys as a function of grain size.

Significant strengthening due to grain refinement arises from the obstruction of dislocation motion at nano-scale grain boundaries. Similar strengthening can also be achieved through the introduction of initially coherent twin boundaries within UFG metals (Fig 1-2). Recent studies [44-46] have shown that when a polycrystalline ensemble of UFG copper (with average grain size in the range of 100 nm to 1000 nm) is populated with initially coherent, mechanically and thermally stable, nano-scale twins (where the twin width or spacing is on the order of tens of nanometers), the ensuing structure exhibits deformation characteristics that mirror those of nano-grained copper whose average grain size is comparable to the twin spacing in the nano-twinned (NT) copper. In other words, when nano-twins are introduced in the UFG metal during pulsed electrodeposition, the material exhibits strengthening characteristics and strain rate sensitivity comparable to those of a nano-grained metal without twins [44, 47, 48] (Fig 1-3(b)). The coherent NT boundaries act as barriers to dislocation motion just as grain boundaries do [46, 49, 50]. The pile up of dislocations at an incoherent GB leads to a stress concentration that can result in the nucleation of new dislocations on the other side of the boundary without altering the character and energy of the GB. Since the structure of the GB is not altered, dislocations usually do not glide along the boundary. This limited capability of GBs to accommodate dislocations during deformation manifests in reduced ductility despite promoting increased strength. On the other hand, the twin boundaries are not only capable of accommodating dislocations, but they also facilitate glide of dislocations along the boundary given their significant local plastic anisotropy [6, 45]. Molecular dynamics simulations [51, 52] have indicated that when a perfect glide dislocation in FCC metals with b = ½ [101] crosses a symmetric (111) TB, a Shockley partial (with b = 1/6 [$\bar{1}\bar{1}2$]) is left behind at the TB, which is indeed observed in Fig. 1-4(b). This

implies that the higher the TB density, the larger the capacity of dislocation accumulation at the TBs, which consequently results in an enhanced ductility due to plastic deformation.

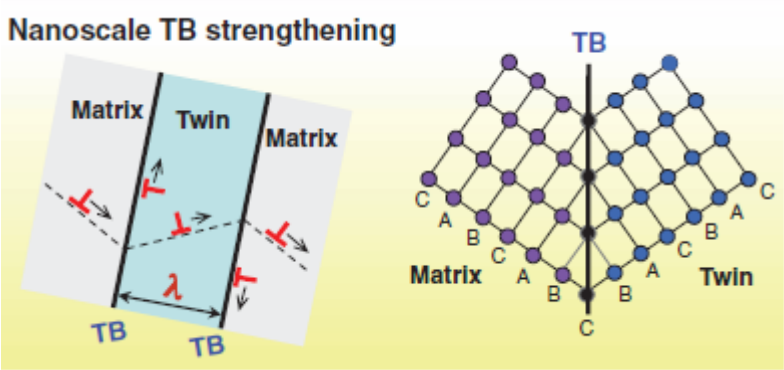

Fig. 1-2 Schematic illustration of a twin boundary [46] : Nanoscale TB strengthening is based on dislocation-TB interactions from which mobile and/or sessile dislocations could be generated, either in neighboring domains (twin or matrix) or at TBs. Gliding of dislocations along TBs is feasible because of its coherent structure [the right panel denotes a $\sum 3$ TB]. Higher strength and higher ductility are achieved with a smaller twin thickness λ in the nanometer scale.

Post deformation studies of nano-twinned (NT) specimens have shown high dislocation density in the vicinity of the twin boundaries [47, 53] as can be seen in Fig 1-4(a). These attributes of NT copper appear to facilitate not only a potent mechanism of strengthening through the control of twin density at the nano-scale without any change in grain size, but they also help retain a significant fraction of ductility when strengthening is achieved through NT refinement. As a result, nano-twinned metals offer the potential for engineering mechanical properties with optimized combinations of strength and ductility for a variety of structural applications by

circumventing issues related to the severe loss of ductility which are serious drawbacks of grain refinement strategies involving nano-grained materials [5, 6]. The fact that the electrical resistivity of coherent twin boundaries is one order of magnitude lower than high angle grain boundaries also enhances its range of applications [54, 55]. Moreover twin boundaries have been shown to have much higher thermal stability than grain boundaries for instance the nano twinned microstructure of sputter deposited sputtered Cu films showed considerable stability even at annealing temperatures close to 800 ^{0}C [56].

Twin boundaries (TBs) within grains can be introduced either during processing (so called growth twins), plastic deformation (deformation twins), or recrystallization of deformed structures upon annealing (annealing twins).

The most commons way of introducing growth twins inside metals is by pulsed electro deposition (Fig 1-3(a)). There does not exist complete scientific understanding of the mechanism of twin formation by pulsed electro deposition but it is the high current density that is possible in pulsed electro deposition and not in direct current deposition that is conducive to formation of twins. . Thermodynamically, twin formation decreases the total interfacial energy as the excess energy of coherent twin boundaries (TBs) is less than those of high-angle GBs. In addition, TBs tend to nucleate at GBs and triple junctions to accommodate mismatch at these locations. The sum of interfacial energies of the GB and TB even after formation of a new TB is less than just the GB alone. The nucleation and growth of twins is highly dependent on the deposition conditions. Experimental observations by Lu [44, 54] show that a high current density , a large pH of the solution and low deposition temperature are conducive to high deposition rates of twins. Besides, formation of twins is favored for low stacking fault energy metals.

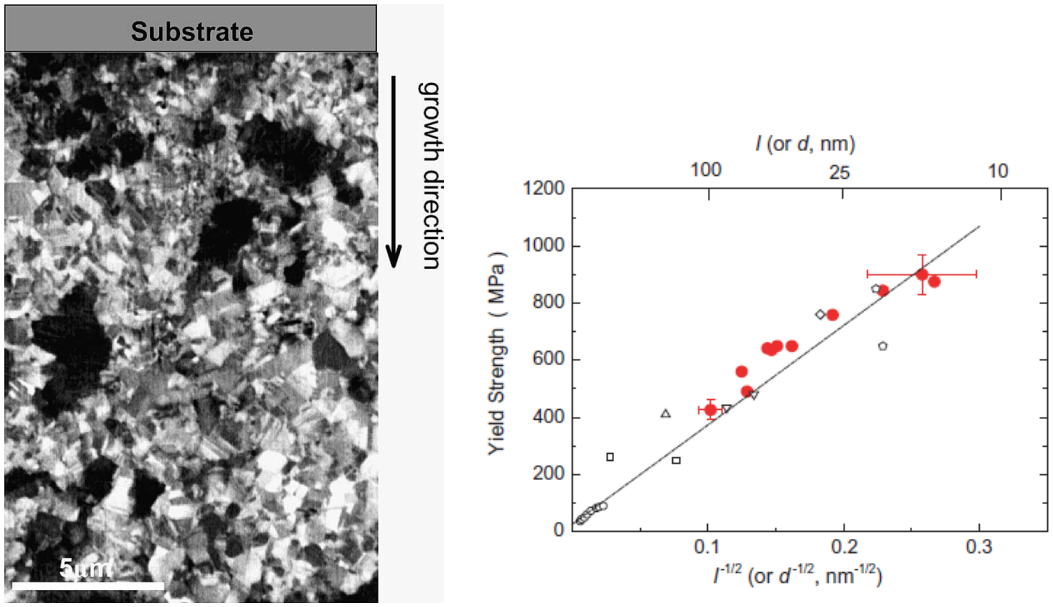

(a) (b)

Fig 1-3 (a) [53]Cross-sectional view SEM micrograph of an as-deposited copper sample using pulsed electro deposition (b) A plot of tensile yield strength as a function of the $l^{-1/2}$ (where l is the average lamellar thickness determined from statistic TEM observations) for the as-deposited Cu samples (solid circles). For comparison, H–P plots for the CG Cu (dashed lines and the opencircles and the nc Cu samples with various grain size were included.

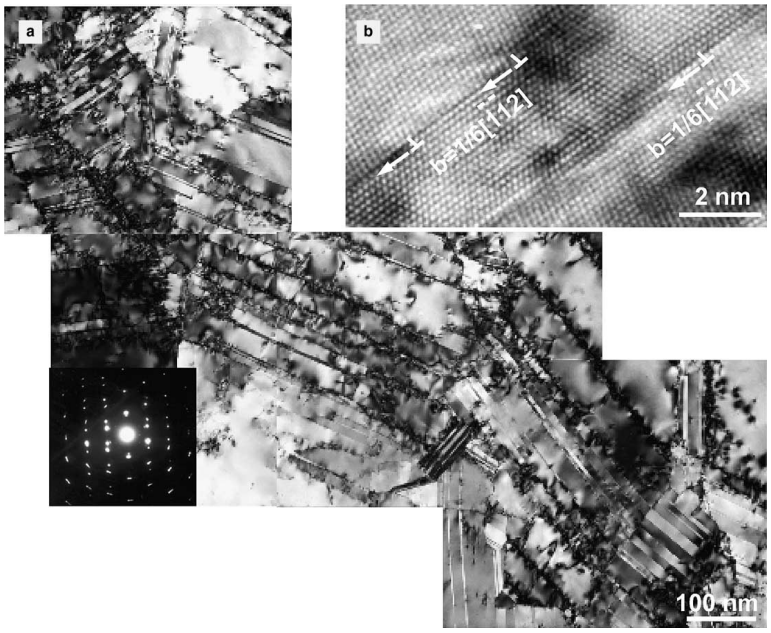

Fig 1-4 A TEM image of the microstructure close to the failure surface of high density nano twinned sample after tensile tests (a), containing lots of Shockley (partials) dislocations (1/6[$\bar{1}\bar{1}2$]) (b).

Controlled introduction of nanoscale twins has been achieved in UFG Cu with a grain size of 400-500nm. Twin boundaries can accommodate high densities of dislocations and thus facilitate plastic deformation leading to significant ductility [57] . The multimodal distribution of length scales in nano-twinned copper in these specimens further benefits ductility [4]. The ultra fine grain is divided into nano meter sized twin/matrix lamellar structures, however the length scale parallel to the TBs (plastically soft direction) is close to 500 nm and the length scale transverse to the TBs (plastically hard direction) is of the order of nanometers. Dislocation glide is easier along the former direction than the latter direction [45]. However, currently it is possible to make nano-twinned specimens of a few micron thicknesses using pulsed electro deposition.

Dynamic Plastic Deformation offers a way of manufacturing materials in bulk form with an abundance of deformation twins. The relative high stacking fault energy (SFE) of Cu makes it deform primarily by dislocation movement. However the high strain rate and cryogenic temperatures involved in this process prompt deformation and strain induced micro structural evolution by twinning because dislocation processes are suppressed at such high strain rates and low temperatures [58, 59] . As the amount of strain imposed on the specimen increases, the area occupied by deformation twin boundaries expands. This is manifested by the visibility of the grey region in the SEM micrographs as can be seen in Fig 1-5(b) which was originally white (Fig1-5(a)) . A higher magnification image shows the presence of deformation twin boundaries in the grey region (Fig 1-6) [59]. Micro structural refinement as a result of the DPD treatment occurs by three main mechanisms [59], (1) fragmentation of nanoscale T/M lamellae leading to grain sizes of about 47nm (2) nano grains formed in shear bands having an average transverse grain size of 75 nm, (3) nano grains formation originating from dislocation cells with an average grain size of 121nm. The specimen that will be used in the current study has been subjected to a strain of ε=2.1 during the DPD treatment and shows a mixed microstructure with nano scale T/M lamella making upto 33 % of the volume and nano sized grains making up about 67%. It has shown to have high tensile yield strength of about 600 MPa and an ultimate tensile strength of 633MPa mainly because of the presence of a combination of high number of deformation twin bundles and nano grains. The tensile elongation to failure is about 11% that is much better than that of NG materials [58, 59] produced by other methods. The DPD process of strengthening Cu also does not adversely affect the electrical conductivity mainly because of the low resistivity of twin boundaries [60]. Deformation twinning in DPD Cu was found to be dependent on texture [61]. Increase in the percentage of deformation twin bundles was shown to improve fracture

toughness [62]. Cold rolling of the DPD sample was shown to increase ductility but with a concomitant reduction in strength [56].

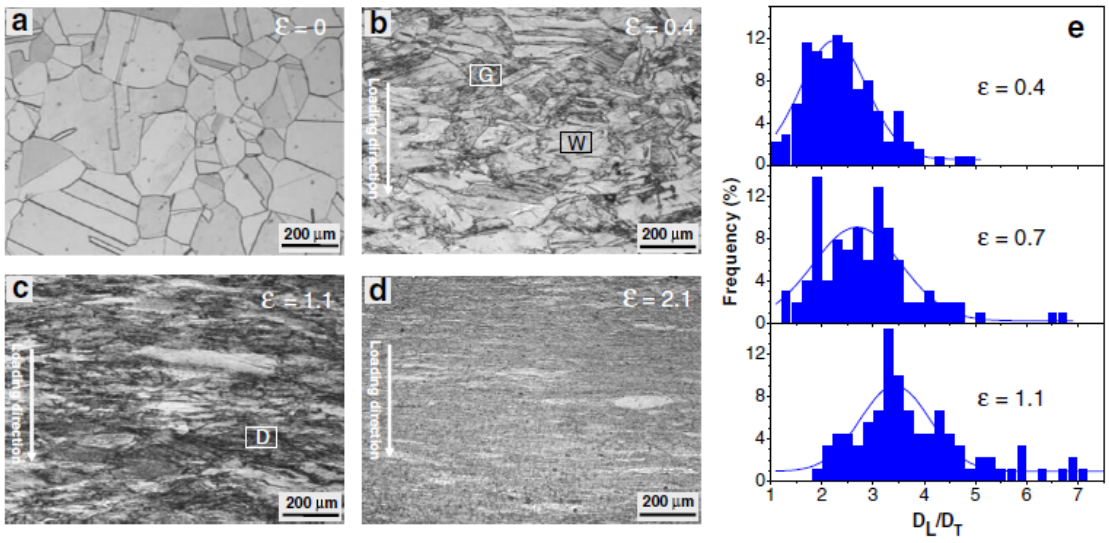

Fig 1-5 (a–d) Cross-sectional metallographic observations of the DPD Cu samples with different strains [59] : (a) $\varepsilon = 0$ (as-annealed), (b) $\varepsilon = 0.4$, (c) $\varepsilon = 1.1$ and (d) $\varepsilon = 2.1$. The letters ‘‘W’’ ‘‘G’’ and ‘‘D’’ denote the white region (hard-to-etch), the gray region (easy-to-etch) and the dark-gray region (very-easy-to etch), respectively. (e) Distribution of aspect ratios of grain sizes (D_L/D_T) in the three samples with different strains.

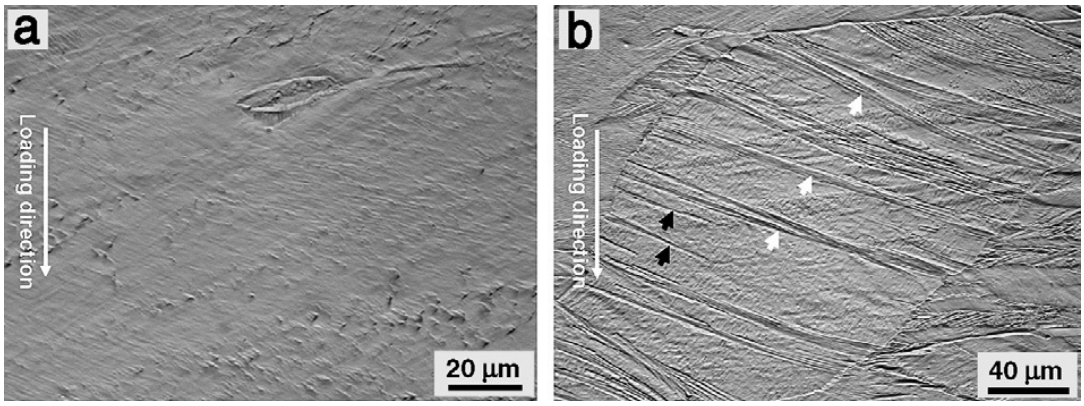

Fig 1-6 High-magnification metallographic images of the W region (a) and the G region (b) as indicated in Fig. 1-5 (b) (ε = 0.4) [59].

In addition to gaining knowledge of the tensile properties, it is critical to develop a deep understanding of the damage resistance and tolerance of nanostructured metals as their usefulness in structural applications is dependent on these properties. Stress controlled fatigue life test is a good measure of the damage resistance of a material as during these tests uniaxial stress less than the yield stress of the material is applied to initially smooth specimens and the number of cycles to failure is recorded. This is repeated at different stress values and the Stress-Number of cycles to fail (S-N) curve gives an idea of the damage resistance since at stress values lower than the yield stress, the greater portion of the life of a material is spent in crack nucleation at the surface than crack propagation. This is in contrast to low cycle fatigue in which high stresses are applied and the specimen life is dependent on the number of cycles required to propagate the fast-nucleated crack at such high stresses. Plastic instability is responsible for nucleation of cracks during fatigue loading. The irreversibility of cyclic slip along the slip bands results in " roughening" of the surface of the material that is manifested in the form of "hills" (extrusions) and " valleys" (intrusions) where the persistent slip bands (PSBs) emerge at the

surface [26]. The intrusions serve as micro-notches and lead to stress concentration that results in additional slip and fatigue crack nucleation.

The uniaxial deformation of metals can also be characterized in terms of the cyclic stress-strain curve (CSS) that is obtained typically by applying constant strain amplitude cyclically and monitoring the stress required to achieve the applied strain. The stress required reaches a stable saturation value after an initial shakedown period. There is a gradual change in dislocation substructure in the shakedown period until a stable configuration of dislocations that represents the stable saturation stress state is attained. It has been seen that word-hardened or cold worked metals undergo cyclic softening under fixed amplitude strain-controlled cyclic loading due to rearrangement of prestrain-induced dislocation networks into energetically optimal configurations and well-annealed metals undergo cyclic hardening due to dislocation multiplication [63, 64]. However, prior loading history, slip planarity, plastic strain amplitude and temperature play a strong role in determining the eventual microstructure attained by the metal during cyclic loading [65, 66]. High stacking fault energy FCC metals with a high propensity to cross-slip harden or soften to a similar steady-state saturation stress after the initial shakedown. The eventual microstructure comprises of a cell structure that is independent of the dislocation structure that existed before the application of cyclic loading. The cell size decreases with increased strain amplitude and increasing temperature but is independent of the loading history of the metal. However if the stacking fault energy is increase by alloying, then the CSS is sensitive to the prior deformation history as cross slip is hindered and this prevents the attainment of a common state of dislocation structure for initially annealed and cold- worked metals, Instead they harden and soften respectively to different steady saturation stress and microstructure. In both these cases, the steady state is approached when the numbers of

dislocations reach saturation and equilibrium between work hardening (dislocation generation) and dynamic recovery (dislocation annihilation) is reached.

Sub-critical fatigue crack growth experiments are also a good measure of damage tolerance and involve applying uniaxial stress cyclically to specimens with a pre-introduced crack and monitoring the length of the crack with the number of cycles applied. The rate of crack growth is expressed in terms of the incremental increase in crack length per loading cycle (da/dN). This crack growth rate is plotted with respect to the driving force for crack growth that is the stress intensity factor range ($\Delta K = K_{max} - K_{min}$), where K_{max} and K_{min} refer to the maximum and minimum values of the stress intensity factor during a fatigue cycle. In that plot three stages of crack growth can be identified. During Stage I of growth, the crack and its associated plastic zone are confined within a few grains and crack growth occurs primarily by single slip along the primary slip system [26]. For Mode I loading, a zig-zag crack path is observed although for Mode 1 loading the crack propagates (on average) in a direction perpendicular to the tensile axis. At higher levels of ΔK, the crack tip plastic zone size becomes large, relative to the characteristic grain dimension, and crack growth occurs via duplex slip (Stage II and the crack advances in a planar fashion between slip bands, normal to the tensile axis [67]. During Stage III, there is a sharp rise in crack growth rates due to the crack length exceeding the sub-critical crack length for fracture and the specimen fails catastrophically. Experimental studies done on mc metals and alloys and in light of the above analysis, we can conclude that grain refinement will lead to an improvement in stress-controlled fatigue life and endurance limit [68]. However, a coarse grained metal would exhibit an increase in the fatigue crack growth threshold stress intensity factor range and a decrease in the rate of crack growth especially in the near-threshold regime of

fatigue crack growth owing to periodic deflections (Fig 1-12) in the path of the fatigue crack at grain boundaries during crystallographic fracture and bigger crack surface asperities[69].

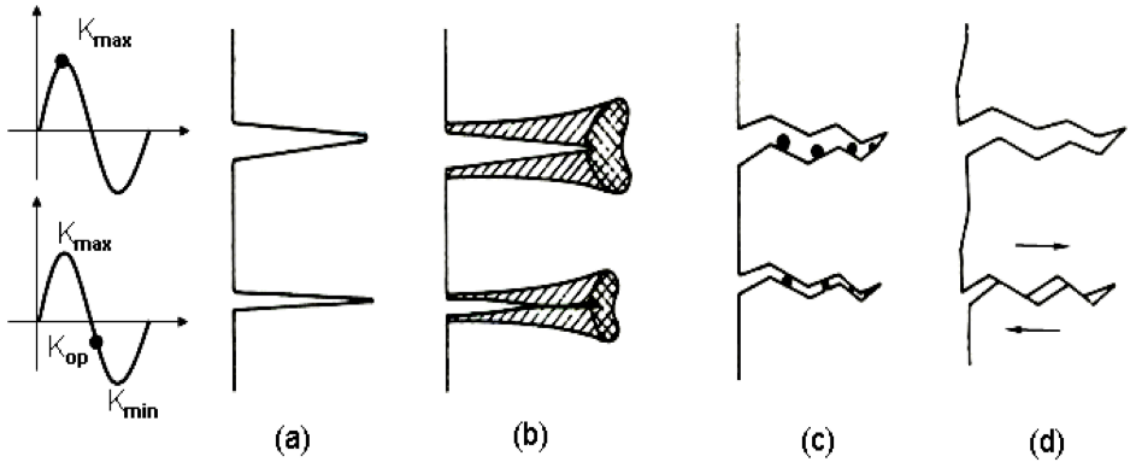

Fig 1-7 Different mechanisms of crack closure: (a) No crack closure (b) Plasticity induced crack closure, (c) Crack closure induced by particles likes corrosion products and (d) Roughness-induced crack closure [26].

This is because the actual manner of crack propagation is quiet complex and very sensitive to extrinsic mechanisms that can influence the apparent crack propagation rates to be markedly different from that expected just from the intrinsic resistance of the material to fracture and the applied stress intensity factor range. It is imminent to understand and study these crack retardation mechanisms in order to develop accurate life prediction models and come up with better microstructural design in order to prolong the stable fatigue crack growth life of the material. The differences between the actual "driving force" and the apparent one can spring

from a variety of factor including (a) premature closing of the crack faces in spite of nominal cyclic tensile loads applied, (b) periodic deflections of the crack path owing to microstructural obstacles like grain boundaries, precipitates etc. or local changes in mode mixity and local stress states, (c) bridging of the crack faces by corrosion products, fibers, grains or particles, (d) residual stresses imposed on the crack tip by stress-induced phase transformation or the cyclic plastic zone. These processes can be triggered and can make a seminal contribution by even a minor variation in the path of the crack, environmental conditions, loading environments and test methods. Some of the main cracks retarding mechanisms (Fig 1-7) are discussed below:

(i) Plasticity induced crack closure: A fatigue crack in reality is not an atomically sharp notch or a saw-cut. It has in its wake envelopes of plastic zones formed during crack propagation. Fig 1-8 shows the wake of material with a fatigue crack under constant amplitude of cyclic tensile stresses. Residual tensile strains are present in the material behind the advancing crack during one cycle of crack growth as only elastic recovery happens after the creation of the crack's new surfaces. The nearby material exerts compressive stresses on the plastically deformed region (with tensile strains) enveloping the crack that leads to crack closure even under positive values of far field tensile loading.

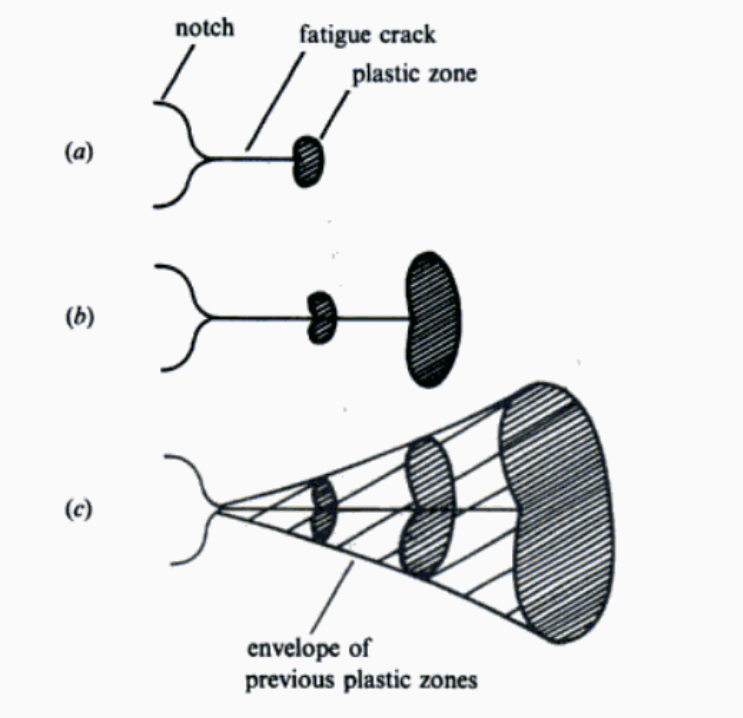

Fig 1-8 Envelopes of plastic zones in the wake of an advancing fatigue crack.[26]

(ii) Oxide induced crack closure: The presence of a moist atmosphere can lead to the oxidation of freshly formed crack faces. In many steels the thickness of the oxidation layer has been found to be comparable to the size of the crack tip opening displacement (CTOD) near the threshold [26]. At near threshold fatigue crack growth regime, due to low values of CTOD, the possibility of repeated crack face contact during tensile fatigue is significant due to serrated nature of crack growth in Stage 1 causing mode mixity. Besides microscopic roughness of the crack faces and plasticity induced crack closure also contribute in enhancing chances of crack closure at non-zero values of nominal stress fields. Besides, at low values of ΔK, there also occurs a continual

breaking and reformation of the oxide layer behind the crack tip [26]. This fretting mechanism can be conducive to building up thicker oxide layers than those formed on a freshly prepared surface that is exposed to same moist environment. These corrosion products formed induce crack closure and lead to an increase in the value of the threshold as can be seen in Fig 1-9. However, this type of crack closure is not very probable at high R-values, when the possibility of crack face contact is bleak because of the larger CTOD values, or at high ΔK values when the crack propagation rate is too fast to promote sufficient oxidation at any value of R (Fig 1-10).

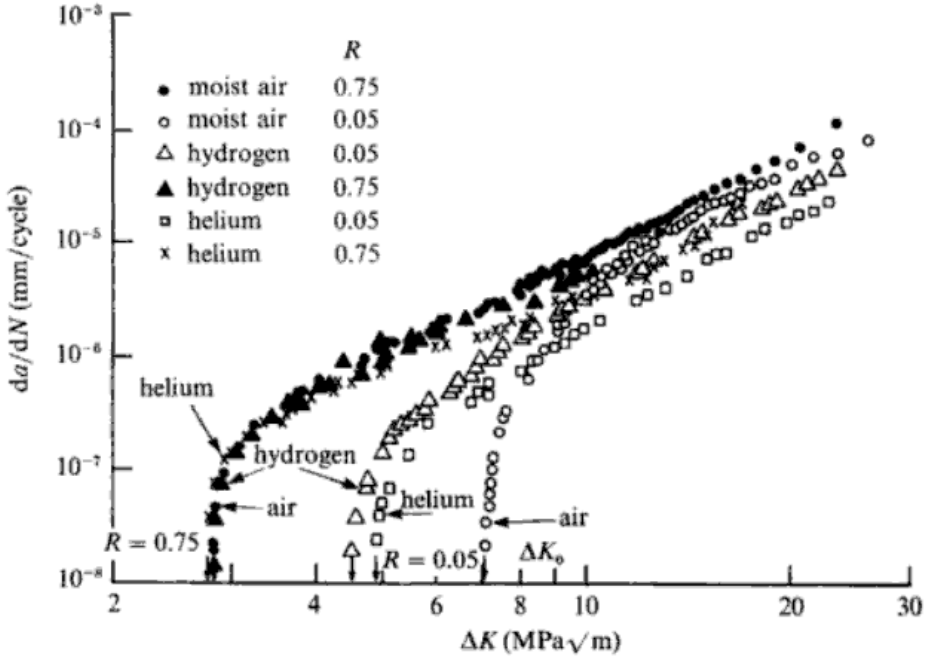

Fig 1-9 Effect of load ratios and dry and moist environment on the stable fatigue crack growth propagation of AISI A542 Steel [26].

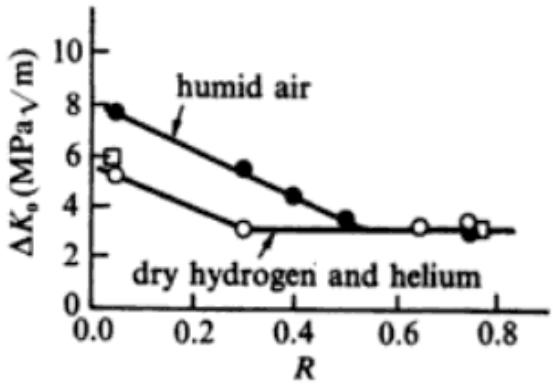

Fig 1-10 Threshold values increase with an increase in humidity, however with an increase in R ratio the effect of environment conditions is not significant [26].

(iii) Roughness induced crack closure: The explanation of the traditionally unexpected poor fatigue crack growth with grain refinement is possible because of the phenomenon of roughness induced crack closure. Crack propagation in Stage I occurs by the mechanism of single slip. Plasticity induced crack closure and the possibility of slip irreversibility due to various factors including corrosion cause mis-match between the fracture surfaces asperities. In situ observations in SEM of the opening and closing of fatigue cracks have recorded a significant Mode II component associated with fatigue crack and the occurrence of premature contact between crack faces asperities [26]. Roughness induced crack closure is enhanced by the following factors (a) low stress intensity levels when the plastic zone size is smaller than the grain dimensions, (b) small values of CTOD such that they are smaller than the crack surface asperity dimensions, (c) microstructure comprising of large grains and least non-shearable obstacles in the path of the crack such that serrated crack path is promoted, (d) periodic deflections in the crack path promoted by grain boundaries, second phase particles and (e) slip irreversibility especially enhanced by slip step oxidation in moist environments.

To date, there is limited information available on the fracture and fatigue properties of ultra-fine-grained (UFG) and nano grained (NG) materials. This can be ascribed to the limitations in manufacturing bulk fully dense nano-structured materials as techniques like electro deposition, e-beam deposition or magnetron sputtering that are capable of producing fully dense specimens of uniform purity and grain size can produce them to thickness of at most a few hundred microns. These processing limitations belie the possibility of conducting a valid plane strain fracture toughness test in accordance with ASTM E399 [70] and the fracture and fatigue studies done up

till now report specimens in plane stress since twenty-five times the plastic zone ahead of the crack is larger than the thickness of the specimen. In addition, to prevent artificial artifacts like out of plane bending and buckling, special care must be taken in gripping the thin test specimens and imposing loads. This imposes additional constraints on the environment, range of loads, stress intensity factors, mean stress levels and cyclic frequencies that can be imposed during the tests. Since compressive loading introduces the risk of buckling of the thin specimens, only tensile loading can be applied to the specimens. Severe Plastic Deformation (SPD) techniques and mechanical alloying/consolidation can prepare bulk specimens that satisfy the requirements of a plain strain fracture toughness tests mentioned in ASTM E399 and thus the results obtained can be compared with the literature values of coarse grained materials. However, it is difficult to gain a fundamental understanding of the mechanisms of crack initiation and propagation and extend the results obtained in these materials to other NG systems since the specimens produced through these methods comprise of highly inhomogeneous microstructures with a considerable variations in grain size, grain structure and defect density. In addition, many grains in such systems have sizes in the ultra fine grain regime (several hundred nanometers) and the specimens have pronounced initial defect densities that further make it difficult to get meaningful connections between structure and damage resistance and tolerance.

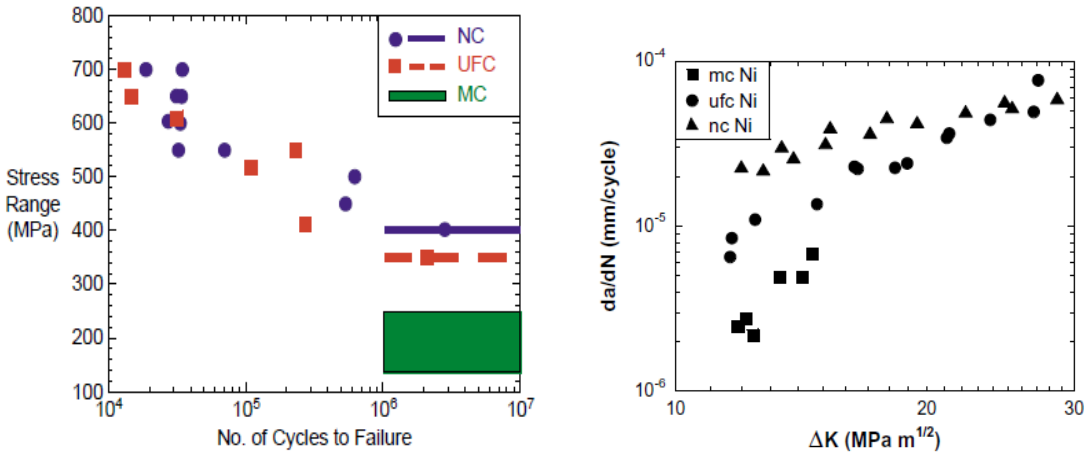

(a) (b)

Fig 1-11 (a) The effects of grain size [27, 28] from the micro to the nano-regime on the cyclic stress vs. total number of cycles to failure plot in pure Ni. (b) Variation of fatigue crack growth rate, da/dN, as a function of the stress intensity factor range, ΔK, for mc pure Ni and for electrodeposited ufc and nc pure Ni at R = 0.3 at a fatigue frequency of 10 Hz at room temperature.

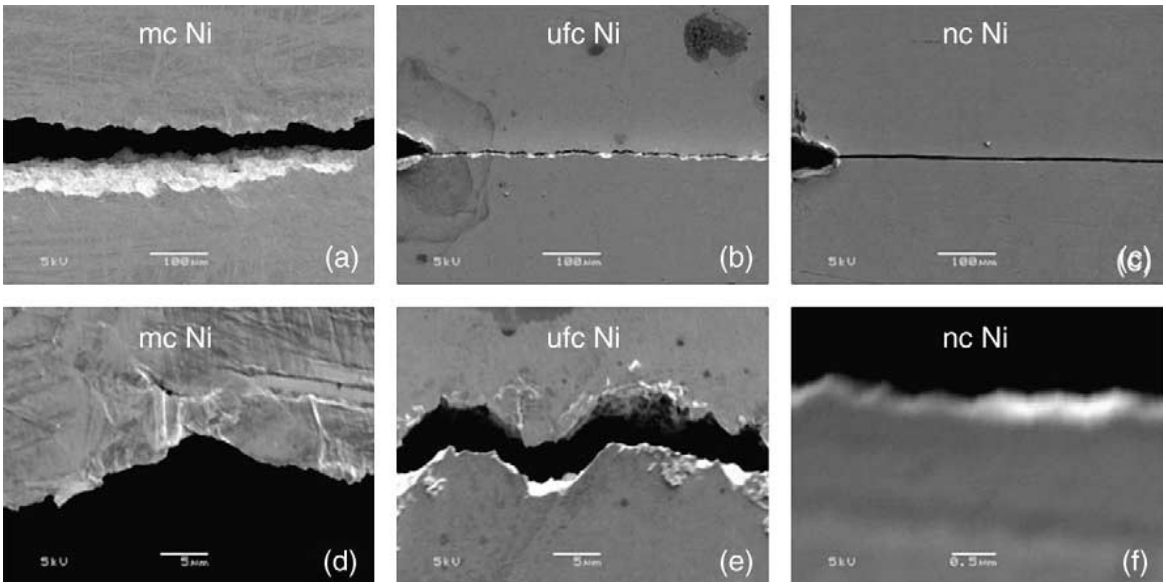

Fig 1-12 Scanning electron micrographs [27, 28] of mc, ufc, and nc Ni subjected to sinusoidal fatigue loading at initial ΔK values of 10, 6.2, and 8.5 MPa $m^{1/2}$, respectively. A cyclic frequency of 10 Hz and load ratio, R=0.3 were used in all cases. Crack path tortuosity clearly decreases with grain refinement. Images (d) through (f) are higher magnification images of (a) through (c), respectively, and the magnification of (f) is 10 times that of (d) and (e).

Earlier studies included high cycle fatigue experiments performed on nanocrystalline Cu produced by inert gas condensation [71] in order to ascertain the stability of microstructure under cyclic loading. These experiments documented 30% increase in grain size due to repeated, cyclic loading along with the surface being populated with parallel "extrusions" seemingly similar to persistent slip bands (PSBs) observed in coarse grained (CG) Cu and single crystals[26]. Strain-controlled fatigue tests [64] comparing UFG Cu prepared by severe plastic deformation (SPD) and CG Cu showed that the latter has a longer total fatigue life than the former, and that the surface of the fatigued UFG specimen showed extrusions similar to those

found in NG Cu [71]. In addition, cyclic softening was observed in Cu prepared by severe plastic deformation (SPD) [63]. However, it has been found [72] that annealing treatment improves the low cycle fatigue life in strain controlled cyclic tests on UFG materials produced by equal channel angular pressing (ECAP). Cyclic softening in UFG Cu produced by ECAP was also ascribed to dynamic recrystallization and subsequent grain growth which was observed after strain controlled cyclic loading on Cu specimens produced by ECAP [73]. Unlike UFG metals prepared from SPD techniques, electrodeposited NG Ni with an average grain size of 40 nm displayed cyclic strain hardening under tension-tension cyclic loading. The deformation was also found to be dependent on the frequency of applied loading [74]. Stress controlled cyclic loading applied on bulk Ni-18wt%Fe alloy with an average grain size of 23 nm and produced by pulsed electrodeposition exhibited an endurance limit of just 13% of the yield stress which was surprisingly low compared to the trend shown by other metals [75]. Fracture and fatigue studies [76] done on the same bulk Ni-18wt%Fe alloy with an average grain size of 23 nm demonstrated limited values of fracture toughness owing to nano-void coalescence at the grain boundaries. In the near threshold regime of stable fatigue crack growth, the crack path was found to be non-tortuous as seen through scanning electron microscopy (SEM). Focused Ion Beam (FIB) confirmed the results obtained earlier from atomistic simulations [77] that the micro cracks are initiated close to the primary crack by the process of nano-void coalescence. Xie *et al.* [78] performed experiments on electrodeposited Ni sheets (average grain size 26 nm) and CG Ni in order to determine the difference in the modes of fatigue crack nucleation. It was found [78] that for CG Ni crack nucleation occurred in a diffused manner in that a population of cracks was observed whereas for NG Ni there was one principal crack and dislocation cell structures with an average size of 108 nm were observed along the main crack.

Mirshams *et al.* [31] found that the fracture toughness of pure NG Ni produced by pulsed electrodeposition decreased with an increase in annealing temperature. Their results were rationalized using the "cluster model" [79]. Here the claim is that a large number of nonequilibrium vacancies formed during the process of recrystallization of nanocrystalline materials would segregate and condense into clusters preferentially residing at the grain boundaries. These clustered vacancies would weaken the material, and the number and size of these clusters would increase with an increase in annealing temperature.

Opposite trends, however, were observed for carbon doped NG Ni in that the fracture toughness increased with an increase in annealing temperature. Charpy impact energy tests on electrodeposited Co showed that the toughness decreases as the grain size is refined close to 18 nm [80]. This trend has also been corroborated by fracture studies on α-Fe and Al [81] which have shown that fracture toughness decreases with grain refinement. Stress controlled cyclic loading experiments conducted on electrodeposited Ni showed an improvement in fatigue life and endurance limit with grain refinement in the < 100 nm regime (Fig 1-11(a)). However, stable crack propagation experiments on CG, UFG and NG Ni revealed diminishing fatigue crack growth threshold values with grain refinement (Fig1-11 (b)) [27, 28].

Only a few cyclic loading studies have been done so far on NT materials and have demonstrated enhanced mechanical stability of twin boundaries. For example, multilayer copper/copper specimens with nanoscale twins produced by magnetron sputtering have been shown to exhibit considerable microstructural stability and hardness retention even under fatigue loading and indentation [82]. The twin lamellae thickness dependence of fatigue endurance limit of the nano-twinned Cu (NT Cu) was also studied by conducting cyclic tension-tension tests under constant

stress amplitude at room temperature [83]. Initial results suggest that both the high cycle fatigue life and fatigue endurance limit increase with a decrease of the twin lamellae thickness [83]. Cyclic studies done on NG Ni-Fe alloy with growth twins have shown considerable grain growth and de-twinning in the path of the fatigue cracks with little microstructure change observed in grains removed from the crack [84]. In addition, large scale atomistic simulations to model the damage tolerance behavior of NG materials (average grain size ~ 20 nm) with nanoscale twins have suggested the possibility of an improvement in fracture toughness with an increase in twin density [85, 86]. Copper produced by dynamic plastic deformation (DPD) under conditions of high strain rate and cryogenic temperatures has a microstructure with a mixture of deformation twins and nano grains. Qin *et al.* [62] have shown that increasing the strain while preparing the specimen leads to an increase in fracture toughness on account of increase in the concentration of deformation twins in the structure. However, the highly heterogeneous microstructure of DPD Cu comprises both deformation twins and nano grains and the percentage of both of them increases with the imposed strain, so it is difficult to elucidate the isolated role of twin boundaries in influencing the fracture toughness. To our knowledge, no experimental studies of the key damage tolerance characteristics involving systematic fracture toughness measurements and fatigue crack growth behavior of nano-twinned metals and alloys have been reported to date.

In addition to high strength, ductility, damage resistance and tolerance, good tribological properties are indispensable for many engineering applications. Design against wear damage is crucial as it is the most common way of material loss in most engineering applications [87]. This is as much true for designing materials that have to cope with frictional sliding against abrasive particles, as it is to MEMS devices with resistance against tribological damage that might result from repeated contact between small scale structures. The effect that the controlled introduction

of nano-twins in UFG Cu will have on the tribological response has not been systematically studied. The wear properties depend in a complex manner on such material properties as elastic modulus, yield strength, ductility, strain hardening exponent, friction coefficient, fracture resistance, and sustained damage tolerance, as well as on the environment in which wear damage occurs. Thus it is not possible to predict the trends in tribological properties by a mere knowledge of basic mechanical properties. Besides, under conditions of repeated sliding, the microstructure and the properties evolve in response to high stresses and strain gradients below the indenter. Consequently, information about the initial structure is often insufficient to predict the wear response under repeated sliding contact fatigue.

Instrumented repeated frictional sliding tests offer a means to assess, in a quantitative and controlled manner, the wear properties of UFG Cu with nanoscale twins. The use of scratch testing dates back to adhesion testing of thin hard coatings several decades ago [88] and its popularity in testing tribological response has since grown. Its direct utility lies in the fact that the indenter tip serves as a model of the abrasive particle that rubs against the surface. One of the parameters recorded was the total friction coefficient for the motion of the diamond indenter over the surface of the specimens. Some of the possible measures of damage in scratch tests are the depth of scratches, the width of scratches, and the volume of material that is removed by the scratching process or the pile up of material on the sides of the scratch. The most appropriate measure is often dictated by the application. Aesthetics may dictate that the most important measure is the width of the scratch; whereas the pile up, depth or volume of material removed may be more important if wear resistance is the main concern.

In addition to monotonic sliding, it is also very necessary to investigate the response of the material to repeated contact sliding using scratch testing. This is important from a practical point of view as it mimics the real life situation in many materials that are subjected to repeated frictional sliding contact. Secondly, there has been no study done previously which systematically investigates the effect of twin density on the wear response of materials under repeated frictional sliding although there have been numerous studies done to investigate the wear response of coarse grained (CG) metals and alloys. There have also been limited investigations done to elucidate the tribological behavior of NG metals and alloys. Most wear studies on coarse-grained materials have shown that as a result of large plastic stresses and strains the microstructure of the region close to the surface is severely affected. The material close to the surface is drastically affected by the wear process and is instrumental in affecting the subsequent wear response of metals under repeated sliding. This tribolayer formed can have structurally and chemical characteristics completely different from the original material. The structure has been classified into cells, sub grains and recrystallized grains [89]. The substructure has often been compared to that observed in metals and alloys after severe deformation processes (SPD) with the size dependence related to the stacking fault energy, applied stress and temperature [90, 91]. Rigney has found out the substructure to consist of equiaxed cells bounded by relatively wide cell walls [92]. These dislocation substructures formed under wear were optimal with respect to energy minimization and were similar to those for sliding and erosion except near the surface where the number of active deformation systems can make a difference in the structure observed [93]. Many wear studies have shown this tribolayer to have boundary spacing in the nanocrystalline regime [94-96] and to differ considerably from the bulk material [92, 97]. Smoothness of sliding and damage incurred in terms of material loss have been found

to be dependent on the nature of the tribolayer [97]. The tribolayer microstructure in Cu-15wt%Ni-8Wt%Sn bronze after sliding resembled that of a heavily rolled FCC alloy with fine grains and nanotwins are observed within the nano grains which is indicative of large stresses and strains incurred by the sliding process [98, 99]. Bellon found a sharp transition between the tribolayer from the bulk material and the presence of the tribolayer to alleviate the wear rate [99]. Boundary spacing of 25nm was observed in the tribolayer for CG Cu after sliding in addition to the presence of newly formed deformation twins, recrystallized grains and largely recovered large subgrains [100]. Formation of twins in the tribolayer has also been reported by Rigney [92] during the dry sliding of CG copper during which the growth of the tribolayer becomes larger and more non uniform with sliding time. Under repeated sliding, a submicron layer has been observed below the nano layer in pure copper [92]. The nano-grained tribolayer has been shown to be conducive to reduce the wear rate and friction coefficient [101, 102]. Dynamically Plastic Deformed (DPD) Cu with an initial microstructure comprising of nano grains and nanotwin bundles exhibited grain coarsening in the tribolayer as a consequence of repeated sliding [103]. Grain coarsening has been observed for Ni-W alloys with an initial grain size ranging from 3nm-10nm to a final grain size close to 20 nm under contact sliding whereas negligible change in grain size was observed for initial grain sizes greater than 10 nm [104]. Although the formation a deformation-affected tribolayer is widely reported, the mechanisms of its formation are still not very clear.

Wear studies on NG Ni have shown that friction coefficient is a stronger function of strength than the grain size for Ni. However, the microstructure did not remain stable with sliding and significant grain coarsening was reported in the sliding track [9]. Grain refinement played a significant role in improving the wear rates of NG Al under frictional sliding [105]. Schuh [7]

has shown that wear damage in Ni decreases with a decrease in grain size but beyond the Hall-Petch breakdown point increased material loss was observed with grain refinement. However, degraded wear response with strengthening has been observed for NG Ni-B alloy film produced by electro deposition [106] and NG iron produced by rolling [107] . Dry sliding wear studies done on NG Cu processed by SMAT and CG copper showed a lower friction coefficient for NG Cu than CG Cu however the distinction diminished at high load values imposed on the indenter [108].

The foregoing discussion of prior work clearly illustrates that there is very little systematic work on the fracture and fatigue crack growth characteristics of nano-grained metals and alloys. Nevertheless the limited experimental information available to date generally appears to indicate a significant reduction in damage tolerance with grain refinement into the nano-crystalline regime, and the loss of resistance to fatigue crack growth with grain refinement in NG metals, especially in the near-threshold regime, mirrors the trend observed in their CG counterparts [27, 28]. However, there is an improvement in damage resistance with grain refinement as can be inferred by the improved high cycle fatigue life and enhanced endurance limit values for NG Ni. The compromise between either damage tolerance or damage resistance is the dilemma faced by material scientists when gran boundary engineering is used to alter the strength of materials. Therefore, in the current study we have tried to gain knowledge of the damage resistance and tolerance characteristics of another class ie. nano-twinned copper. The aim of the current work is to further the understanding of the role of microstructural length scale TB spacing vs. grain size in affecting the fracture and fatigue of metals. Another important objective of the current study is to investigate the tribological response of NT copper and DPD copper and contrast it against

UFG and CG Cu respectively. The present thesis will address the following hitherto unanswered questions related to nanostructured metals:

1. How are TBs in nanotwinned copper produced by pulsed electro deposition different from GBs in NG metals in affecting the sub-critical fatigue crack growth characteristics?
2. How is the fracture toughness affected by twin-lamellae refinement?
3. What is the effect of twin density in NT copper on the wear response and damage evolution under monotonic and repeated frictional sliding?
4. What is the role of twin density in influencing the microstructural stability under the high stresses beneath a sharp indenter during monotonic and repeated contact sliding? How does the hardness of the tribolayer evolve with repeated sliding?
5. Is there an improved wear response in DPD Cu with a microstructure comprising of an abundance of deformation twin boundaries and nano grains in comparison to CG Cu in terms of lower frictional coefficient and less wear damage?
6. What is the hardness evolution of the tribolayer in DPD and CG Cu as a consequence of repeated frictional sliding? (Tao [103] has studied the micro structural evolution entailed by the nano scratch process for DPD and CG Cu.)

The thesis is organized in the following sequence.

Chapter 2 describes in detail the material systems investigated, as well as the experimental methods employed. The strengths and limitations of the processing and testing techniques are discussed. Although there exists analytical expressions to relate the P-h (Load vs.

depth) response obtained after indenting on a flat surface to the elasto-plastic properties of the material, no such expressions are known for indenting on a grooved surface. Since inorder to determine the hardness evolution with repeated frictional sliding, the indentations were made on the grooved surface of the sliding track. Large deformation FEM computations were performed modeling indentation on a grooved surface with a conical indenter and analytical expression was obtained relating the indentation response to the elasto-plastic properties in the vicinity of the scratch.

Chapter 3 reports the outcome of systematic experiments on the effects of controlled variations in nano-twin density in a UFG copper with a fixed grain size of approximately 450 nm. The use of pulsed electric deposition (PED) to produce nano-twinned copper, while enabling the manipulation of the grain size and twin density by controlling such parameters as current density and time, has thus far resulted in producing fully dense NT specimens in the form of thin foils only. As a result, it is presently not feasible to perform "valid", plane strain fracture toughness or subcritical plane strain crack growth studies of fully-dense, pure nano-twinned copper produced by pulsed electrodeposition. Despite this limitation, careful experiments could be designed to critically assess the structural effects of introducing nano-twins in UFG Cu on the relative intrinsic resistance to fracture toughness, fatigue crack growth, and damage tolerance by performing linear elastic fracture experiments under plane stress conditions.

The present investigation therefore allows the effects of varying yield strength through the control of nano twin density on fracture resistance and fatigue crack growth response to be isolated from any effects of grain size. Tensile tests were conducted on three specimens with different twin densities but with the same grain size, and their strength and ductility were

determined. Damage tolerance was studied by introducing a crack of known length and applying displacement controlled loading to the specimen until the onset of stable fracture. Subsequently, the stable crack propagation response was studied in pre-cracked specimens by optically monitoring the length of the crack until catastrophic failure. Possible mechanistic origins of the observations are postulated and comparisons are made between the relative roles of grain and twin boundaries in influencing subcritical fatigue crack growth characteristics and fracture toughness under plane stress conditions [109].

Chapter 4 reports the effect of twin density on the friction coefficient as a function of number of repetitions of contact sliding has been studied. Pile up material around the indenter was also investigated for all the specimens with different twin densities. Prior work on NG Ni has shown that high stresses underneath the indenter cause microstructure changes during repeated tribological contact [9]. Here we quantify such microstructure evolution during repeated frictional sliding not only through microscopy observations, but also by recourse to quantitative indentation tests along the wear tracks performed at periodic intervals. These measurements are accompanied by large deformation finite element method (FEM) computations. Through such experiments and computations, we demonstrate the effects of the introduction of a population of coherent nano twins in ultra-fine-grained Cu on the sliding contact fatigue characteristics. Earlier work on constant amplitude strain controlled fatigue has shown that pure FCC metals under repeated uniaxial loading transform to a characteristic steady state saturation flow stress and microstructure that is dependent on the strain, strain rate and temperature [65, 66] . We have tried to elucidate the similarities and differences between strain-controlled fatigue and repeated sliding in terms of attaining a final saturation stress, microstructure, damage accumulation and the mechanisms leading to it.

Chapter 5 presents the results of the investigation of the tribological response of DPD Cu and CG by scratch testing under monotonic and repeated sliding conditions. Friction coefficient and pile up height are reported as a function of pass number. We have probed into the deformation induced hardness evolution by indenting on the scratches and have made connections of the tribological properties and damage accumulation under repeated sliding to the hardness and microstructure evolution. Cyclic indentation experiments have also been done on DPD and CG Cu and the ratcheting of the indenter is monitored with the number of cycles. Repeated contact loading was found to be similar to strain controlled uniaxial fatigue loading in that both of them lead to a transformation of microstructure and properties with the increase in load cycles which is dependent on the specific state of stresses, temperature and strain rate applied but is independent of the load history for high stacking fault energy metals [65, 66].

Chapter 6 provides a brief summary and principal achievements of this thesis and introduces the future pertinent directions of investigation related to nano-twinned copper.

Chapter 2

Materials, Experimental Methods and Modeling

2.1 Introduction

The materials studied in this thesis, and all associated experimental techniques are described in full detail below. All of the specimens in the current study were procured from Institute of Metal Research (IMR), Chinese Academy of Science, Shenyang, China. NT Cu specimens produced by PED were taken in order to gain a fundamental understanding of the effect of TBs on the sub-critical fatigue crack growth, fracture toughness and wear properties and with the eventual aim of extending the understanding to other FCC systems. DPD copper specimens were studied for their tribological response firstly because they contain a different kind of TBs: deformation TBs and secondly they are closer to be used in actual structural applications because they can be produced in bulk form.

2.2 Materials Investigated

2.2.1 Electrodeposited nano-twinned (NT) copper

Pulsed electro-deposition was used to synthesize high purity copper specimens with nanoscale growth twin lamellae from an electrolyte of $CuSO_4$. The grains were equi-axed and the average grain size for all the specimens was 400–500 nm, but the twin density was varied by modifying the electrodeposition parameters. Three specimens, one with the highest concentration of twin

boundaries with an average twin lamellar spacing of 15±7nm (hereafter referred to as HDNT Cu, i.e. high density nano twinned Cu), the second with a medium density of twins with an average twin lamellar spacing of 32±7nm (MDNT Cu: Medium density nano-twinned Cu) and the third with a relatively low density of twins with an average twin lamellar spacing of 85 ± 15 nm (LDNT Cu: Low density nano-twinned Cu), were produced. The fourth control specimen, UFG Cu with essentially the same grain size but with no significant concentration of twins, was prepared by direct-current pulsed electrodeposition. The density of the as-deposited specimens was measured to be 8.93±0.03 g/cm^3. The purity of the as-deposited copper was found to be more than 99.998 at% with less than 8 ppm S content. Chemical analysis also showed hydrogen and oxygen levels to be less than 15 ppm and 20 ppm, respectively. The specimen preparation procedure and the structural characterization of the NT Cu are discussed in detail elsewhere [54].

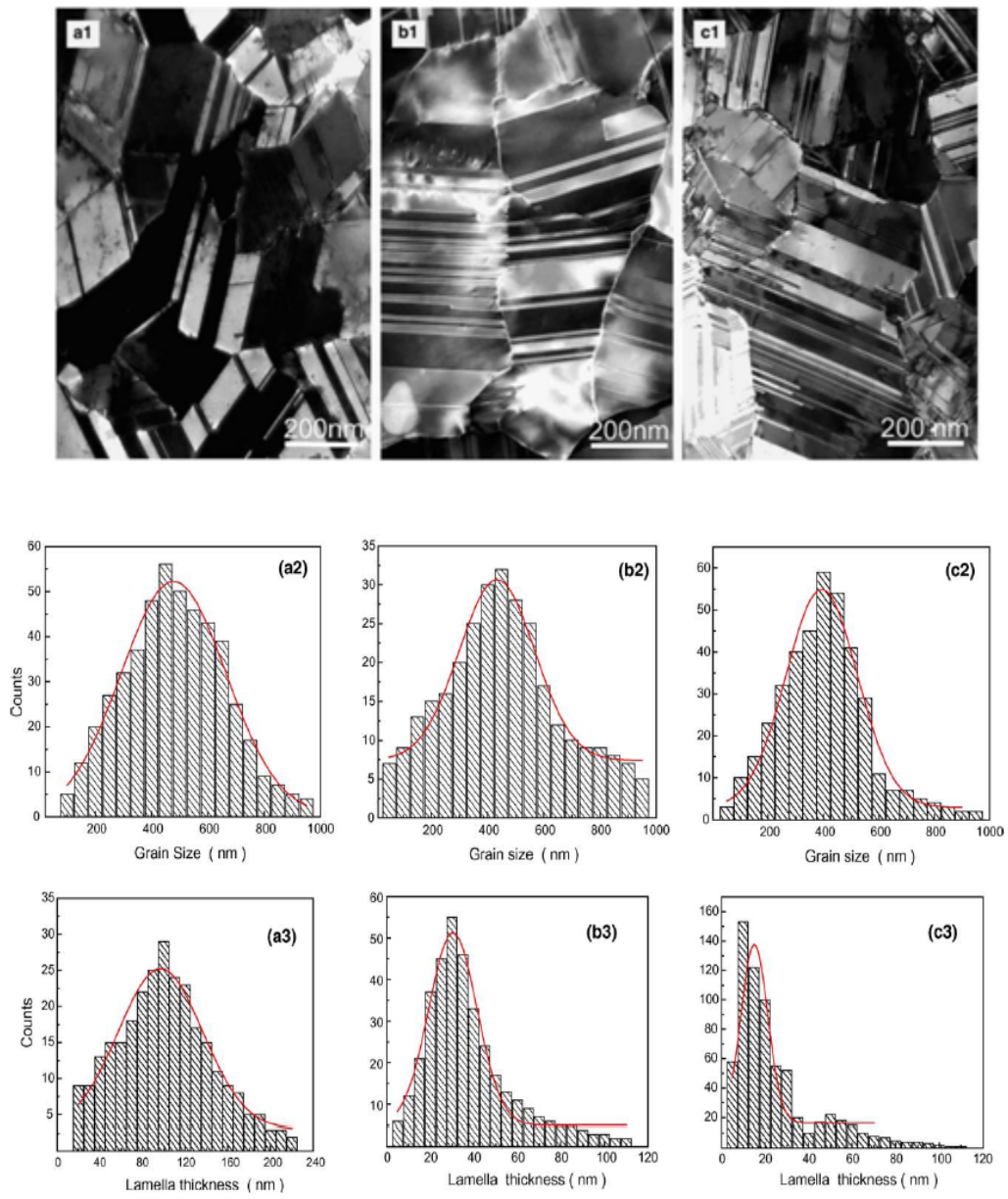

Fig 2-1 Bright field TEM images (a1, b1, c1), statistics of grain size distributions (a2, b2 and c2) and twin lamellae thickness distributions (a3, b3, andc3) in three as-deposited Cu samples (A, B and C), respectively [53].

TEM observations (Fig 2-1) of specimens in prior studies prepared by the same method show that most grains are subdivided further into twin/matrix lamellar structure by a high density of TBs. Fig. 2-1a1, b1 and c1 show typical TEM images for three as-deposited samples (A, B, and C) with different twin densities, respectively. Most of them have coherent $\sum 3$ boundaries. The twins separate grains into nano-meter thick twin/matrix lamellar structures with an average twin lamellar spacing of 85nm, 30nm and 15nm for the A, B and C samples respectively. Inside the ultra-thin lamellar crystallites almost no lattice dislocation can be seen.

2.2.2 Severely Plastically Deformed (DPD) and Coarse Grained (CG) copper.

Two copper bars with an initial size of 8x8x12 mm^3 were taken and mechanically polished with SiC papers and subsequently annealed for 120 minutes in vacuum at 700^0C to achieve a final grain size of 200-300 um. DPD treatment was applied to one of them and the specimen obtained after the treatment would be subsequently addressed as DPD Cu whereas the second bar was directly used for the experiments and would be hitherto addressed as CG Cu. DPD treatment was applied by placing the former bar on a lower anvil and compressing cyclically with an upper impact anvil at a strain rate of 10^2-10^3 s^{-1}. The sample was cooled by Liquid nitrogen before each impact that ensured that the temperature of the sample before each impact was close to -100^0 C to prevent dynamic recovery and recrystallization during the process. No flaws or porosity was reported in the sample and the final density and purity was found to be similar to the original CG sample. The deformation strain defined as $\varepsilon = \ln (L_0/L_f)$ where L_0 and L_f are the initial and final thickness of the specimen respectively was 2.1. The microstructure comprised of 67% of nano grains and 33 % of deformation twin bundles by volume. The yield strength has

been found to be 600 MPa and ductility to be 11% [58]. There was negligible strain hardening observed. More details of sample preparation and microstructural and mechanical characterization can be found in [58].

2.3 Experimental Methods

Three different kinds of mechanical experiments were performed in order to determine mechanical properties involving smooth tensile specimens, fracture toughness tests, and stable fatigue crack propagation experiments. Details of these experimental methods and data analysis are described below

2.3.1 Fracture toughness determination

Two specimens of each condition (MDNT, LDNT and UFG Cu) with similar dimensions were tested (Fig 2-2(a)). A fatigue pre-crack was initiated to a depth of 1.5mm in all the specimens. The specimens were gripped all along their width as shown in Fig 2-2(b). Subsequently, monotonic loading was applied under displacement control mode at a rate of 0.5mm/min on the Tytron 250 micro-force testing system. The displacement was allowed to increase until the crack propagated catastrophically to fracture. The displacement, δ, was plotted as a function of load, P, and a tangent line was drawn to the linear part of the initial P *versus* δ curve and subsequently a line having a slope of 95% of the tangent line was drawn. The point at which the 95% line intersected the load–displacement curve was the taken as the load, $P_{Q,}$ at which unstable crack growth ensued. This load was used to determine the fracture toughness estimates for the different materials studied, as described below. Further details of this method can be found in [110].

The Mode I stress intensity factor (K_I) directly ahead of a sharp crack can be expressed in terms of the nominal stress applied on the specimen (σ), crack length (a), the specimen width (w) and the shape factor $f(\frac{a}{w})$ [26]

$$K_I = \sigma \sqrt{a} f(\frac{a}{w}) \qquad (1)$$

The shape factor $f(\frac{a}{w})$ depends on the geometry of the specimen and the loading conditions [26]. Fixed end displacement loading was used in the present study for both fracture toughness estimation using the P–δ curve and subcritical crack growth studies rather than pin-loading (which can induce bending and wave form degradation); rigid grips help ensure uniform waveforms especially at frequencies above 5 Hz. A model based on the finite element (FEM) that employs the commercial software package ABAQUS (SIMULIA, Providence, RI, USA) was constructed for geometry shown in Fig 2-2(b) and computations were performed with the final aim of estimating $f(\frac{a}{w})$ in terms of $\frac{a}{w}$ for the present loading configuration and geometry. The J integral for $\frac{a}{w}$ values ranging from 0.1 to 0.7 was obtained through the simulations. The value of $f(\frac{a}{w})$ in turn was extracted from J from Eq. 2 for plane stress [26].

$$f(\frac{a}{w}) = \sqrt{\frac{JE}{a\sigma^2}} \qquad (2)$$

Using the above analysis the shape factor was found as given in Eq. 3 and it is used to evaluate the stress intensity factor in all the cases

$$f(\frac{a}{w}) = 1.94 + 0.81\times(\frac{a}{w}) - 2.40\times(\frac{a}{w})^2 + 4.42\times(\frac{a}{w})^3 \quad (3)$$

Fracture toughness is obtained by using Eq. 4 where B is the specimen thickness, w is the width of the specimen and a is the crack length at which the crack begins to propagate catastrophically.

$$K_C = \frac{P_Q}{Bw}\sqrt{a}f\left(\frac{a}{w}\right) \quad (4)$$

However, in order to evaluate K_C for the imposed loading conditions using Eq. 4, it is necessary to ensure that the small-scale yielding (SSY) condition of linear elastic fracture mechanics (LEFM) analysis is valid. This condition requires that the size of the plastically deformed material ahead of the crack tip should be small compared to all characteristic dimensions including the length of the crack and the size of the uncracked ligament. The values of plastic zone radius, r_p, under conditions of plane strain and plane stress are given, respectively, by [111]

$$r_p = \frac{1}{6\pi}\left(\frac{K_I}{\sigma_y}\right)^2 \quad \text{plane strain} \quad (5)$$

$$r_p = \frac{1}{2\pi}\left(\frac{K_I}{\sigma_y}\right)^2 \quad \text{plane stress} \quad (6)$$

where σ_y is the material yield strength. According to the ASTM Standard E 399 [70], $(a, w-a, B) \geq 25r_p$ for a valid plane strain fracture toughness test. Evaluating $25r_p$ using Eq. 5 and comparing it to the thickness B of the specimens lead to the inference that $B << 25r_p$ for the present specimens. Therefore all the specimens tested in this work are more representative of plane stress conditions than plane strain. Thus Eq. 6 is used to determine r_p for all the cases to assess the validity of the data points. As discussed earlier, high quality NT Cu specimens can only be made at this time in

relatively thin foils less than a few hundred micrometers. Consequently, the fracture toughness values reported here should be taken to represent broad material trends that arise due to controlled micro- and nano-structural variations, and relative values of damage tolerance characteristics of the different material conditions studied, and not as true indicators in intrinsic, geometry-independent material fracture resistance.

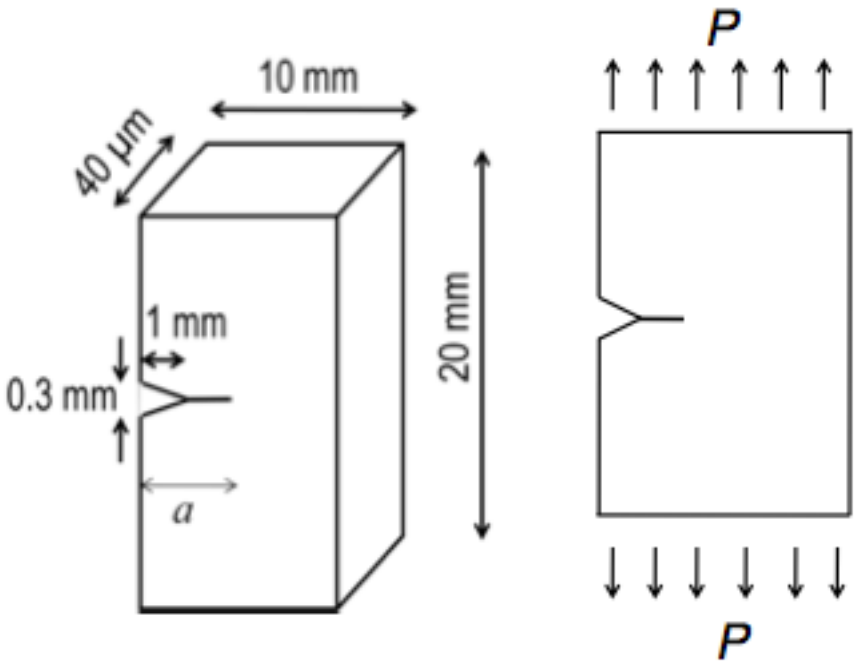

(a) **(b)**

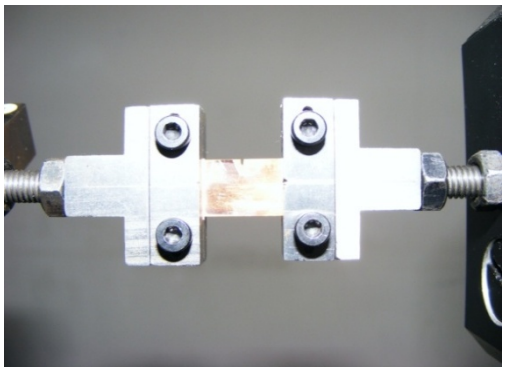

(c)

Figure 2-2: (a) Specimen geometry for fracture toughness test and stable fatigue crack propagation experiment. (b) Loading configuration for applying monotonic load to determine fracture toughness using the *P–δ* method. (c) Experimental set-up for studying the fatigue crack propagation, where the specimen was subject to tension–tension cyclic loading, with the ratio of the minimum load (stress intensity factor) to the maximum load (stress intensity factor), *R* = 0.1.

2.3.2 Sub-critical fatigue crack growth

Fatigue crack growth experiments were performed on two specimens of each condition (MDNT, LDNT and UFG Cu) at room temperature (25 ^{o}C and 50% relative humidity). The specimen dimensions are indicated in Fig. 2-2(a). An initial sharp cut was made using a sharp razor ahead of the notch tip before subjecting the specimen to fatigue in tension–tension cyclic loading in order to facilitate the formation of a pre-crack. The specimens were subsequently electropolished to relieve any surface residual stresses that could possibly arise from the introduction of the notch and specimen preparation. Subsequently an initial mode I fatigue pre-crack was introduced at the notch-tip to a distance of 0.36 mm ahead of the notch tip (tip radius ~ 250 mm) by applying tension–tension cyclic loading at a load ratio of 0.1 and frequency of 10 Hz through a servohydraulic machine. Data gathered during this initial fatigue pre-cracking process were not included in subsequent fatigue crack growth rate analysis in order to avoid possible effects of initial notch-tip region on the inferred fatigue fracture characteristics. The specimen was gripped along its entire width as can be seen in Fig. 2-2(c) and the experiment was performed under load-controlled conditions. The crack length was monitored through an optical microscope, and the crack length a was continuously tracked as a function of the number of fatigue cycles N. The value of K_I was determined from Eq. 1 by using the value of $f(\frac{a}{w})$ given by Eq. 3.Fatigue crack growth rates and fracture toughness for all the specimens were estimated from a plot of $\log_{10}(da/dN)$ vs. $\log_{10}\Delta K$.

Microstructural characterization on the surface of fatigued samples was performed in a scanning electron microscopy (SEM, Nova Nano-SEM 430) at a voltage of 18 kV.

2.3.3 Sliding Contact Fatigue

An instrumented nanoindenter, NanoTest™ (Micromaterials, Wrexham,UK), was used to conduct all sliding contact fatigue experiments. Force transducers mounted on either side of the indenter tip monitored tangential loads generated during scratch experiments, and a conical diamond tip (70.3^{o} half angle and 2 μm tip radius) was used in each test. Tips were replaced after every experiment to avoid material transfer between specimens. Initial contact was made between polished specimens (thoroughly cleaned in an ultrasonic ethanol bath) and the indenter tip, after which a prescribed normal load was applied as the specimen stage was displaced at a constant rate of 5 μm/s. The normal load was ramped to its maximum value of 500 mN over the first 50 μm of stage motion, and remained constant thereafter. A 500 μm scratch at the maximum normal load was then introduced, followed by a 15 μm tip retraction from the surface. The sample stage was subsequently returned to its initial position, and the scratch was repeated in this unidirectional fashion. Figure 2-3 illustrates this repeated contact sliding procedure. Through this method 1, 17, 34, 50, 66, 82 and 98 sliding cycles were imposed in seven different tracks which were sufficiently spaced out so that the possibility of interaction between the stress induced deformation zones of different scratches is eliminated. Normal and tangential loads were acquired throughout the entire length of the scratch.

In order to investigate the hardness evolution under repeated sliding, indentations were performed on the seven tracks left after scratching using instrumented nanoindentation. The indenter tip was conical and made up of diamond with a half angle of 70.3^{o} and a tip radius of 2

μm. The indentations were depth-controlled and the load required to reach a depth of 1 μm was recorded. All these indentations were performed at a loading rate of 10mN/sec.

After the experiment, a series of at least 30 cross-sectional residual profiles were obtained over the steady state regime by using a Tencor P10 profilometer (KLA-Tencor, San Jose, California, USA). The profilometer was equipped with a conical diamond probe that had an apex angle of 45^{o} and a tip radius of 2 μm. From these profiles the pile-up height for all of the specimens for all the pass numbers was determined.

In order to assess deformation-induced microstructure changes, specimens were ground on a 320 grit SiC paper followed by a 1000 grit SiC paper to reach the center of the length of the sliding tracks with continuous cooling maintained during the entire grinding process. Focused Ion Beam (FIB) was subsequently used to polish the cross section of the scratch. The cross section was observed under a high resolution FEI Quanta 600 scanning electron microscope (SEM) (FEI Company, Hillsboro, Oregon, USA).

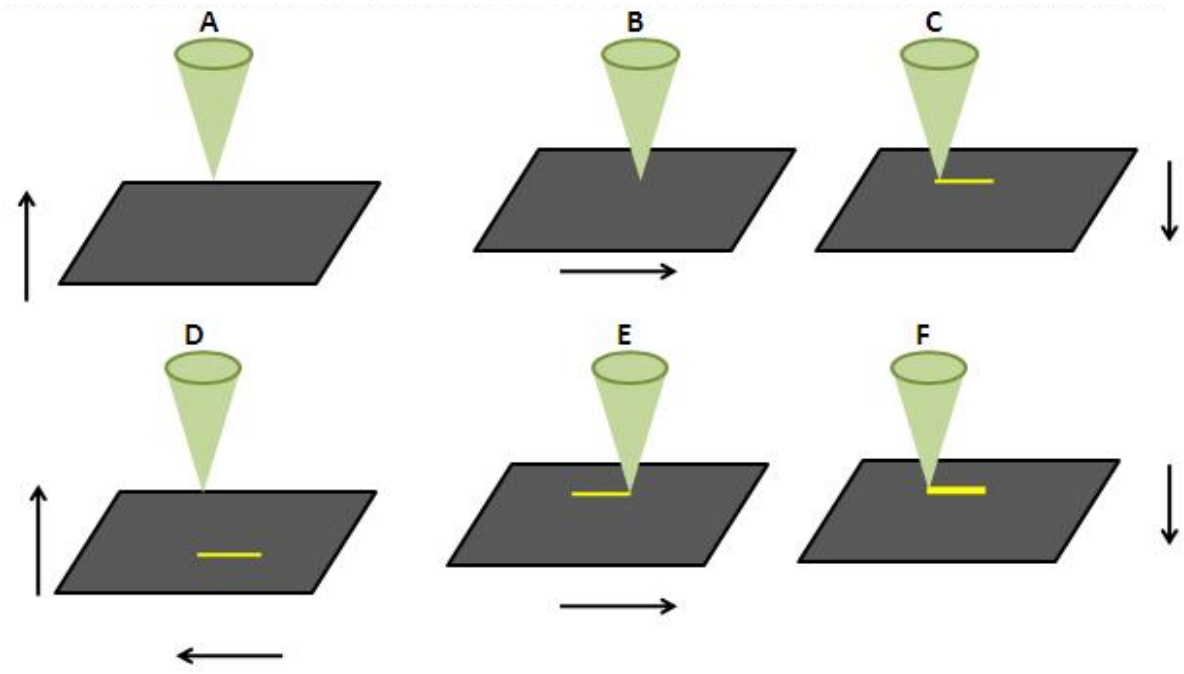

Figure 2-3. A schematic drawing of the repeated contact sliding experiment. (A) Sample Stage is brought close to the tip. (B) Sample Stage is moved to the right to make a scratch. (C) Sample Stage is moved away from the tip. (D) Sample Stage is restored to its original position and brought in contact with the tip to repeat sliding at the same position. (E) Sample Stage is moved to make another scratch along the same track. (F) Two cycles of sliding completed.

2.3.4 Cyclic Indentation

A fresh area on the specimens was chosen and cyclic indentation experiments were performed using the same-instrumented micro-indenter and conical diamond tip that was used for the previous indentation experiments. An initial contact was introduced between the tip and the sample –stage subsequent to which 500 cycles of load controlled indentations at a loading and unloading rate of 50mN/sec were performed. The loading was applied to a maximum value of 500mN subsequent to which that load was held steady for 10 seconds. Unloading was programmed to reach a minimum load of 20 percent of the maximum load that is 100mN. This was followed by loading to the maximum load again while the sample stage was not displaced laterally. This process was repeated till 500 cycles of indentation were imposed on the specimen at the same spot. The depth and load were monitored during the entire process.

2.4 Finite Element Modeling of Indentation on a grooved surface.

Recent advances in mechanical testing equipments have made it possible to record forces and distances to an accuracy of microNewton and nanometer respectively. An example of such equipment is Micromaterials (UK) that has been used in the current study to indent on the sliding tracks with the aim to ascertain deformation induced mechanical property changes. However, most of the analytical studies in the literature relating indentation data to elasto-plastic properties were for the case of indenting on a flat surface. Currently no analytical expression exists which can either yield the indentation response while indenting on an inclined surface or can extract the elasto-plastic properties from the indentation data obtained from indenting on a slanted surface.

To achieve the objective of assessing deformation induced property change as a function of number of sliding passes as well as twin density from the indentation data, analytical functions that can relate indentation data to elasto-plastic properties are needed. For this we resorted to large deformation FEM computations. Large equivalent plastic strains of the order of 25-36% below a sharp indenter [112] require large deformation analysis to model instrumented sharp indentation. Since the NT Cu used in the present study has relatively low strain hardening, the strain-hardening exponent has been taken as zero. In order to cover the entire span of pure and alloyed engineering metals, E was varied from 10 to 210 GPa, σ_y from 30 to 3000 MPa and ν was kept fixed at 0.33. Dimensional analysis was used to construct functions to relate the loading curvature while indenting on a slanted surface as a function of elasto-plastic properties. These functions and FEM computations were then used to extract the analytical relationships between the indentation response and elasto-plastic properties.

2.4.1 Dimensional analysis

Assuming the materials whose indentation response we wish to investigate manifest elastic perfectly plastic behavior, the indentation response is completely determined by the Young's modulus (E), yield strength (σ_y), and Poisson's ratio (ν) of the material. A number of dimensionless functions have been proposed using dimensional analysis and FEM computations [113, 114]. Here a new dimensionless expression for indentation on a grooved surface will be formulated as a function of the above-mentioned material parameters.

The load P required for a conical sharp indenter to penetrate a depth h into an elastic perfectly plastic material can be written as

$$P = P(h, E, \nu, \sigma_y, E_i, \nu_i) \quad (7)$$

where E_i and ν_i is the Young's modulus and Poisson's ratio of the indenter respectively. The elastic effects of the indenter and material can be incorporated into a single parameters E^* where

$$E^* = \left[\frac{1-\nu^2}{E} + \frac{1-\nu_i^2}{E_i} \right] \quad (8)$$

Using (2), Eq. (1) can be rewritten as

$$P = P(h, E^*, \sigma_y) \quad (9)$$

Applying the $\prod$ theorem in dimensional analysis, equation (9) can be transformed as

$$P = \sigma_y h^2 \prod_1 \left(\frac{E^*}{\sigma_y} \right) \quad (10)$$

Figure 2-4(b) shows the typical indentation response of an elasto-plastic material in terms of the load, P, required to penetrate depth, h. The loading curve follows the Kick's law [115, 116] $P = Ch^2$ for sharp indentation. The parameter C, also known as the curvature of the loading curve can be expressed using Eq. (10) as

$$C = \frac{P}{h^2} = \sigma_y \prod_1 \left(\frac{E^*}{\sigma_y} \right) \quad (11)$$

where $\prod_1$ is the dimensionless function used in Eq. 10. For simplicity, here we assume the indentation size effect can be ignored, and consequently C is a material constant. Equation (11)

and FEM computations would be used to determine the analytical expression for C as a function of the elasto-plastic parameters.

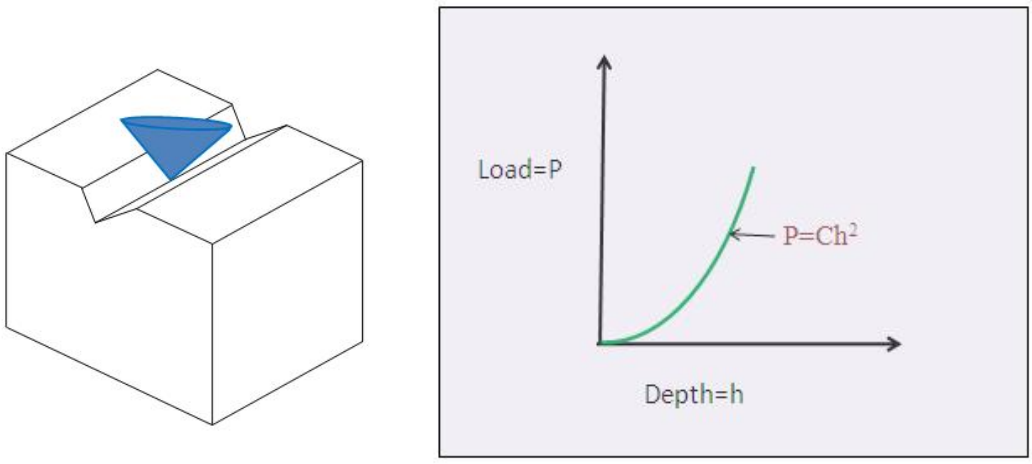

(a) **(b)**

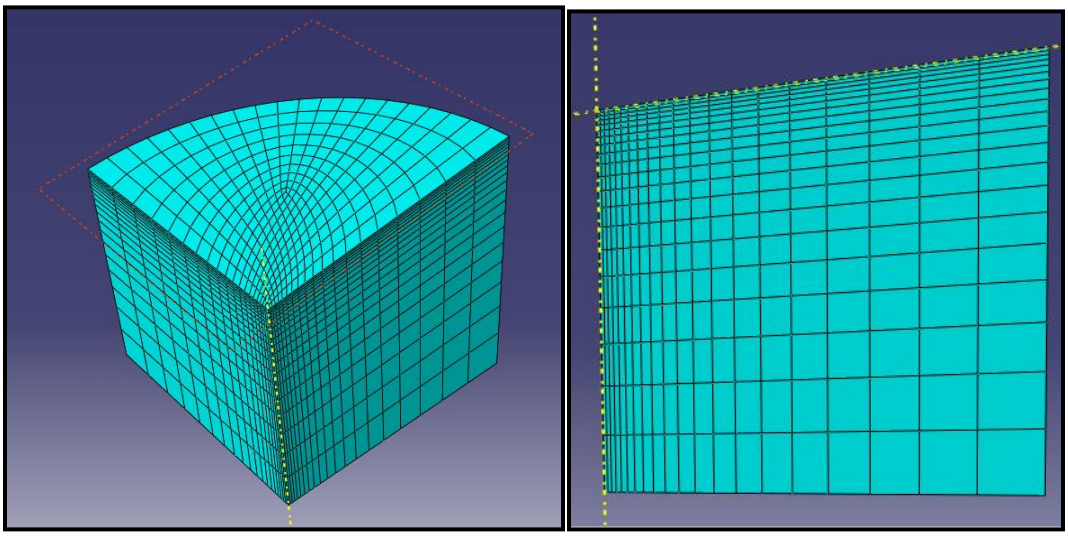

(c) **(d)**

Figure 2-4 (a) A schematic drawing of the process of indenting on a grooved surface. (b) Typical loading response in the form of a load (*P*) versus depth (*h*) curve obtained after indenting an elastic plastic material. (c) Isometric view of the FEM mesh design, where inherent symmetry of the geometries enabled the ¼ model construction. (d) Front view of the FEM mesh showing the inclined surface of the specimen being indented.

2.4.2 Computational Model

General purpose FEM package ABAQUS (SIMULIA, Providence, RI, USA) was used to construct full 3 dimensional model of the indented material and the indenter and to perform the computations. The specimen was modeled using 6000 eight noded linear brick elements and mesh biasing was done to ensure a finer mesh close to the region where the indenter makes contact with the specimen as can be seen in Fig. 2-4(c) and 2-4(d). Minimum number of elements in contact with the indenter at the maximum load was not less than 20 in each FEM computation. The mesh was determined to be insensitive to the far field boundary conditions and satisfied the convergence criteria. Indenting on a grooved surface was found to be self-similar in that for all combinations of material properties the curvature of the *P-h* curve was constant with the depth of penetration of the indenter. The diamond indenter was modeled as a rigid body cone with half included angle of 70.3^{o} and the contact between the indenter and the specimen was specified as frictionless.

2.4.3 Computational Results

Large deformation FEM computations were performed using the model described in Section 2.4.2. A total of 12 different cases of material properties which span σ_y from 30 to 3000 MPa and E from 10 to 210 GPa were input to the model in order to extract C. Using the obtained values of C from the FEM simulations, the dimensionless function (C/σ_y) was plotted as a function of ln (E^*/σ_y) with diamond symbols for indentation results on a grooved surface as can be seen in Fig. 2-5. This specific functional form was inspired by what was used in literature [113] for the case of indenting on a flat surface with a conical tip in which (C/σ_y) was found to have a cubic dependence on the natural logarithm of E^*/σ_y.

$$\frac{C}{\sigma_y} = -1.131\left[\ln(\frac{E^*}{\sigma_y})\right]^3 + 13.635\left[\ln(\frac{E^*}{\sigma_y})\right]^2 - 30.594\left[\ln(\frac{E^*}{\sigma_y})\right] + 29.267 \qquad (12)$$

This relationship of indenting on a flat surface is also plotted with square symbols in Fig. 2-5. We repeated the computational study of indenting on a flat surface and found our results to be in close fit to the above equation.

It can be concluded by looking at the figure that indenting with a 70.3^0 conical indenter on a grooved surface made by prior sliding offers more resistance then indenting on a flat surface. Using the parametric FEM simulation results (shown with diamond symbols) in Fig. 2-5 and Eq. (11), the dimensionless function for indenting on a grooved surface was found to be

$$\prod_1 = \frac{C}{\sigma_y} = -2.208\left[\ln(\frac{E^*}{\sigma_y})\right]^3 + 29.45\left[\ln(\frac{E^*}{\sigma_y})\right]^2 - 81.21\left[\ln(\frac{E^*}{\sigma_y})\right] + 92.53 \quad (13)$$

In order to extract the deformation induced flow stress changes, the value of C would be ascertained from the P-h response obtained from indenting on the tracks and Eq. (7) would be used to extract the flow strength for all the passes and different specimens.

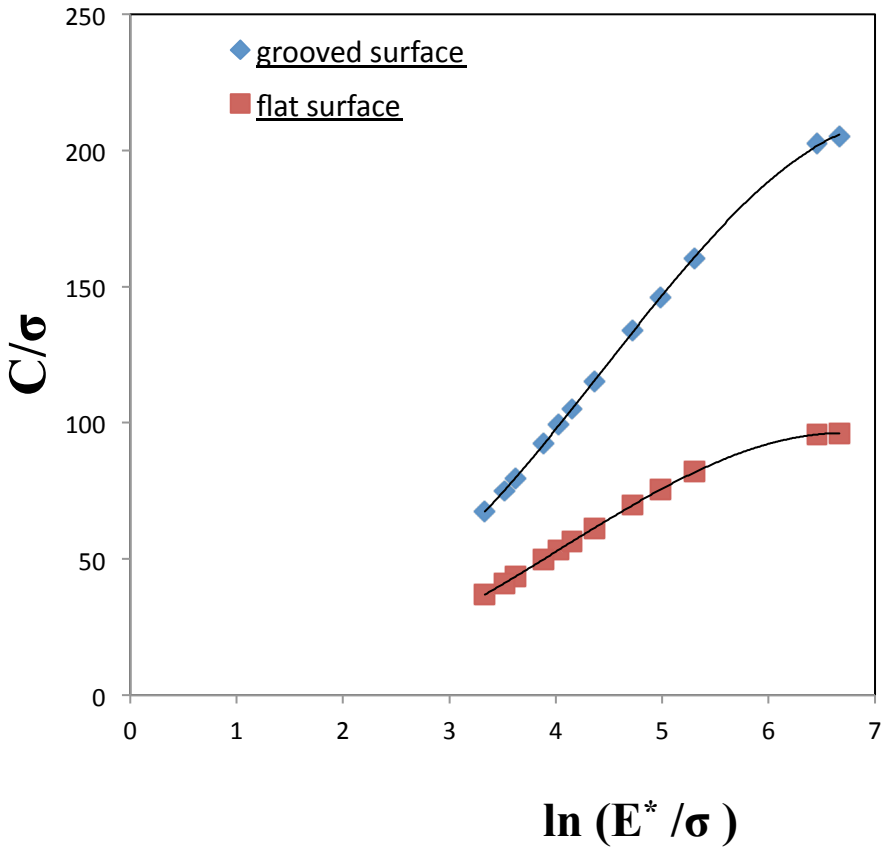

Figure 2-5. Dimensionless function $\prod_1$= (C/σ_y) as a function of ln (E^*/σ_y) obtained from FEM simulations of indenting on a (a) grooved and (b) flat surface using a conical indenter with half included angle of 70.3°.

Chapter 3

Stable Fatigue Crack Growth and Fracture Toughness of Nano-Twinned (NT) Cu.

3.1 Introduction

Recent studies have shown that nano twinned copper (NT Cu) exhibits a combination of high strength and moderate ductility. However, most engineering and structural applications would also require materials to have superior fracture toughness and prolonged subcritical fatigue crack growth life. The current study investigates the effect of twin density on the crack initiation toughness and stable fatigue crack propagation characteristics of NT Cu with an average grain size of 450 nm. Specifically, we examine the effects of tailored density of nano twins, incorporated into a fixed grain size of ultra-fine-grained copper, on the onset and progression of subcritical fracture under quasi-static and cyclic loading at room temperature. It is shown here that processing-induced, initially coherent nanoscale twins in ultra-fine-grained copper lead to a significant improvement in damage tolerance under conditions of plane stress. This work strongly suggests that an increase in twin density while keeping the grain size constant in NT Cu is beneficial not only for desirable combinations of strength and ductility but also for enhancing damage tolerance characteristics such as fracture toughness, threshold stress intensity factor range for fatigue fracture, and subcritical fatigue crack growth life. Possible mechanistic

origins of these trends are discussed along with issues and challenges in the study of damage tolerance in NT Cu.

3.2 Results

3.2.1 Tensile Properties

The tensile properties of all the specimens were measured at room temperature, and they are listed in Table 1. It is seen that increasing twin density leads to high values of strength without compromising ductility. This is consistent with the previous work done to investigate the effect of twin density on the tensile properties of NT Cu.

Specimen	$\sigma_{0.2}$ (MPa)	σ_{ts} (MPa)	ε_f (%)	K_{IC} $(MPa\sqrt{m})$ from P-δ method	K_{IC} $(MPa\sqrt{m})$ from da/dN vs ΔK curve
UFG Cu	340 ± 30	430	12	12.9	14.9
LDNT Cu	500 ± 50	530	2.7	14.8	17.5
MDNT Cu	720 ± 50	820	5.6	17.2	22.3

Table 3-1: Values of yield strength, tensile strength, ductility and fracture toughness for MDNT, LDNT and UFG specimens. It can be seen that MDNT Cu shows the highest value of yield strength and tensile strength without a significant loss of ductility. Values of fracture toughness obtained from the $P-\delta$ curve and from the da/dN versus ΔK curves indicate that increasing twin density leads to increased fracture toughness values.

3.2.2 Fracture Toughness Estimation from P-δ Curve

Figure 3-1 shows a plot of engineering stress versus displacement for all the specimens. To normalize the force variations due to sample thickness variations, nominal engineering stress (P/Bw) is used instead of the loading force P. Table 1 shows the values of the fracture toughness obtained from the $P-\delta$ curves illustrating that decreasing twin lamellae spacing leads to enhanced fracture toughness.

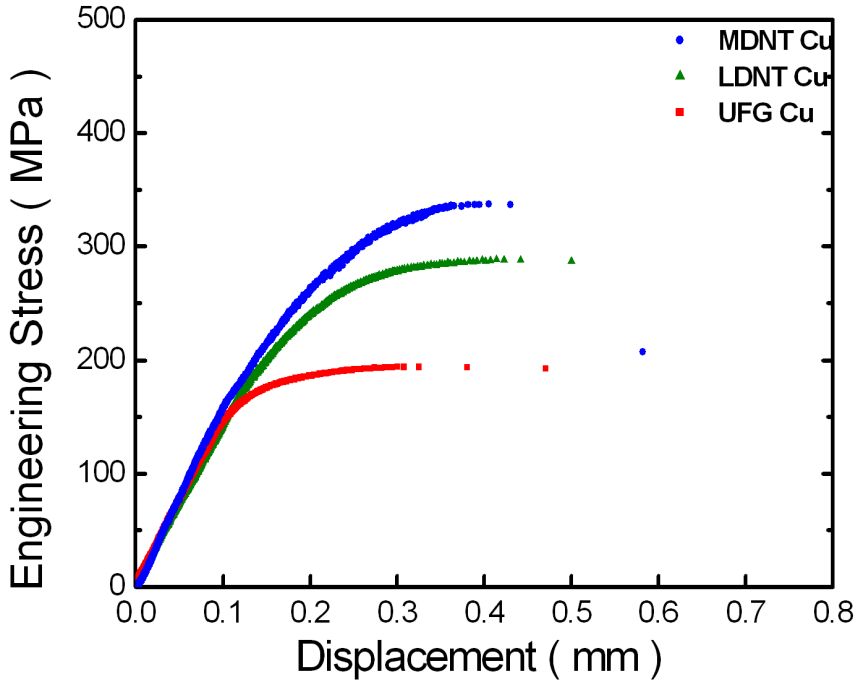

Figure 3-1: Engineering stress versus displacement plot of MDNT, LDNT and UFG specimens which were pre-cracked to 1.5 mm prior to the fracture experiment.

3.2.3 Stable Fatigue Crack Propagation

Figure 3-2 shows a plot of change in crack length versus the number of cycles when multiple load-controlled cycles with an initial ΔK of 6 MPa$\sqrt{m}$are imposed on the specimens. This leads to the inference that a decrease in twin lamellar spacing leads to smaller crack length change over the full range of cycles. In addition, the rate of increase of crack length with respect to the number of cycles, as can be seen from the slope of the curves at any point, is also smaller in the case of MDNT specimen. Thus increasing the twin density appears to lead to an improvement in fatigue life under stable crack propagation.

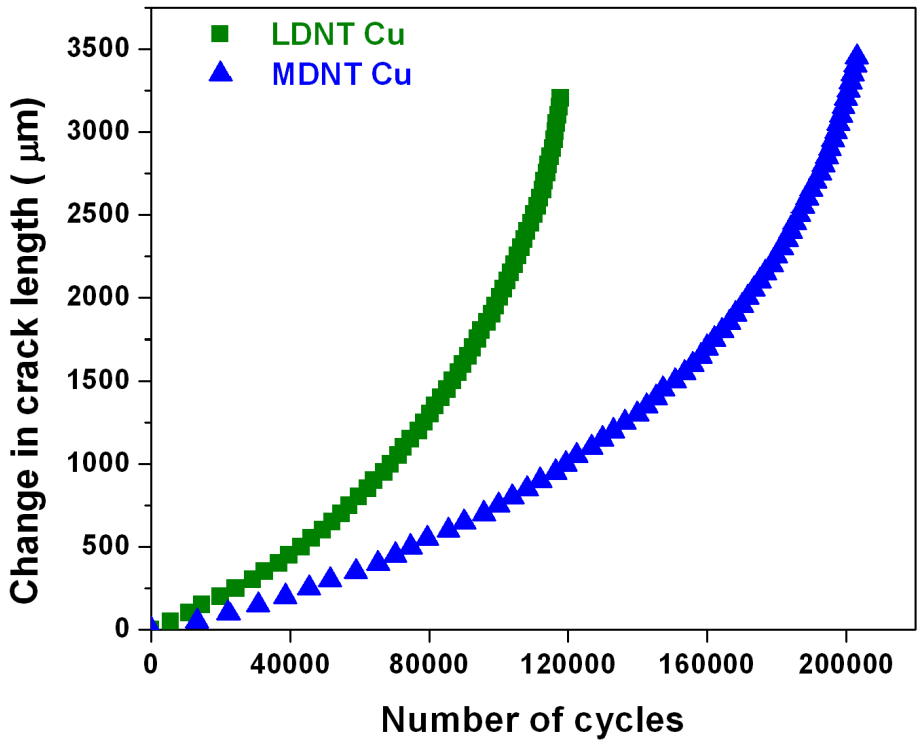

Figure 3-2: A plot of change in crack length versus the number of cycles with an initial ΔK of 6 MPa$\sqrt{\text{m}}$ for the MDNT and LDNT specimens demonstrating that increasing twin density leads to a decreased rate of fatigue crack growth.

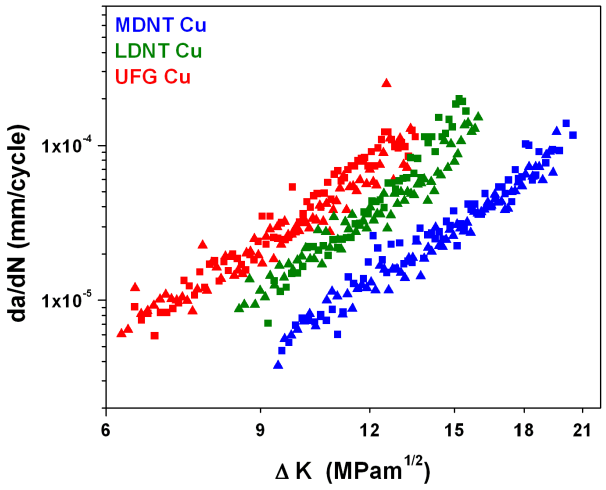

(a)

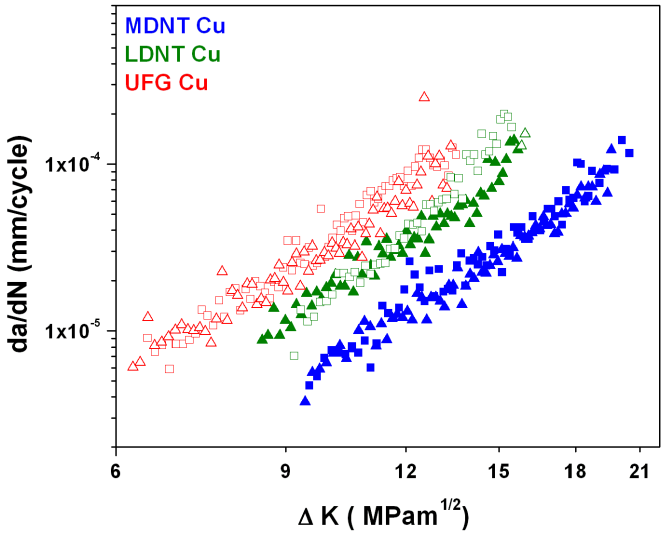

(b)

Figure 3-3 (a) Variation of da/dN versus $\log_{10}\Delta K$ showing that increasing twin density leads to the highest value of fatigue transition threshold ΔK_T and lowest crack growth rates for all values of ΔK. The validity condition for small scale yielding is taken to be (a, w-a) $\geq 15r_p$ for use of LEFM to characterize crack growth using ΔK. (b) Illustration on how some data points in (a) become invalid (marked by open symbols in (b)) if the small scale yielding condition is made stricter to require that (a, w-a) $\geq 25r_p$.

Using a less stringent condition than prescribed in ASTM 399 [70] for the validity of small-scale yielding, i.e., (a, w-a) > 15r_p, Fig. 3-3(a) shows the variation of fatigue crack growth rate $\log_{10}(da/dN)$ vs. $\log_{10}\Delta K$. If we define the fatigue transition threshold ΔK_T as the value of stress intensity factor range at which the crack growth transitions from Stage I (near threshold mechanisms of crack growth) to Stage II (Paris regime [26]) of subcritical crack growth, then it can be seen from the plot that with an increase in twin density the fatigue transition threshold is increased. The high twin density specimen also displays the smallest crack growth rate at any value of ΔK. Thus introduction of nanoscale twins appears to impart improved fatigue crack growth life in UFG Cu. This behavior of nano-twinned metals is in distinct contrast to prior results on nano-grained metals that show a higher endurance limit but poorer resistance to fatigue crack growth upon grain refinement [27, 28]. However in our experiments MDNT Cu shows higher yield strength and thus greater crack initiation resistance as well as a longer stable crack growth life. Figure 3-3(b) shows that some of the data points become invalid if the stricter validity condition for small-scale yielding required in the ASTM E-399 standard is imposed for the use of K in characterizing fatigue crack growth, which is (a, w-a) > 25r_p from Eq. 5. However, even after imposing this stricter condition, the data obtained for both the specimens of MDNT Cu remain valid and for LDNT Cu data one specimen out of two continues to be valid. For UFG Cu, the data turns out to be invalid. However, since UFG Cu has the lowest yield strength, and hence the largest plastic zone size at any given K, among the three conditions employed in this study, any effect of plasticity would be expected to be more "forgiving" for fatigue fracture in that UFG Cu would be expected to result in slower crack growth rates if violation of SSY were to alter the trends. With such an expectation, it is evident even with the

stricter specimen size requirement for valid use of stress intensity factor in Fig. 3-3(b) that increasing twin density leads to an increase in resistance to fatigue crack growth.

Fracture toughness can also be estimated using the value of K_{max} at which fatigue crack growth rapidly transitions from subcritical to catastrophic failure. Specifically, this transition is taken as the maximum stress intensity factor corresponding to the ΔK, at which there is a rapid rise in the slope of the $\log_{10}(da/dN)$ vs. $\log_{10}\Delta K$ curve immediately preceding catastrophic fracture in Fig. 3-3(a). (Note that $K_{max} = \Delta K/(1-R)$.) Table 3-1 lists the relative fracture toughness estimates so obtained for the three materials studied in this work. Fracture toughness estimated in this way also shows the highest crack initiation toughness for the largest density of nano twins, fully consistent with the estimates obtained from the $P–\delta$ curves in the quasi-static fracture toughness tests described earlier. Thus increasing the twin density in UFG Cu appears to render it more defect-tolerant.

3.3 Discussion

Many studies on conventional microcrystalline materials have shown that decreasing the grain size leads to a lower value of fatigue crack growth threshold ΔK_{th}, lower fatigue crack growth transition threshold ΔK_T and higher nominal driving force for fatigue crack growth close to the threshold regime[26] [27]. In the present study the grain size was kept constant for all specimens but another structural length scale i.e. the nano-twin lamellar spacing, was varied. The impediment to dislocation motion due to the presence of twin boundaries is seen to result in

higher strength; but the nano twins also lead to higher values of ΔK_T (Fig. 3-4), lower crack growth rate, and higher fracture toughness.

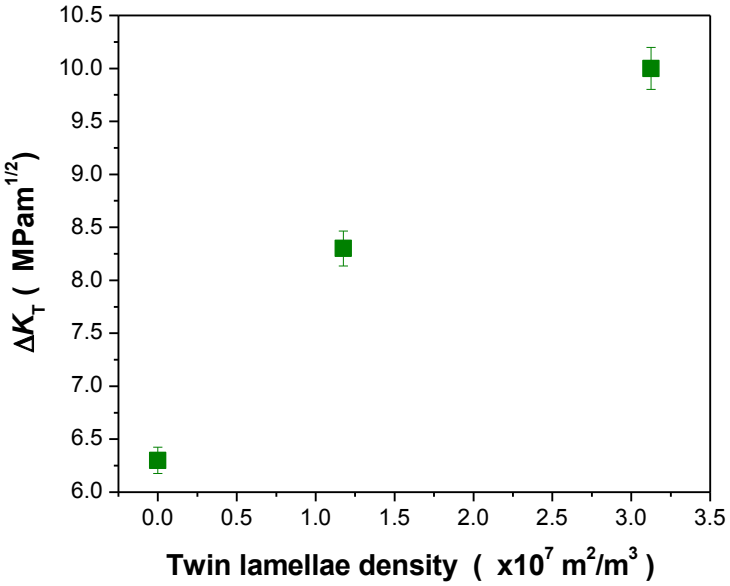

Figure 3-4: Variation of the fatigue crack growth transition threshold (ΔK_T) as a function of twin density. Increasing twin density is beneficial for damage tolerance as $\Delta K_T$is increased with a decrease in twin lamellar spacing.

It is well known from studies of microcrystalline materials that fatigue crack growth rates close to the threshold regime are very sensitive to the microstructure, loading ratio and environment [26]. During stable near-threshold fatigue crack growth in microcrystalline metals and alloys, the plastic zone size is typically smaller than the grain size and crack growth occurs predominantly by planar slip in the direction of the primary slip system (so-called Stage I crack growth). Since such crack growth occurs by single shear, the crack can continue to propagate locally along the primary slip plane within the grain, away from the nominal mode I growth

plane, until deflected by an obstacle such as a high-angle grain boundary. As can be seen in [28] a larger grain size leads to higher tortuosity as the crack continues along a non-mode I deflected path. Higher tortuosity in crack growth leads to smaller driving force for crack advance and smaller effective crack growth rate [26]. Besides, larger grain size can promote bigger surface asperities which also contribute to enhanced crack closure; this results in reduced crack growth rates [26, 69] at a given nominal value of stress intensity factor range.

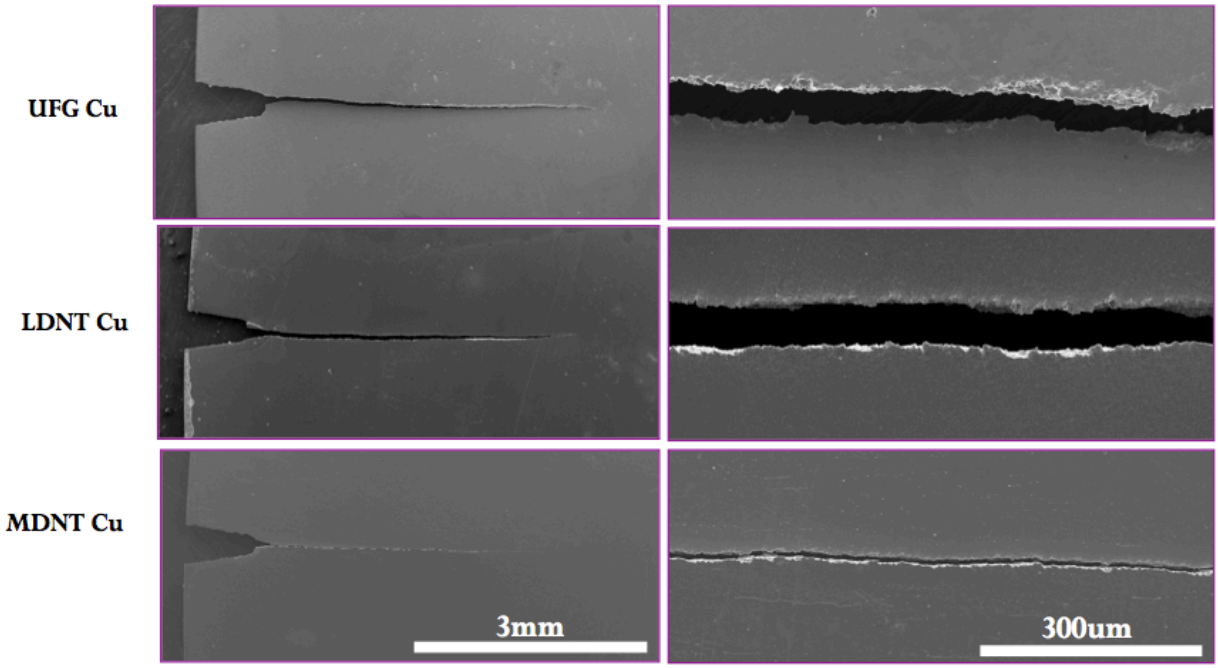

Figure 3-5: SEM images of UFG (a), LDNT (b) and MDNT Cu (c) subjected to load controlled cyclic loading at a frequency of 10 Hz. (d), (e) and (f) are higher magnification images of (a), (b) and (c) respectively. The three crack profiles are similar in terms of crack path tortuosity, deflection angle and surface roughness showing that these parameters are not influenced by the twin density (given that the grain size is essentially the same for the three cases).

In the present study the grain size was kept constant in all the materials but the twin density was varied. The fact, that increasing the twin density leads to an improvement in fatigue crack growth life, may be better understood in terms of the following arguments. First, grain boundaries and twin boundaries influence subcritical fatigue crack growth in Stage I in different ways due to the strong dependence of crack propagation on crystallography. The twin boundaries inside each grain are parallel to one another and for face centered cubic (FCC) metals the twin boundaries are also the (111) slip planes. Due to the strong plasticity anisotropy, shear deformation parallel to the twin boundaries is much easier than that in slip systems that have slip planes not parallel to the twin planes [6, 47]. This crystallographic preference to move along a single slip plane would not be seen in UFG Cu without twins in which the crack can move along all slip systems (where the direction within each grain along the crack path would be determined by the local driving force). In nano-twinned Cu, a Stage I fatigue crack would likely be parallel to the twinning planes within a grain, since twin boundaries unlike grain boundaries cannot veer the propagating crack back to the direction perpendicular to the loading direction (until the crack hit the next grain with a different twin boundary orientation). Thus the crack path tortuosity, size of the crack surface asperities and mismatch between the crack faces would be mainly influenced by the grain size but not the twin lamellae spacing. SEM images of the crack profiles also reveal this, as can be seen in Fig. 3-5, where the crack profiles of all the specimens bear close resemblance to each other in terms of crack path tortuosity, surface roughness and deflection angle on account of having similar grain sizes. Secondly, since decreasing twin lamellar spacing improves fatigue life, it implies that strength alone as a parameter could be beneficial for stable crack growth life if other parameters are kept fixed for the present materials. Indeed, higher yield strength leads to a lower value of the maximum crack tip opening displacement. The value of the maximum or

instantaneous crack tip opening displacement (CTOD) at K = 6MPa√m for the 3 specimens can be estimated using the formula:

$$CTOD = d_n \frac{K_I^2}{E\sigma_y} \quad (7)$$

The value of d_n varies from 0.3 to 0.8 as n changes from 3 to 13 [117]. It is found that CTOD values for the MDNT, LDNT and UFG specimens are estimated to be 250 nm, 360 nm and 528 nm respectively when d_n is taken as 0.6. The previous discussion showed that the height of the microstructural surface asperities depends on the grain size and not on the twin density and hence it can be deduced that a higher twin density would induce relatively more roughness induced crack closure due to a smaller value of CTOD leading to better stable crack growth life under cyclic loading. Some earlier studies that formulated empirical models to ascertain the fatigue crack growth threshold and fatigue transition threshold as a function of mechanical properties also support this observation. For example, models proposed by Donahue *et al.* [118] suggest that the threshold for the beginning of perceptible crack growth occurs when the crack tip opening displacement becomes comparable to the critical microstructural length scale.

$$\Delta K_{th} \propto \sqrt{\sigma_y E l^*} \quad (8)$$

where l^* is the relevant microstructural length scale. It has been shown by Yoder *et al.* [119] that cyclic plastic zone size instead of the CTOD needs to reach a critical microstructural length scale in order to reach the transition threshold leading to the formulation

$$\Delta K_T \propto \sigma_y \sqrt{l^*} \quad (9)$$

Proceeding on the same lines, threshold is also postulated to be attained when the shear stress needed to nucleate and move a dislocation reaches a critical value [120]:

$$\Delta K_{\mathbf{th}} \propto \tau\sqrt{b} \tag{10}$$

where *b* is the magnitude of the Burgers vector. Although all these formulations do not exactly capture all the complexities of the structural variations possible, they underscore the notion that threshold decreases with a decrease in structural length scale but increases with an increase in strength. In the present study the grain size is kept constant for all the cases, however the strength increases with an increase in twin density. These models capture our result of the fatigue transition threshold increasing with twin density as the grain size and not the twin lamellar thickness is the critical microstructural length scale.

For Stage II fatigue crack growth, the crack advances by a process of duplex slip along two slip systems [67]. This results in a planar (Mode I) crack advance normal to the loading axis. The growth in Stage II is not found to be microstructure sensitive unlike Stage I. Unlike the faceted fracture surface in Stage I, the fracture surface in Stage II normally shows striations. The crack advance is shown to occur via crack tip blunting and the striations manifest the amount of crack extension in one cycle in most ductile FCC metals. In the current study, no obvious striations were observed in all specimens tested. However as can be seen in Fig. 3-3, the rate of crack growth is lowest for MDNT Cu and increases with a decrease in twin density.

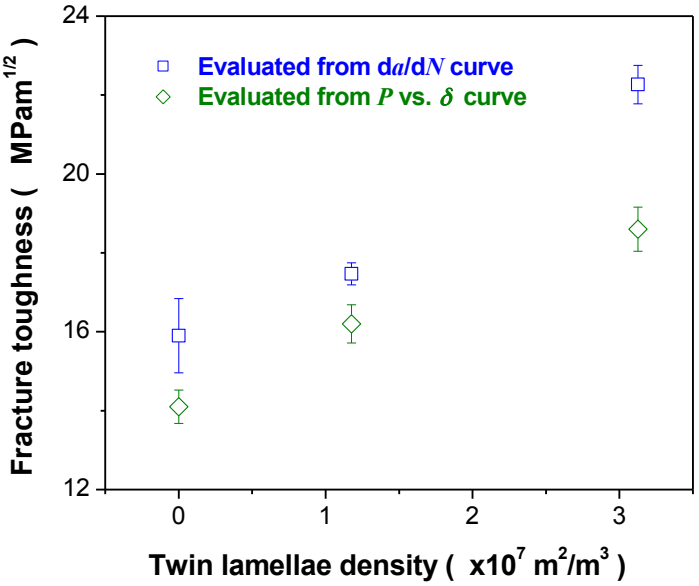

Figure 3-6: Variation of fracture toughness with changes in twin density. The figure depicts the effect of twin density (or twin lamellar spacing) on the fracture toughness obtained both from the *P*-δ experiments and the crack propagation experiment, respectively. Increasing twin density enhances the fracture toughness of nanotwinned copper.

Subsequent to Stage II fatigue crack growth, the crack advances rapidly and the specimens are expected to fail in a ductile manner by void nucleation and growth. It can be seen in Fig. 3-6 that fracture toughness of Cu is enhanced by decreasing the twin lamellar spacing. However, an opposite trend has been observed in earlier studies for nano grained materials where grain refinement leads to poor damage tolerance and diminished values of fracture toughness [31, 80]. Strain energy accommodation by plastic work is limited in nano grained materials due to curtailed dislocation activity which is also the reason behind the poor ductility of NG materials. In displacement controlled testing, high stress concentration at the grain boundaries arises due to limited plasticity for NG metals, which makes the process of void nucleation at the

grain boundaries even more severe. However, increasing twin density can lead to enhanced plastic strain accommodation due to the high area of twin boundaries which are principal sites for accumulation and pile-up of partial dislocations. This in turn could contribute to enhanced values of fracture toughness as has been observed in the current study.

3.4 Conclusion

This work reveals for the first time that high twin density in ultra-fine-grained copper provides a unique combination of strength, ductility, fracture initiation resistance and damage-tolerance during stable fatigue crack growth. The fracture toughness values show marked improvement with the introduction of nano-twins. During fatigue crack growth, grain and twin refinement are different mechanistic processes in terms of their influence on crack path tortuosity and crack surface roughness because twin planes are also slip planes in FCC metals. This suggests that Stage I fatigue crack propagation is likely to occur parallel to the twin planes within each grain along the crack path and thus these intra-grain twin planes, unlike grain boundaries, can more easily facilitate Stage I, serrated (and locally non-mode I) fracture trajectory. Electron microscopy investigations would be helpful to further confirm these inferences. However our study has shown that MDNT Cu which has the highest strength also showed relatively the best fatigue crack growth resistance. On the other hand, UFG Cu with essentially no nano twins showed the poorest plane stress fatigue initiation toughness and sub-critical fatigue crack growth response among the three materials studied here. In spite of their unique combination of properties, it is challenging at this time to produce homogeneously nano-twinned Cu in bulk which is essential to employ it in any structural applications. It is also not an easy task to

introduce nano twins in many other important structural materials. Further progresses in processing methods would help exploit the beneficial damage-tolerant properties identified in this work for metals containing coherent nano-scale twins.

Chapter 4

Deformation Evolution of Nano-Twinned (NT) Cu under Repeated Frictional Sliding.

4.1 Introduction

Nano-twinned metals have the potential for use as structural materials by virtue of having a combination of high strength and reasonable ductility. In the current study the tribological response of nano-twinned materials has been characterized under conditions of repeated frictional sliding contact with a diamond indenter. Pure ultra-fine-grained copper specimens of the same grain size (~ 450 nm), but with three different structural conditions involving high, medium and negligible nano-twin density, were studied. The effects of twin density and number of repetitions of sliding cycles on the evolution of frictional coefficient and material pile up around the diamond indenter were studied quantitatively using depth-sensing instrumented sliding indentation. Cross-sectional focused ion beam (FIB) and scanning electron microscopy (SEM) observations were used to systematically monitor deformation-induced structural changes as a function of the number of frictional sliding passes. Nano indentation tests on the sliding tracks coupled with large-deformation finite element modeling (FEM) simulations were used to assess local gradients in mechanical properties and deformation around the indenter track. The results indicate that friction evolution as well as local mechanical response is more strongly influenced by local structure evolution during repeated sliding than by the initial microstructure. An increase in twin density was shown to result in smaller pile up height and friction coefficient.

Comparing to low density nano-twinned samples, high density nano-twinned copper showed significantly higher resistance to surface damage and structural changes, after the initial scratch using a nanoindenter. However with an increase in the number of sliding passes, friction coefficient and rate of increase of pile up for all specimens acquire a steady value which does not change significantly in subsequent scratch passes. The frictional sliding experiments also lead to the striking result that Cu specimens with both high and low density of nano twins eventually converge to a similar microstructure underneath the indenter after repeated tribological deformation. This trend strongly mirrors the well-known steady-state response of microcrystalline copper to cyclic loading. General perspectives on contact fatigue response of nano-twinned copper are developed on the basis of these new findings.

4.2 Results

4.2.1 Friction Coefficient

Figure 4-1 shows the evolution of friction coefficient at a normal indentation load of 500mN, as a function of the number of unidirectional scratch passes in all the specimens. It can be seen that the total friction coefficient decreases as the number of sliding passes increase. A 'steady-state' friction coefficient is reached after approximately 80 passes. It is also evident from the figure that increasing the twin density leads to a lower value of total friction coefficient.

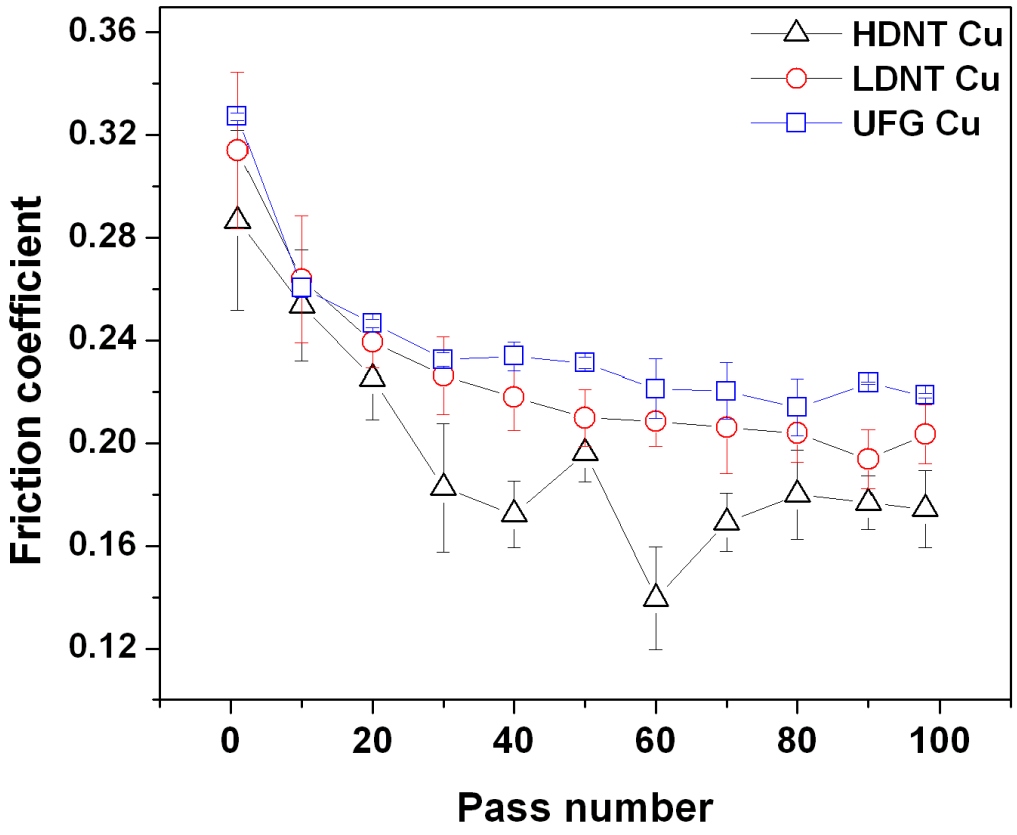

Figure 4-1. Total friction coefficient as a function of sliding contact pass numbers or cycles for HDNT, LDNT and UFG Cu. The friction coefficient decreases with increasing passes and eventually reaches a plateau value for each case. The friction coefficient deceases with an increase in twin density.

4.2.2 Pile-up Height

The ploughing of the indenter over the specimens leads to a pile up of material around the scratch groove. From the instrumented depth-sensing frictional sliding experiments, the height of the pile up as a measure of deformation and damage is plotted as a function of pass number in Fig. 4-2. It can be clearly seen that the additional pile up height per each pass versus the pass number decreases for all the specimens and eventually reaches a constant rate after about 66 passes. It can be inferred that HDNT Cu has the lowest pile up for all pass numbers and the pile up increases as the twin density decreases. However, eventually all the specimens show similar rates of pile up height increase per each new sliding pass.

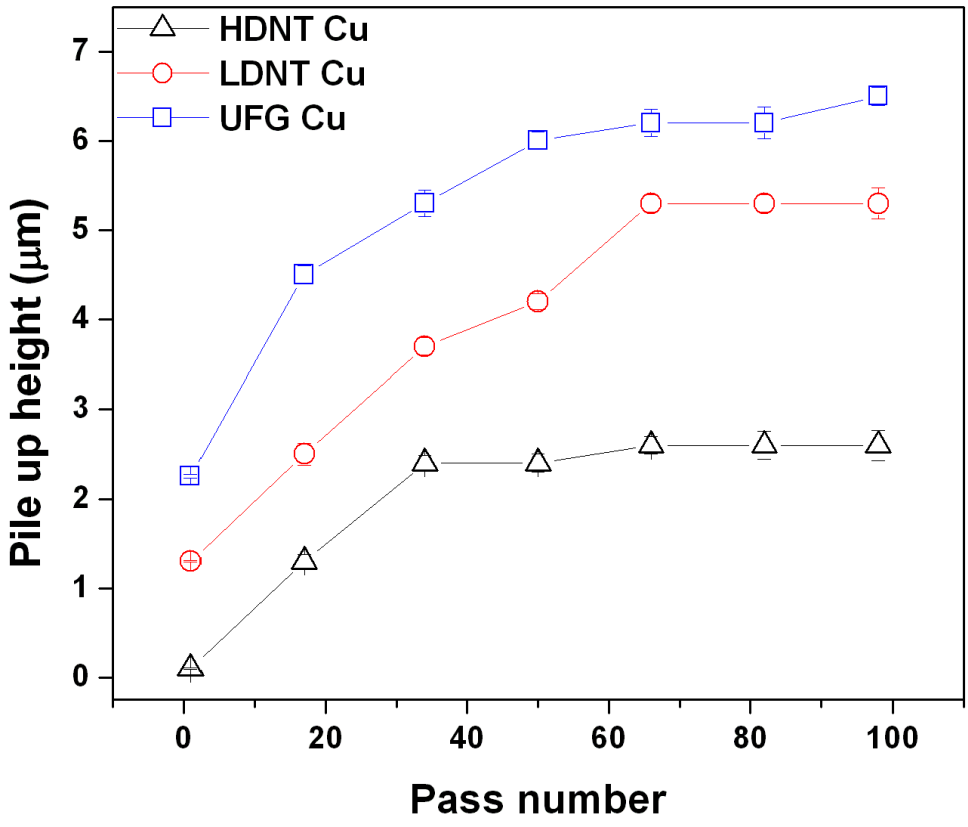

Figure 4-2. Pile up height, for HDNT, LDNT and UFG Cu as a function of sliding pass numbers, showing that pile up is a decreasing function of twin density.

4.2.3 Structural Evolution

The deformation affected zone for all the specimens after the 1st and 82nd passes was examined under an SEM after sectioning with FIB. Figure 4-3 shows a comparison of the deformation-induced microstructure change after the 1st sliding cycle for the HDNT and LDNT Cu specimens. It can be seen that there is a significant microstructure change even after just one pass of contact sliding for the LDNT Cu specimen. The micrograph for the LDNT specimen shows considerable grain refinement close to the surface of the scratch. As the distance beneath the contact surface increases, the changes to microstructure from deformation progressively diminish and the microstructure appears coarser as the depth from the surface increases. Figure 4-4 shows grain size distribution for the LDNT and HDNT specimens after the 1st scratch. The deformation-induced area can be broadly divided into 2 zones (also see Fig 4-9 and 4-10 in later discussion) The first zone for LDNT Cu has an average grain size of about 80 nm and extends up to a depth of 0.7 μm below the surface of the scratch. However the minimum grain size in the first zone goes to as low as 30 nm for a few of the grains. The second zone has an average grain size of 200 nm and extends up to a depth of 2.5 μm below the first zone. No obvious grain size change can be identified for the HDNT Cu specimen after the 1st pass. The original microstructure that comprised equiaxed grains close to the surface and columnar grains with grain size of 400-500 nm having high density of twins is retained (also see Fig 4-10).

As can be seen in Figs. 4-5 and 4-6, repeated sliding over 82 passes leads to drastic microstructure change that is evident from the significant grain size change close to the surface in LDNT Cu. The deformation-affected zone is much larger than that after the 1st pass of sliding. HDNT Cu, with grain size largely unaffected after the 1st pass, exhibits similar final

microstructure compared to LDNT Cu after 82 passes of sliding. The deformed area for both the specimens can be broadly classified into 3 zones beyond which the original microstructure is preserved. The first zone has an average grain size of about 45 nm for LDNT Cu and 40 nm for HDNT Cu and extends up to a depth 1.4 μm below the scratch surface. The smallest grain size in this zone is as low as 15 nm. The second zone has an average grain size of 120 nm and 110 nm for LDNT and HDNT Cu, respectively, and extends up to a depth of 1.8 μm below the first zone. Beyond the second zone, there exists a large region in which LDNT and HDNT Cu have an average grain size of 280 nm and 305 nm, respectively.

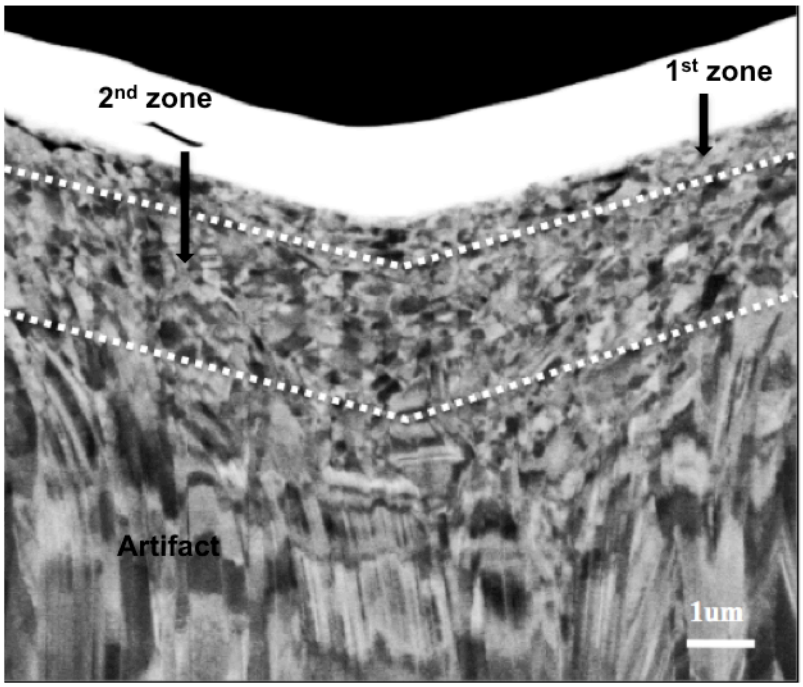

(a)

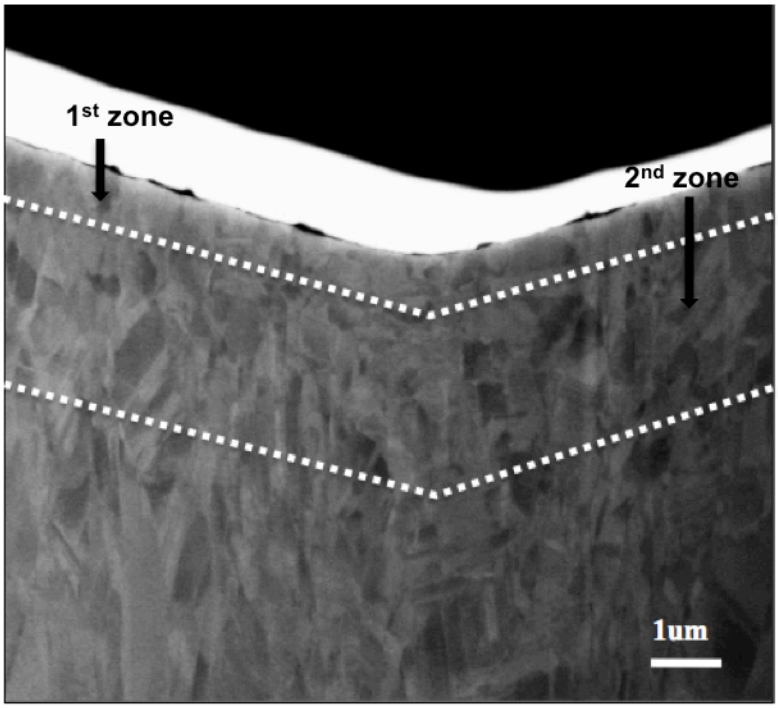

(b)

Figure 4-3. SEM images of (a) LDNT Cu and (b) HDNT Cu specimens showing deformation induced microstructure change in the vicinity of the scratch after 1st pass of frictional contact sliding. Grain refinement near the surface can be observed in LDNT Cu while no apparent change in the grain size for HDNT Cu is observed in spite of the high strains induced by the nano-scratch process.

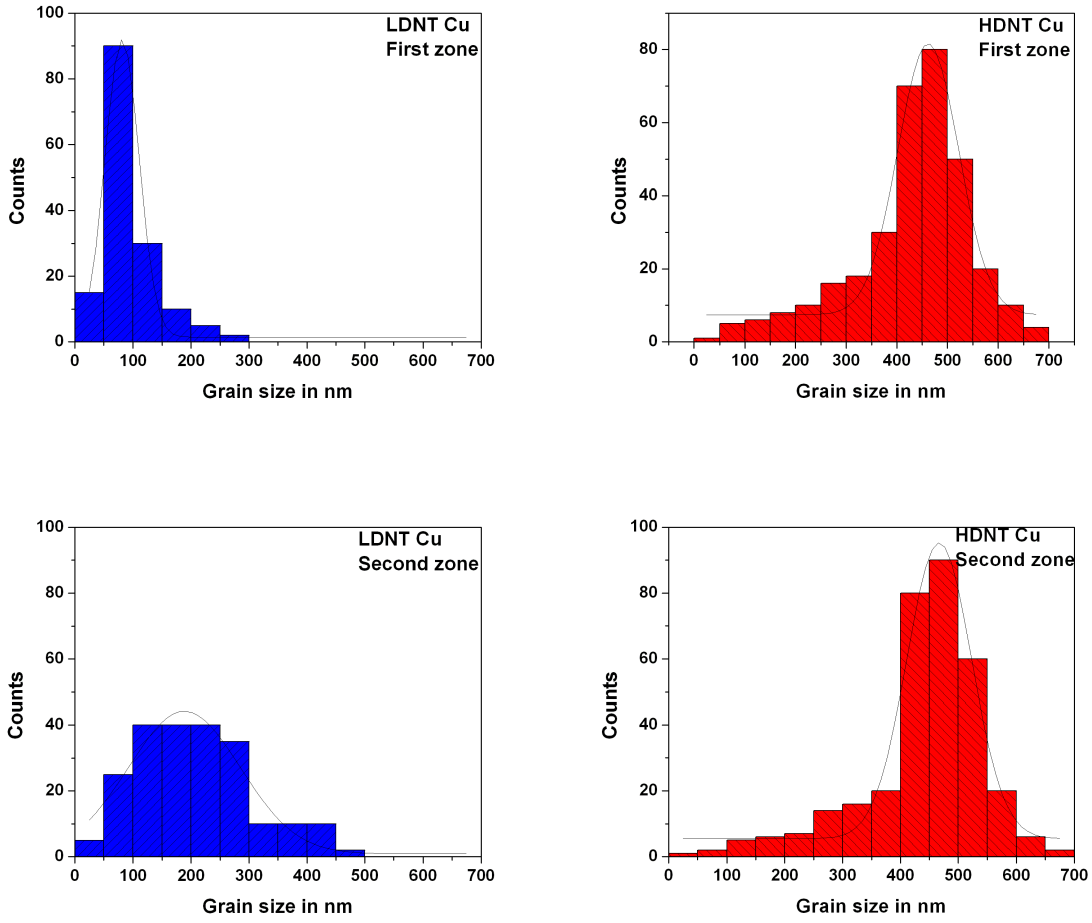

Figure 4-4. Grain size distribution of LDNT and HDNT specimen just below the contact surface of the specimen after the 1st pass of sliding. There is little change in the microstructure below the HDNT specimen. Significant grain refinement is observed in the vicinity of the scratch for the LDNT specimen.

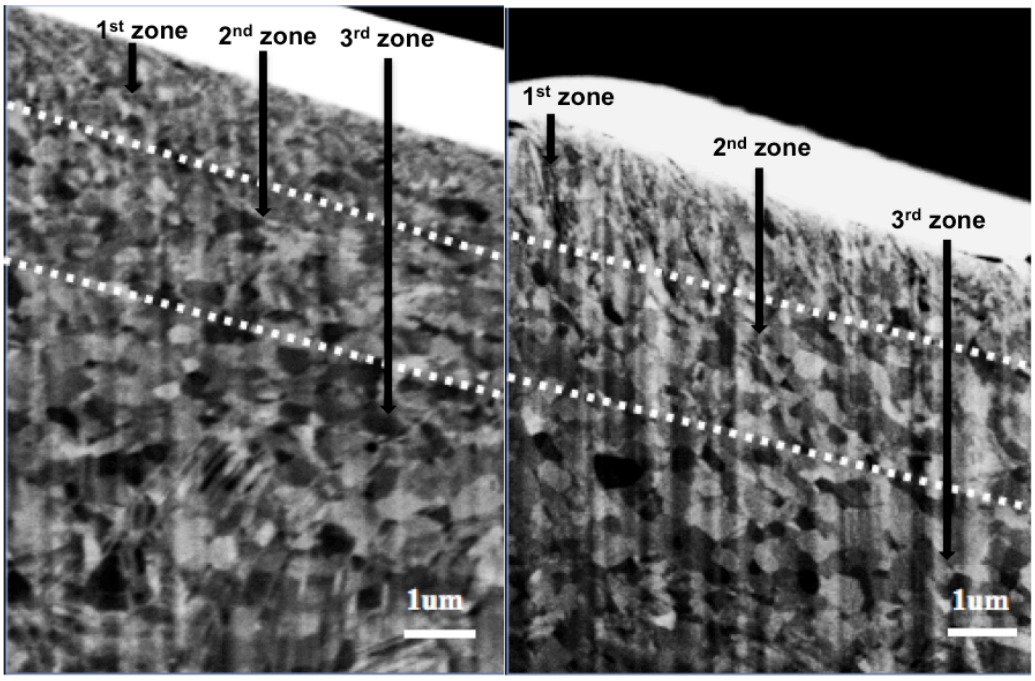

(a) **(b)**

Figure 4-5. Comparison of the SEM images of (a) LDNT Cu and (b) HDNT Cu just below the scratch after 82 passes of sliding showing that after repeated contact sliding both specimens have similar microstructure in the vicinity of the scratch.

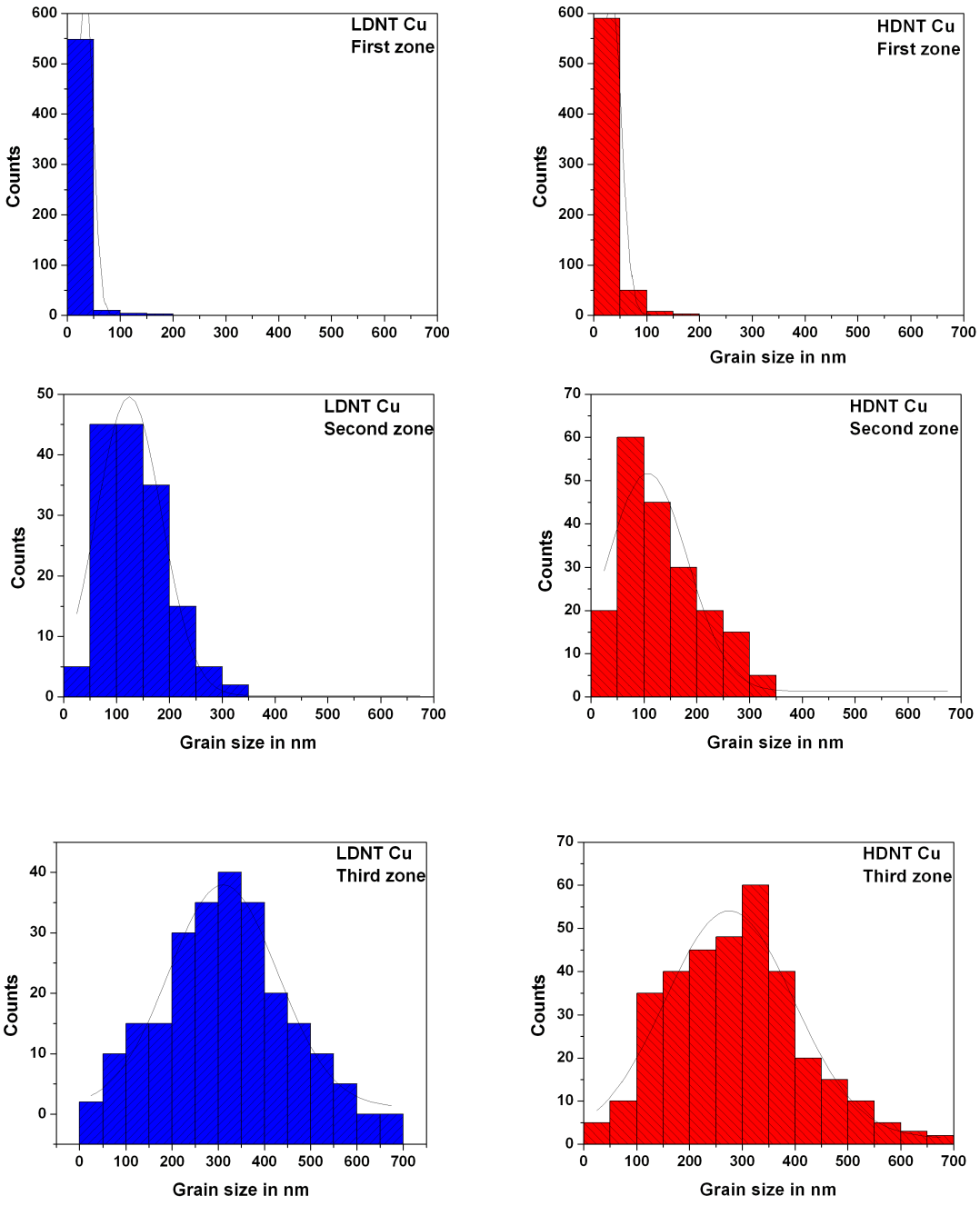

Figure 4-6. Plots of grain size distribution after 82 passes of sliding in the 3 deformation zones in LDNT Cu and HDNT Cu. It can be seen that grain size distribution for both the specimens bear great resemblance in all 3 deformation zones.

4.2.4 Evolution of Flow Strength

Analysis of the load (P) versus displacement (h) curves obtained after indenting on the scratch groove led to the extraction of the yield strength of the HDNT and LDNT Cu as a function of the sliding passes using the procedure described in the Section 2-4. The deformation induced flow strength change in all the specimens was plotted as a function of the number of sliding passes in Fig. 4-7. The evolution of the flow strength in the close vicinity of the scratch surface correlates well with the observed deformation induced microstructure changes shown earlier. It can be seen that HDNT Cu manifests its peak yield strength in the first pass and with an increase in the number of sliding passes the material in the vicinity of the scratch surface softens. LDNT Cu on the other hand displays low strength in the first cycle but undergoes a monotonic increase in flow strength and eventually the flow strength of both HDNT and LDNT Cu converges to a common value.

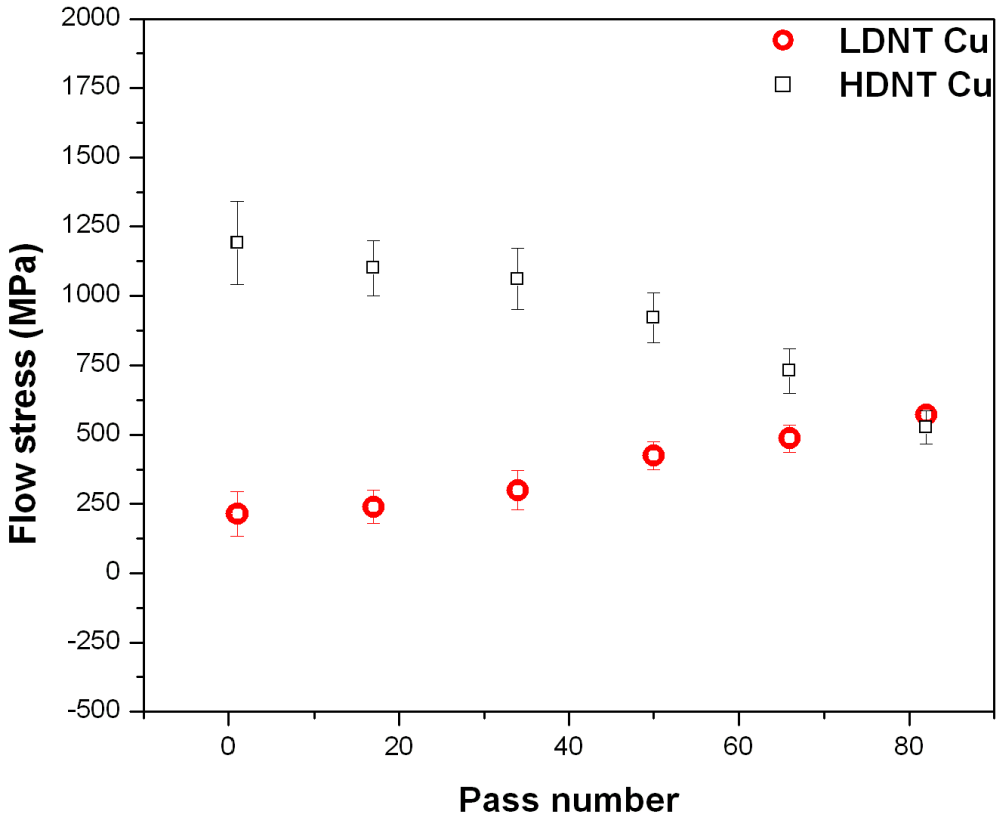

Figure 4-7. Estimated surface flow strength of HDNT and LDNT Cu specimens as a function of sliding passes obtained by nanoindentation within the sliding tracks up to 1 mm deep. LDNT specimen hardens with an increase in the number of sliding cycles as a result of deformation induced microstructure changes whereas HDNT specimen softens. The flow strength close to the surface of the specimens after 82 sliding passes is similar for both specimens.

4.3 Discussion

A wear resistant material should exhibit minimal pile up height after being scratched by the indenter. It can be clearly seen in Fig. 4-2 that an increase in twin density leads to a reduction in pile up height. Besides, the differential change in pile up height versus pass number keeps on diminishing with an increase in pass number. This can be explained by the fact that the indenter would penetrate the material most in the first pass and therefore remove the maximum amount of material. In subsequent passes the indenter makes first contact with a deeper grooved surface and FEM simulations have shown the effective hardness of indenting a grooved surface solely due to the nature of geometric constraints to be significantly higher than that of indenting a flat surface (see Section 2-4). Thus the amount of depth that the indenter penetrates below the scratch in subsequent passes at the same value of the applied load is much less in subsequent passes and this leads to diminishing rate of pile up height increase with respect to the number of passes. Eventually the rate of pile up height change appears to reach a steady state for all the specimens after 82 passes as can be seen in Fig 4-2. This trend is consistent with the repeated contact sliding studies done on stainless steel [121] that showed that the depth of penetration per cycle reaches an almost constant value after multiple cycles after an initially transient regime.

Friction coefficient between two surfaces is a parameter that depends on many factors like elastic modulus, yield strength, strain hardening exponent of materials. In this case, on account of high loads imposed on the indenter while scratching, significant ploughing of material occurs and thus the fracture toughness of the materials would also contribute to friction. Thus friction is a complex function of many independent mechanical properties. Previous studies have tried to

assess the contribution of hardness and grain size in isolation from each other in determining the friction coefficient by varying strength by recourse to cold work and annealing while keeping the grain size values close to each other (average grain size values of 340 and 420 nm respectively) [9]. It has been found that hardness has a stronger effect on friction coefficient and friction coefficient decreases with an increase in strength. The present study is consistent with that observation as the friction coefficient was shown to decrease with an increase in hardness that was in turn controlled by monitoring the twin density.

Repeated contact sliding demands a much more involved explanation of the observed friction coefficient variation with pass number for all the specimens. This is because the harsh environment due to high stresses entails microstructure and properties change that adds more complexity to understanding of the wear process. Previous repeated sliding studies done on ceramics have concluded that friction is determined primarily by two main factors. First is the force required to initiate deformation (this includes plastic deformation and fracture). Second is the force needed to counter the adhesive force that is generated between the diamond tip and the surrounding material [122]. In addition to these two factors, it is evident through the present study that the amount of material ploughed by the indenter can also be an important factor in determining the total friction coefficient as the indenter has to bear the tangential load of moving the ploughed material in front or piling it towards the sides. Indeed the total friction coefficient decreases with pass number as the material ploughed by the indenter (measured by pile up height increase per each pass) keeps on decreasing. Thus after successive passes, we observe constant rate of pile up height increase and a steady friction coefficient. We suspect that this may be because the material underneath the scratch acquires a steady state microstructure that does not

change with subsequent sliding cycles. However, we need to perform greater number of sliding than those in the current study to validate this.

Under sufficiently high loads nano scratch process entails localized high stresses and deformation. Microstructure changes incurred by repeated sliding were reported previously in many studies for microcrystalline metals [92, 94-96]. In the present study microscopic observations of the area below the first scratch for LDNT Cu (Fig. 4-9(a)), reveal that the microstructure refines as far as the grain size is concerned in the first zone and evolves into nanoscale grains. The variation of the strain and strain rate of deformation with an increase in depth below the indenter leads to a gradient in microstructure with the grain size getting coarser with an increase in depth. No apparent grain size changes could be perceived for the case of HDNT Cu specimen after the first pass of sliding (Fig. 4-10(a)). This may be attributed to high density of twin boundaries that curtail grain boundary motion and at the same time are capable of storing significant amount of strain energy by accommodating large number of dislocations along the twin boundaries. Stability of nanotwinned structure in Cu under severe conditions of localized stresses has also been previously reported [82].

In addition to microstructure refinement induced by wear, there have been earlier instances of grain refinement as a consequence of excessive dislocation activity under high imposed strains in processes like cold rolling, equal channel angular pressing (ECAP), surface mechanical attrition treatment (SMAT) and dynamic plastic deformation (DPD) [5, 59, 123]. During these processes grain refinement occurs when dislocations propagate and tangle with each other under the high stress and rearrange spatially forming sub-structures like cells and cell blocks where there is a high concentration of dislocations at the cell walls but the interior is

relatively dislocation free [124-126]. The misorientation between adjacent cell-blocks increase with increasing strain and the average size of the cells become smaller. Thus grain refinement via dislocation processes is achieved when these cell walls eventually transform to high angle boundaries. Grain refinement via initial twin lamellae formation and subsequent dislocation-twin interactions has also been observed [127] in SMAT process in the top surface layer of CG Cu. The minimum size of these grains has been observed to be close to 10 nm. Initial microstructure refinement is proposed to have been taken place by dislocation rearrangements, however with grain refinement dislocation activity is suppressed and deformation is speculated to be occurring via twins at the higher strain rates in the layer close to the surface. Molecular dynamics simulation of the deformation of nanotwinned copper [128] have in addition shown full and partial dislocation emission from the GBs , TB migration (TBM) , partial dislocation– twin boundary interaction and formation of twinning faults as some of the microscopic processes. In addition at higher deformation stages excessive number of dislocations interacting with TBs appear to break most of the TBs. HPT studies on UFG Cu-30wt%Zn done by Wang [129] claim that due to a decrease in SFE of Cu by alloying with zinc, there is an increased propensity of deformation by twinning than dislocation processes leading to the formation of twin lamellae of thickness ~ 13 nm through partial dislocation emission from the GBs. Transmission electron microscopy (TEM) observations [130] have shown that these newly formed GBs serve as sites for emission of partial dislocations and secondary deformation twins are formed and the intersection of these twins and the new GBs lead to the formation of smaller cell blocks within the twin lamellae leading to the microstructure refinement even across the larger dimension of the twin lamellae parallel to the TB. These newly formed TBs are transformed into high angle GBs and grain refinement results after dislocation interaction with the new TBs and possible

grain rotation [131, 132]. In light of the previous studies it is suspected that under the high strain imposed, deformation occurs by twinning in addition to dislocations processes due to the not so high stacking fault energy of copper. Nanotwins have also been observed in the tribolayer in earlier wear studies [98, 99]. Processes such as new twin lamellae formation, dislocation –TB interaction, TB migration, detwinning of TBs and transformation of TBs into high angle grain boundaries could have a major role to play in the deformation similar to what had been observed in earlier wear and SPD studies. Formation of dislocation blocks inside the twin lamellae is also highly probable contributing to grain refinement

After 82 passes, there is significant refinement in LDNT Cu in a much bigger region than after the 1stpass with the grain size progressively increasing with the distance from the surface. There had not been much microstructural change after the 1st pass in HDNT Cu. However after the 82 passes the grain size distribution for HDNT Cu is similar to LDNT Cu as can be seen in Fig 4-5 and 4-6. The minimum grain size is as low as ~15 nm in both the specimens after 82 passes of deformation which is similar to the finest grain size (10nm) obtained after high strain rate SMAT process in copper the 1st pass. The transformation of HDNT and LDNT Cu to a similar microstructure however was feasible only after repeated passes of sliding and not after the 1st pass in spite of the similar imposition of stress beneath the indenter in both the cases. This underscores the significance of repeated contact sliding that makes possible interactions of defects like dislocations and TBs and simultaneous rearrangements such that the final microstructure is dependent solely on the state of stresses and strains and not on the initial twin density. In this process, it is suspected that the nano twinned structure gradually disappears near the contact surface after many repeated sliding passes, since excessive dislocation activities can result in a twin boundary losing its coherency [78].

The effect of the drastic change in the microstructure of the specimens subsequent to repeated sliding is also evident in the strength evolution of the material at the site of the scratch. After the first pass, there is significant grain refinement close to the surface in LDNT Cu. When a 1 μm deep indentation is made (within the grooved scratch scar), the grains near the surface have an average grain size of about 180 nm. The estimated average flow stress in the scratch groove was found to be close to 200 MPa and decreases with an increase in the maximum indentation depth from the surface. This value is what would be expected for the corresponding grain size (~180 nm) in the absence of nanoscale twins that was suspected as elaborated in the previous discussion. Further, the flow stress evolution in LDNT Cu with the number of passes shows that the strength of the material increases with the increase in the number of sliding cycles. This seems logical by the fact that there is increased grain refinement with an increase in the number of sliding cycles.

The flow stress close to the 1st sliding track in HDNT Cu is close to an average of 1 GPa. This is because the region in the vicinity of the scratch has still retained the twinned microstructure as discussed before and has also been subjected to strain hardening. Residual stresses also might be contributing to the high flow strength. It can also be seen in Fig 4-7 that HDNT has high flow stress to begin with, but softens to similar value of flow stress as LDNT Cu after 82 passes of sliding that is close to 670 MPa. The average size of the grains sampled during the 1 um deep indentation in this case was close to 40-50 nm. This is consistent with the observations in the study by [133] in which the flow stress for NG Cu with an average grain size of 54 nm was reported to be 680 MPa. However, the final grain size sampled by the indenter after 82 passes is larger than the initial smallest microstructural length scale of 15nm leading to softening of HDNT Cu.

Fig 4-5 and 4-6 clearly illustrates that repeated frictional sliding after 82 passes leads to a clear zoning of microstructure such that the finally attained microstructure is consistent with the state of stress, strain and strain rate in that zone and is independent of the initial twin density. This observation of materials with different initial microstructures converging eventually to the same strength and microstructures after multiple cycles of contact sliding falls in place with traditional constant strain amplitude fatigue experiments (Fig. 4-8) in which FCC metals with high stacking fault energy but with different loading histories and microstructures attain similar steady state saturation flow strength after multiple strain controlled uniaxial fatigue cycles [65, 66] . This steady state microstructure is independent of the prior loading history and is solely dependent on the temperature, strain rate and specific amplitude and kind of stresses and strains just below the indenter. It has been postulated in earlier studies that this convergence of microstructure is due to the high stacking fault energy of metals that promotes significant amount of cross slip for the formation of a cell structure irrespective of the microstructure before cyclic straining. However based on our observations and previous work on several SPD processes and wear studies on copper, we think that both dislocation processes and twinning mechanisms can operate in copper by because of it having a medium stacking fault energy ($40x10^{-3}J/m^2$). The dominant mechanism would depend on the strain, strain rate and temperature imposed. This is evident in Fig 4-5 where we can see that after 82 passes of sliding there is a gradient in microstructure which is dependent on the strain rate and strain but not on the initial twin density. Pure FCC metals harden or soften to a steady state saturation stress and microstructure under strain-controlled fatigue till failure after an initial transient regime. Apparently the microstructure attained after multiple contact sliding cycles might be steady even after an increase in number of sliding passes similar to strain controlled fatigue**.** The stabilization of the friction coefficient and rate of pile up

height increases also hint towards this. However, we need additional experiments with pass numbers greater than 82 to confirm this hypothesis.

=

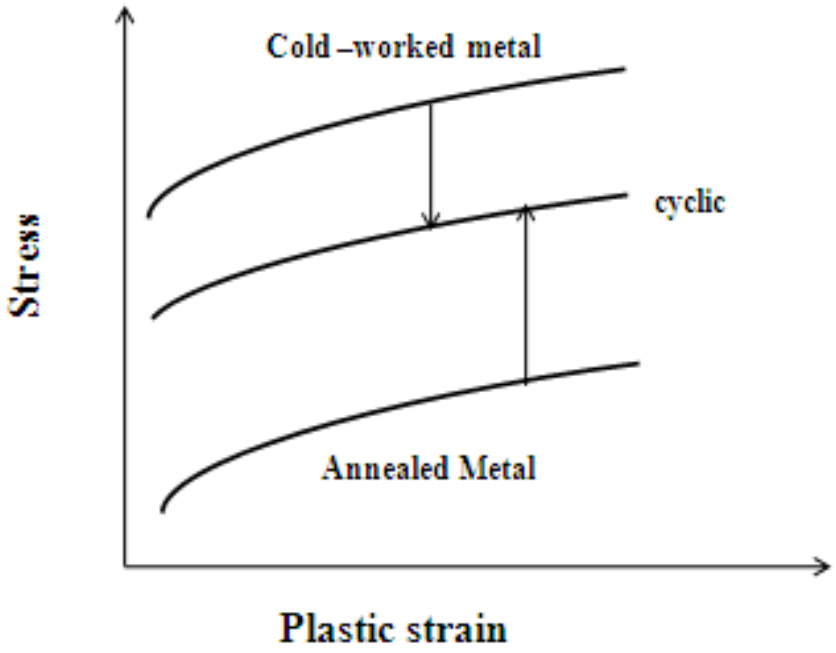

Figure 4-8. A schematic of the strain amplitude as a function of the stress required to impose it in the case of conventional fatigue. It can be seen that for high stacking fault energy materials, after repeated loading initially softer material hardens and harder material softens to the same value of stress. [26, 65, 66]

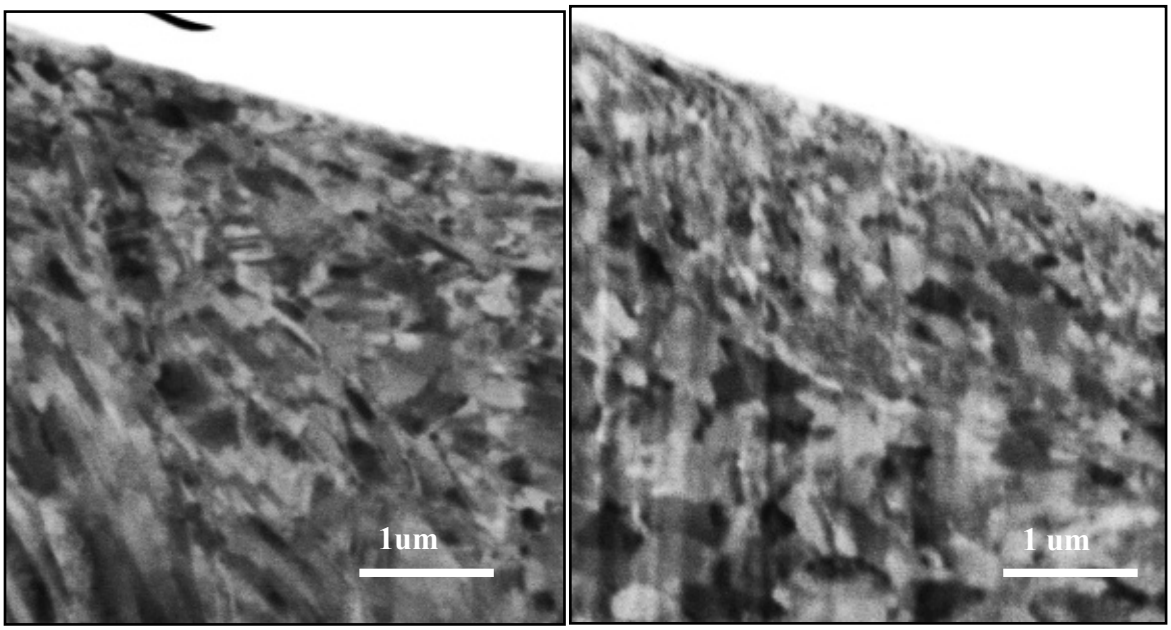

(a) **(b)**

Figure 4-9. Close-up SEM observations of the region just below the scratch surface for LDNT Cu (a) after the 1st pass (b) after the 82nd pass. Grain refinement occurs close to the surface after 1st pass of sliding and can be attributed to dislocation manipulation , rearrangement and twinning processes. After the 82nd pass the deformation affected zone expands and grain size distribution conforms to the strain and strain rates beneath the scratch.

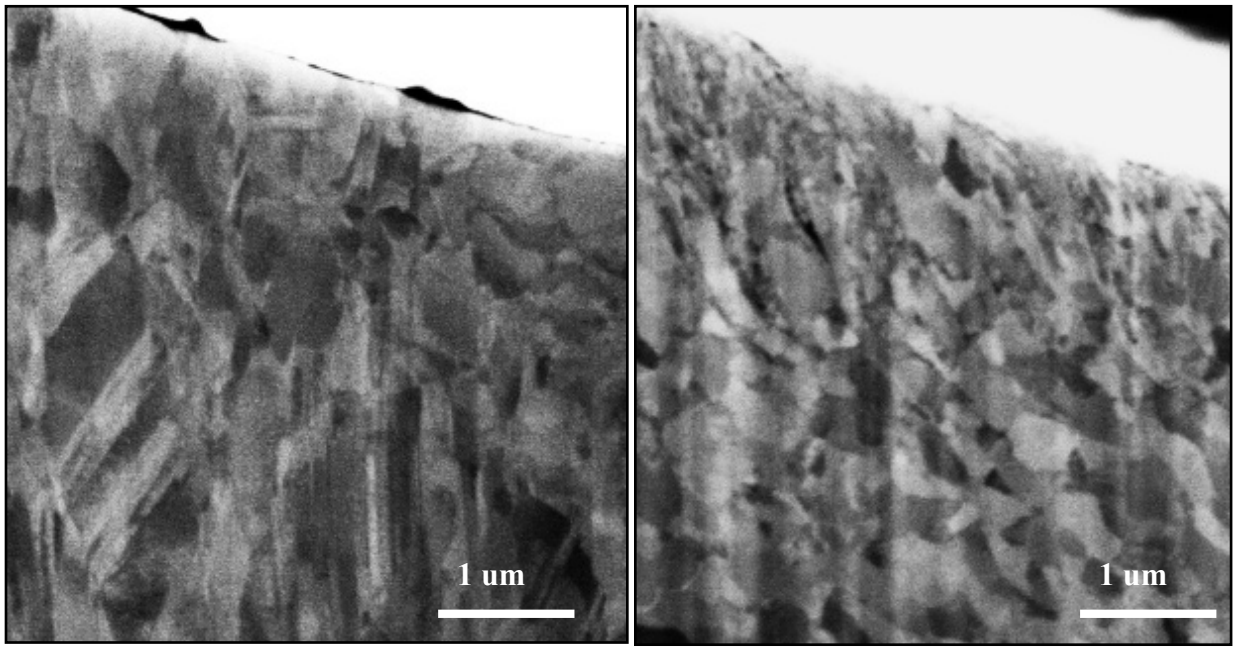

(a) **(b)**

Figure 4-10. Close-up SEM observations of the region just below the scratch surface for HDNT Cu (a) after the 1st pass and (b) after the 82nd pass. The microstructure after the first pass is not severely affected after the 1st pass as most of the plastic deformation can be accommodated by the high density/area of twin boundaries. However, after the 82nd pass, grain refinement occurs possibly via dislocation rearrangements and twinning processes.

4.4 Conclusions

The wear response of UFG Cu having different twin lamellae thickness were examined under monotonic and repeated contact sliding.. To the author's knowledge this is the first study that systematically investigates the effect of coherent growth twin density introduced by electro deposition on the tribological response, microstructure and hardness evolution of UFG Cu under

repeated frictional sliding. An increase in twin density has been shown to result in smaller pile up height and friction coefficient values. It was also inferred that with increase in the number of sliding passes, friction coefficient and rate of increase of pile up for all specimens acquire a steady value that does not change significantly in subsequent passes.

We showed the striking difference between the effects of monotonic and repeated frictional sliding on the deformation induced microstructure change. HDNT Cu exhibited robustness against the high stresses and strains beneath the indenter after the 1st pass of sliding. This is in contrast to LDNT Cu that undergoes grain refinement in the vicinity of the scratch just after the 1st pass. However after 82 passes of sliding, we observe that both LDNT and HDNT Cu incur significant microstructure change and the grain size distribution varies with the depth below the scratch. We have tried to explain through various deformation processes the significant zoning of the grain size distribution after repeated sliding that was not observed after monotonic sliding. The finest grain size observed by us (15nm) is close to the finest grain size observed in repeated sliding of CG Cu and also for SPD processes like SMAT, HPT when twinning processes operate in additional to dislocation activity.

The grains size distribution for both the specimens displayed striking similarity after the 82nd pass and was shown to be dependent on the strain and the strain rate in the zone and independent of the initial twin density. The hardness of the region in the vicinity of the scratch for both the specimens was also found to be similar after 82nd pass. It has been shown through previous studies that cold worked and annealed specimens of the same metal converge to have the same steady state hardness after multiple cycles under uniaxial strain controlled cyclic loading if the metal has sufficiently high stacking fault energy. This takes place primarily through dislocation

processes. In the current study it has been shown experimentally that this hold true under repeated contact sliding as well. However we propose that the convergence of the microstructure and hardness for LDNT and HDNT Cu occurs by twinning processes, dislocation –TB interactions and TB-TB interactions in addition to dislocation processes because of copper being a medium stacking fault energy metal. TEM studies will be needed to further confirm this.

The fact that LDNT specimens showed a considerable increase in hardness with repeated sliding has applications in designing materials. The initial hardness close to the surface matters for an application involving single sliding over the surface. But for applications involving multiple sliding the initial hardness close to the surface is not much consequential as the surface will harden under the influence of repeated sliding and the properties close to the surface would reach a steady value after some passes of sliding. However for single pass sliding HDNT Cu is the best candidate in lieu of exhibiting lowest friction coefficient, pile up height and mechanical stability under the high stresses below the indenter.

Chapter 5

Damage Evolution in Dynamic Plastically Deformed (DPD) and Coarse-Grained (CG) Copper under Repeated Frictional Sliding and Cyclic Indentation

5.1 Introduction

Dynamic Plastic Deformation (DPD) offers a way of manufacturing bulk nano structured materials that manifest a combination of good strength and ductility on account of having a microstructure containing nano grains and nano twin bundles. The tribological properties of DPD Cu have been investigated in his study and compared with coarse-grained (CG) Cu. In addition to the wear response under monotonic sliding, the response of DPD Cu and CG Cu under repeated frictional sliding has been studied. The hardness evolution in the vicinity of the scratches as a function of the repetitions of sliding has also been found out. The depth penetrated by the indenter as a function of the number of cycles has been recorded as a measure of damage under cyclic indentation with a diamond tip. Connections of the wear response in DPD Cu and CG Cu have been made in this study to the original microstructure, the deformation induced micro structural evolution and hardness change. DPD and CG Cu tend to attain similar

microstructure and hardness in the deformation-affected zone that is consistent with what would be expected from strain controlled fatigue experiments for medium to high stacking fault energy metals.

5.2 Results

5.2.1 Hardness Measurements

It can see from Table 1, that DPD Cu which is obtained by cold working on CG Cu at high strain rates and cryogenic temperatures enhances its hardness considerably as compared to the starting material. CG Cu has a hardness of 0.70 GPa while DPD Cu exhibits a hardness value close to 1.90 GPa. An abundance of nano grains and deformation twin bundles formed as a result of low temperature high strain rate deformation are responsible for the higher hardness of DPD Cu than CG Cu.

Sample	**Mean hardness in GPa**
DPD Cu	1.90
CG Cu	0.70

Table 5-1: Hardness of DPD Cu and CG Cu . DPD Cu is much harder than CG Cu due to an abundance of deformation twin bundles and nano grains.

5.2.2 Friction Coefficient

Figure 5-1 shows how the total friction coefficient between the indenter and the specimens evolves as a function of the number of passes of sliding. The friction coefficient for both DPD and CG Cu monotonically decreases with an increase in the number of sliding cycles; however the rate of decline is higher initially and after about 60 passes the friction coefficient values does not decrease significantly which points towards attainment of a steady microstructure. Friction coefficient values for DPD Cu are similar to those observed for nano twinned Copper (Chapter 4) and thus are consistent with what is expected for a high strength nano structured material. CG Cu exhibits similar values of friction coefficient as DPD Cu inspite of different initial microstructure and consequently different initial hardness. This as will be discussed later is owing to the higher strain-hardening exponent of CG Cu.

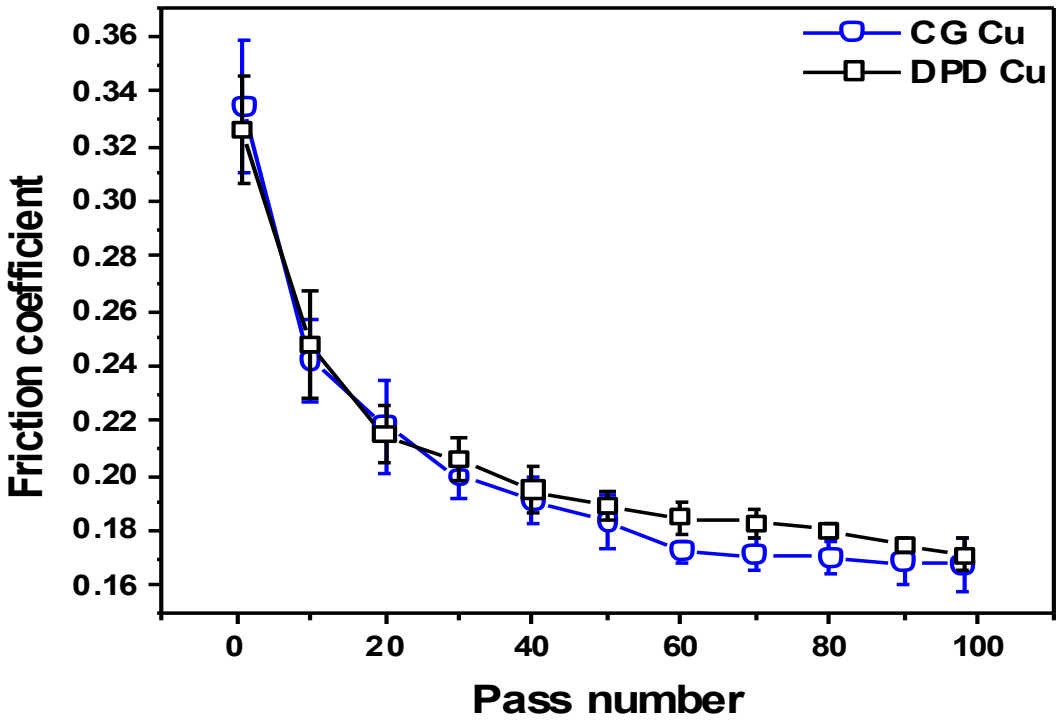

Figure 5-1 Friction coefficient as a function of pass number for both the specimens showing similar values of friction coefficient for both DPD Cu and CG Cu .The friction coefficient for both the specimens decreases with an increase in pass numbers.

5.2.3 Pile-Up Height

Owing to the penetration of the tip into the specimen and the subsequent motion of the sample stage, the specimen surface is worn and the material removed from the specimen is piled up along the sides of the scratch and is referred to as the pile up height. Pile up gives a measure of the wear damage incurred by the frictional sliding process. Minimal damage in the form of pile up height is desired as if there is a contact between the tip and the piled up metal then there might be increased adhesion and thus an increase in the tangential force required to perform

subsequent sliding. The amount of material needed to be dragged forward by the indenter also increases with a higher pile up height. It can be seen in Fig 5-2 that the pile up height increases with an increase in the number of sliding cycles however the rate of pile up increase keeps on decreasing till it acquires an almost constant value after about 60 passes. This steady-state rate of pile up increase is similar for both DPD and CG Cu although CG Cu showed a much higher initial pile up height owing to its lower initial hardness than DPD Cu.

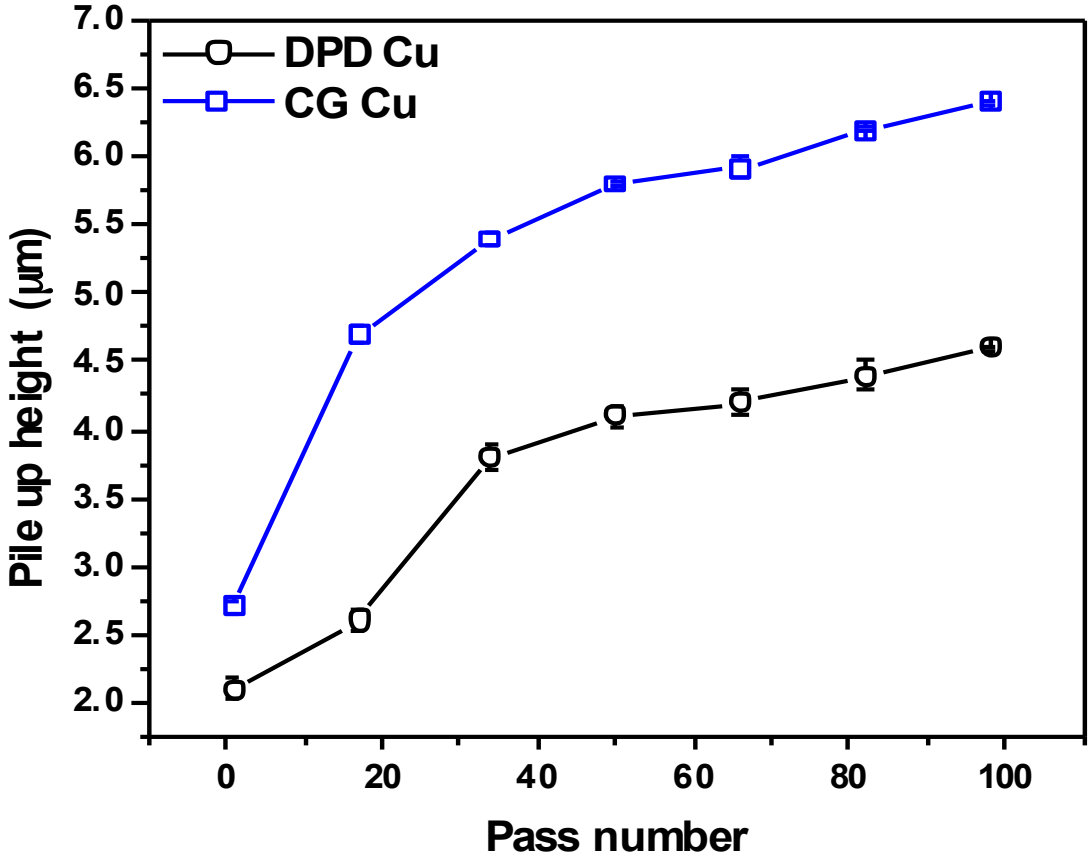

Figure 5-2 Pile up height as a function of pass number for DPD and CG Cu . DPD Cu has a lower pile up height by virtue of being harder than CG Cu.

5.2.4 Evolution of Flow Strength

The method outlined in Section 2.4 was used in order to extract the flow strength of the deformation-affected zone just below the scratch from the P-h (Load vs. depth) response obtained after indenting on the scratches with a conical diamond tip with a half angle of 70.3^0. Subsequently the flow strength in the vicinity of the scratch for both DPD and CG Cu was plotted as a function of the number of sliding cycles. It can be seen in Fig 5-3 that high stresses beneath the indenter lead to strengthening of the deformation affected zone in CG Cu and the hardness monotonically increases with an increase in the number of passes. However, repeated frictional sliding has a softening effect on DPD Cu in that the flow strength decreases from its peak value after the first pass with subsequent sliding cycles and after 98 cycles of sliding both CG and DPD Cu exhibit similar flow strength in the deformation affected zone.

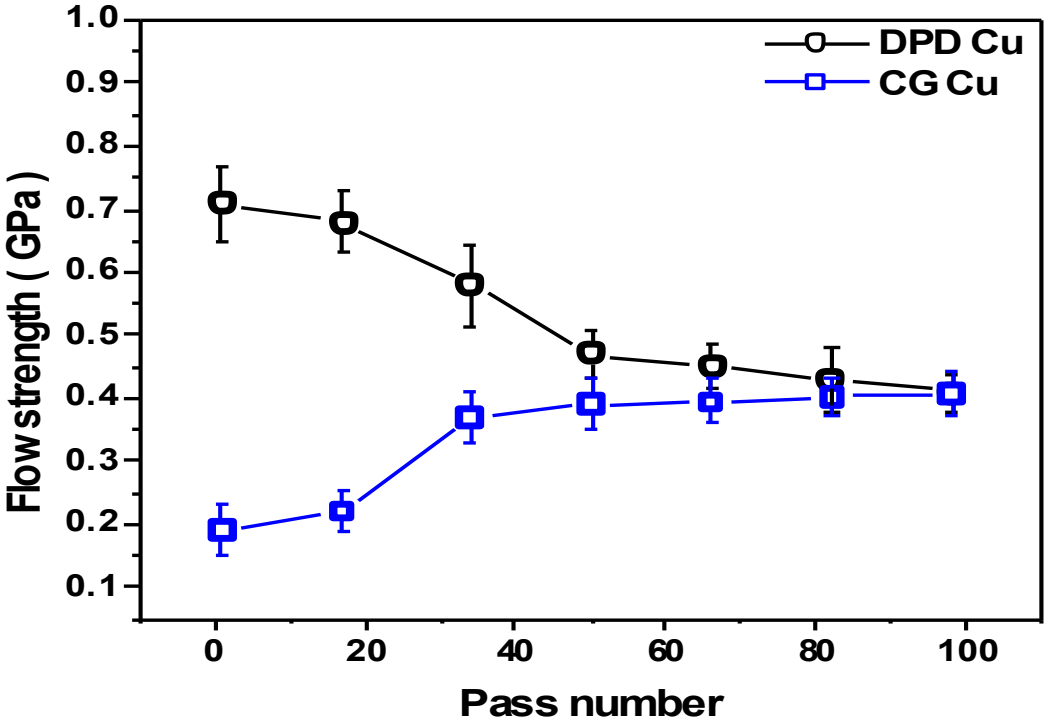

Figure 5-3 Flow strength evolution of the deformation affected region just below the scratch in DPD and CG Cu with the increase in number of sliding cycles. The region below the scratch for CG Cu gets harder whereas for DPD Cu it gets softer with repetitions in sliding.

5.2.5 Cyclic Indentation

The maximum depth penetrated by the indenter at the end of each cycle was plotted as a function of the number of indentation cycles imposed in Figure 5-4. It can be seen that for both DPD Cu and CG Cu with an increase in the number of cycles of indentation the indenter keeps on penetrating deeper into the specimens. DPD Cu has a lower depth of penetration after the first cycle than CG Cu on account of having a greater hardness. CG Cu exhibits a higher initial rate of

ratcheting in the first 250 cycles than DPD Cu. However the rate of ratcheting for both the specimens keeps on decreasing with an increase in the number of cycles and acquires an almost constant average value of 15um per cycle eventually.

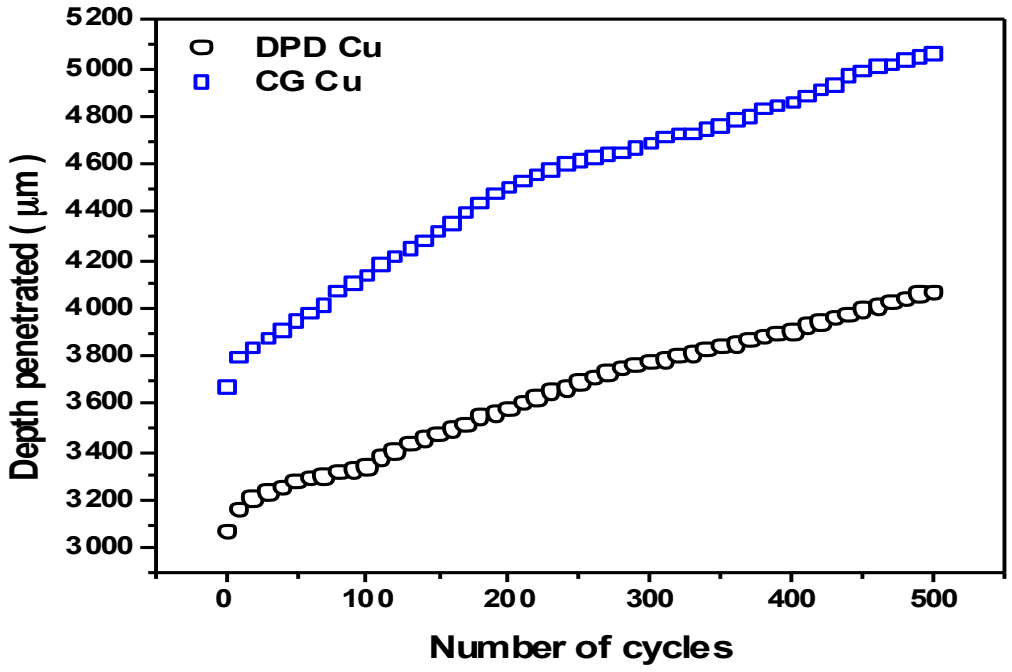

Figure 5-4 Depth penetrated by the indenter as a function of the number of cycles when a maximum load of 500mN was applied cyclically at a loading rate of 50mN/sec. The initial rate of penetration is high but keeps diminishing until a constant rate of penetration is attained for both the specimens.

5.3 Discussion

It can be seen in Table 1 that DPD process leads to significant strengthening as the hardness of DPD Cu is much higher than CG Cu from which it is prepared. This is owing to the high number of deformation twin boundaries that have been shown to harden metals by blocking dislocation

motion [49]. Contribution to the increase in hardness also comes from the grain refinement as nano grains occupy about 67% of the volume of DPD Cu.

DPD Cu shows a lower pile up height when compared to CG Cu. The pile up height of both DPD Cu and CG Cu increase with pass number but the rate of increase diminishes with an increase in sliding cycles till it acquires an almost constant rate after about 50 passes. Pile up height is an indirect measure of the material removed by the motion of the sharp indenter and thus gives an idea of the material loss incurred by the sliding process. It is also not desirable as in repeated sliding it increases chances of adhesion between the indenter and the piled up material leading to increased tangential loads required to perform sliding. Rate of pile up height as discussed in Chapter 4 will diminish because of the indenter making contact with a grooved surface in subsequent passes. A grooved surface offers higher resistance to penetration (Section 2.4) than a flat one. The attainment of similar rate of pile up height increase for both DPD and CG Cu eventually is consistent with similar microstructure attained in the vicinity of the scratch after 50 passes which comprises of equiaxed ultrafine grains with an average grain size of 250-300 nm for both the specimens [103].

Friction coefficient of the relative motion between the indenter and specimen is a complex function of elastic modulus, strain hardening exponent, elastic modulus and fracture toughness when the load applied to the indenter is sufficiently high and consequently the indenter penetrates into the material. Fig 5-1 shows that DPD Cu and CG Cu show similar values of friction coefficient at all pass numbers in spite of having very different hardness. Bellamare [123, 134] has shown that though the friction coefficient decreases with an increase in strength, poor strain hardening leads

to an increase in friction coefficient. It has been shown in [58] that DPD Cu exhibits negligible strain hardening whereas CG Cu shows considerable work hardening. Thus CG Cu with a poor strength but with a high strain hardening exponent manifests similar values of friction coefficient as DPD Cu. Friction coefficient decreases with an increase in pass number for both the specimens as the amount of material worn with subsequent passes of sliding decreases as discussed previously. Such similarity in the friction coefficient values has also been observed for CG and SMAT processed Cu at high loads [108].

Tao[103] has shown that the microstructure of both DPD and CG Cu specimens changes drastically due to the high stresses entailed by the nano scratch process. A strain-induced contrast was observed in the vicinity of the scratch after the first pass of sliding on CG Cu, which suggests a significant density of dislocations induced by the localized deformation [103]. After 50 passes of sliding, equiaxed grains with an average grain size of 300 nm are observed in the deformation-affected zone and this zone extends to a depth of about 10 um beyond which the original microstructure is retained [103]. Ultra fine grains with blurred boundaries are observed in DPD Cu after the 1st pass of sliding and the depth of this tribolayer increases with number of passes of sliding and after 50 passes, equi-axed ultra fine grains with an average grain size of 235 nm are reported up to a depth 10 um below the surface of the scratch [103].

Fig 5-3 shows that the hardness is affected profoundly as result of the microstructure change. After the first pass DPD Cu exhibits high flow strength of 700 MPa that is even higher than its yield strength. This can be accounted for by the high residual stresses expected from the indentation process. However the hardness of DPD Cu decreases with an increase in the number

of sliding cycles and this change is more drastic in the first 50 passes. After about 98 cycles the flow strength is close to 400 MPa. CG Cu exhibits a low strength of 150 MPa after the first sliding cycle however with an increase in the number of sliding passes, CG Cu gets hardened and after 98 cycles, it attains flow strength similar to that of DPD Cu after 98 passes. This is consistent with the studies on deformation induced microstructure change done by Tao [103] in which after repeated sliding both DPD Cu and CG Cu acquire similar microstructure. Tao [103] showed that CG Cu undergoes grain refinement and equiaxed ultrafine grains are observed. DPD Cu exhibits grain coarsening and it is suspected that there is also loss of deformation twin boundaries with the nano scratch process. Detwinning has also been observed with cyclic loading in Cu thin film layers with growth twins [82]. Deformation twin boundaries are even more unstable because of having a higher energy than growth twin boundaries. Thus owing to the high localized stresses below the indenter, both DPD Cu and CG Cu undergo significant microstructure evolution and after 98 sliding cycles the hardness in the vicinity of the scratch for both of them converges to a similar value. This is consistent with our earlier study done on nano twinned materials in which high density nano twinned Cu and low density nano twinned Cu acquire similar microstructure and hardness after repeated sliding (Chapter 4). However, the steady microstructure attained by NT Cu was much finer with lowest grain size close to 15-30nm in the close vicinity of the scratch.

Fig 5-4 shows the indentation creep response of DPD and CG Cu and it can be seen that the indenter penetrates deeper after the first cycle for CG Cu than DPD Cu. The initial rate of ratcheting for the first 250 cycles is also greater for CG Cu .However after about 250 cycles both DPD and CG Cu exhibit similar rate of penetration of the indenter with an increase in the

number of indentation cycles. Although no microscopy studies have been done by us to investigate the microstructure change in the vicinity of the indent, it is suspected that after multiple indentation cycles, the microstructure for both DPD and CG Cu would evolve in similar ways as it has been seen for the case of nano scratching. The similar rate of depth penetration in the later duration of cyclic indentation hints towards attainment of similar microstructure for both DPD Cu and CG Cu. This hypothesis is also consistent with the pile up height evolution observed under repeated sliding of DPD and CG Cu. Investigation of the region in the vicinity of the indent through microscopic studies is needed to confirm the hypothesis.

Strain controlled uni-axial fatigue loading [65, 66] , has been shown to transform the microstructure and strength of medium to high stacking fault energy metals as can be seen in Fig 4-8. Under repeated uniaxial loading cold worked high strength metals soften and annealed softer metals harden till their hardness and microstructure converge if they have sufficiently high stacking fault energy such that cross-slip of dislocations is not hindered. In our current study Copper which has relatively high stacking fault energy ($40x10^{-3}J/m^2$) showed similar behavior to uniaxial fatigue under repeated contact sliding and cyclic indentation too. DPD and CG Cu though had different initial microstructure but the nano scratch and cyclic indentation experiments were performed at similar strain rate and temperature for both the specimens. The similarity in the application of stresses and strains below the indenter led to the development of similar microstructure and strength evolution in the vicinity of the scratch for both the specimens eventually after multiple cycles of scratching and indenting. Thus, the microstructure of neither DPD nor CG Cu was stable under the high stresses entailed by the nano scratch process and evolved to an ultrafine grained structure. Even though the microstructure and hardness attained

by DPD and CG copper was similar but it was different from those of NT Cu that attained a nano-grained microstructure in the vicinity of the scratch after repeated sliding.

5.4 Conclusion

The wear response of DPD and CG Cu was studied and it was found that the DPD process not only improves the hardness but is also good for tribological properties as the pile up height under contact sliding was lower for DPD Cu than CG Cu. The friction coefficient of DPD and CG Cu was found to be similar in spite of a significant difference in their hardness. This was because of higher strain hardening capability of CG Cu than that of DPD Cu. The microstructure of DPD and CG Cu was not found to be stable under contact sliding. We studied its effect on the hardness evolution and found that DPD Cu softens and CG Cu hardens under repeated sliding and eventually both of them converge to similar values of hardness. Strain controlled uniaxial cyclic loading has been known to entail microstructure change in high stacking fault energy through excessive dislocation activity after which cold worked hard specimen softens and annealed specimen hardness to acquire similar microstructure and hardness. The high stresses induced by the nano scratch process are shown in our current study to result in similar evolution though in a small area in the vicinity of the scratch in copper. Pile up height evolution for repeated sliding and depth penetration in cyclic indentation showed a constant rate with respect to the number of passes after multiple cycles which is consistent with the attainment of a steady microstructure as was reported in [65, 66]. Thus, DPD Cu was found to be unstable in its

properties and microstructure under repeated sliding in the localized region close to the scratch. In order to improve its stability under high stresses addition of alloying elements might be useful.

Chapter 6

Concluding Remarks and Suggested Future Work

6.1 Conclusion

The fracture toughness, sub-critical fatigue crack growth life and the tribological response under monotonic and repeated frictional sliding of nano-twinned specimens with different densities of coherent growth twin boundaries has been characterized for the first time in this study using experimental, analytical and computational tools. Besides, this is also the first study to investigate the tribological response of DPD copper with a microstructure comprising of an abundance of deformation twin boundaries and nano grains and compare it with CG copper. The key contributions of this thesis are as follows:

1. This work shows for the first time that high twin density in ultra-fine-grained copper provides a unique combination of strength, ductility, fracture initiation resistance and damage-tolerance during stable fatigue crack growth. This is in contrast to grain boundary engineering where the dilemma of either sacrificing damage resistance or damage tolerance was an impediment to designing stronger materials. There is also a marked improvement in fracture toughness values with an increase in twin density. Furthermore, this work introduces the concept that modifying different microstructural length scales: twin lamellae spacing vs. grain size has opposite effects on the stable fatigue crack growth life because Stage I fatigue crack propagation is likely to occur parallel to the twin planes within each grain along the crack path and thus these intra-grain twin planes, unlike grain boundaries, can more easily facilitate Stage I, serrated (and locally non-

mode I) fracture trajectory. The crack surface roughness and tortuosity was shown to depend strongly on the grain size and not on the twin lamellar spacing whereas a smaller twin lamellar spacing leads to smaller value of crack tip opening displacement (CTOD) facilitating fatigue crack closure. This study has shown that MDNT Cu that has the highest strength also showed relatively the best fatigue crack growth resistance. On the other hand, UFG Cu with essentially no nano twins showed the poorest plane stress fatigue initiation toughness and sub-critical fatigue crack growth response among the three materials studied here.

2. In addition to improved fracture toughness and stable fatigue crack growth propagation life, an increase in twin density resulted in improved wear damage and lower values of friction coefficient under monotonic and repeated frictional sliding. It was also inferred that with increase in the number of sliding passes, friction coefficient and rate of increase of pile up for all specimens acquire a steady value that does not change significantly in subsequent passes. Although the specimen with a twin lamellar spacing of 85 nm was not micro structurally stable under the high stresses beneath the indenter, twin lamellar refinement to 15 nm significantly improved the robustness against microstructure change during monotonic sliding thus highlighting the role of increased twin density in enhancing the microstructural stability under high stresses. However after 82 passes of sliding, it was observed that both LDNT and HDNT Cu incur significant microstructure change and the grain size distribution varies with the depth below the scratch and the finest grain size observed (20nm) in the tribolayer is similar to the finest grain size observed for SPD processes like SMAT, HPT when twinning processes operate in additional to dislocation activity. The grains size distribution for both the specimens displayed striking similarity after the 82^{nd} pass and was shown to be dependent on the strain in the zone and independent of the initial twin density. The hardness of the region in the vicinity of the

scratch for both the specimens was also found to be similar after 82nd pass. It has been shown through previous studies that cold worked and annealed specimens of the same metal converge to have the same steady state hardness after multiple cycles under uniaxial strain controlled cyclic loading if the metal has sufficiently high stacking fault energy. This takes place primarily through dislocation processes. In the current study it has been shown experimentally that this hold true under repeated contact sliding as well. However in this study it was suggested that the convergence of the microstructure and hardness for LDNT and HDNT Cu occurs by twinning processes, dislocation–TB interactions and TB-TB interactions in addition to dislocation processes because of copper being a medium stacking fault energy metal. TEM studies will be needed to further confirm this.

3. The tribological response of DPD and CG Cu was studied and it was found that the DPD process not only improves the hardness but also enhances the tribological properties, as the pile up height under contact sliding was lower for DPD Cu than CG Cu. The friction coefficient of DPD and CG Cu was found to be similar in spite of a significant difference in their hardness. This was because of higher strain hardening capability of CG Cu than that of DPD Cu. The hardness evolution under repeated sliding of the specimens was also investigated and it is found that DPD Cu softens and CG Cu hardens under repeated sliding and eventually both of them converge to similar values of hardness. This trend was similar to the wear studies of nanotwinned copper produced by PED, however the final steady microstructure attained in both cases is different: the grain sizes of the tribolayer for NT copper were less than 100 nm, however the grain size for DPD and CG Cu converged to 200-300nm in the tribolayer thus underscoring the role of initial microstructural characteristics in affecting the final saturation microstructure. Pile up height evolution for repeated sliding and depth penetration in cyclic indentation showed a

constant rate with respect to the number of passes after multiple cycles which is consistent with the attainment of a steady microstructure.

6.2 Future Work

The current study has laid down the initial steps and the possibility towards designing metals with a combination of high strength, ductility, fracture toughness, wear resistance and prolonged sub-critical fatigue crack growth life. However, TEM studies need to be undertaken in order to gain a deeper understanding of the deformation mechanisms operating in nano-twinned materials ahead of the advancing crack during sub-critical fatigue crack growth. Grain growth has been observed ahead of the advancing crack for most NG metals [5]. However, the effect of the stress intensification ahead of the crack tip on the nano-twinned microstructure is still unknown. TEM observations during in-situ crack propagation studies will be able to shed a better light on the microstructure evolution ahead of the crack tip.

The current study involved studying the sub-critical fatigue crack growth at low load ratio values at which the effect of roughness–induced crack closure becomes significant. It would be interesting to test the stable fatigue crack propagation response at different values of the load ratio values ranging was 0.1 to 0.9. It is expected that at higher values of load ratio, the effect of roughness induced closure would be less important since the CTOD at all times can be set to be larger than the surface asperities and in that case the fatigue crack growth threshold would be similar for all values of twin densities.

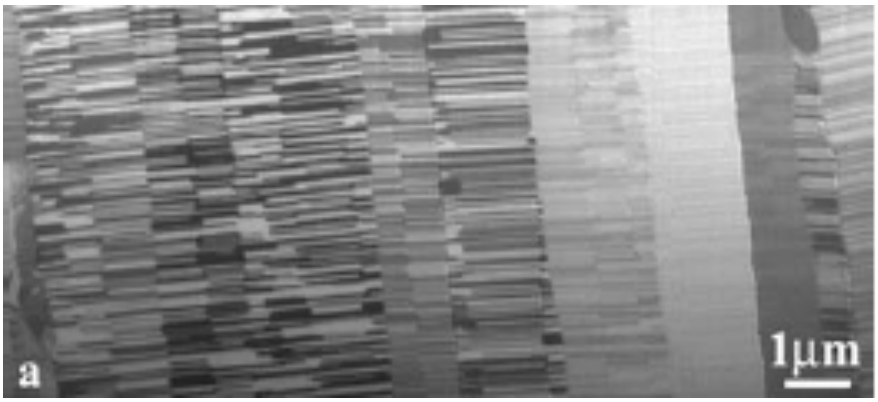

Figure 6-1: Microstructure of nano-twinned copper produced by magnetron sputtering showing columnar grains with the twin orientation parallel from grain to grain.

Nano-twinned copper has also been produced by magnetron sputtering [82] and the microstructure is different from the specimens used in the current study. The twins in adjacent grains are also parallel to each other in the former specimens (Figure 6-1). It would be interesting to do stress controlled fatigue experiments, sub-critical fatigue crack growth experiments and fracture toughness studies on the specimens produced by magnetron sputtering and check whether the trends observed in the current study hold true for specimens with a different design of twinned microstructure.

It has been shown that an increase in the strain applied during the DPD process leads to an improvement in fracture toughness. However, the stress–controlled fatigue life and sub-critical fatigue crack growth propagation of DPD copper has not been studied yet. An increase in the strain applied leads to grain refinement and also increases the amount of deformation twin boundaries in the microstructure during the DPD treatment. Grain refinement has been shown to degrade the fatigue crack growth threshold values and twin-lamellae refinement leads to an improvement in fatigue response as was shown in the current study, so the sub-critical fatigue

response of a microstructure comprising of a combination of nano-grains and deformation twin boundaries is difficult to predict. Since DPD copper can be produced in bulk form and exhibits high yield strength, ductility and fracture toughness, it is crucial to study its response under cyclic loading.

The frictional sliding studies done for the current study involved repeated sliding only till a pass number of 100. In order to further confirm the attainment of a stable microstructure after repeated sliding, additional studies can be undertaken in which the number of passes of sliding can be increased to above 100. This is critical in light of the observation that HDNT and LDNT specimens converged to a nano-grained microstructure in the vicinity of the scratch and DPD copper and CG copper converged to an ultra-fine grained microstructure after repeated sliding under same sliding conditions. It is possible that the presence of an initial significant density of twin boundaries was responsible attainment of an eventual nano-grained structure. Grain refinement mediated by twin-boundaries has been shown in prior studies. It is probable that CG and DPD Cu attained an ultra fine-grained structure because there were no stable twin boundaries to facilitate twin refinement. Therefore, the deformation-affected zone needs to be examined more carefully using TEM, so that more light could be shed on the microstructural features and deformation mechanisms that were not probably revealed by SEM that was used in the current work.

In order to use nano-twinned materials in high stress and high temperature applications, it is also important to study their creep response. The traditional way to measure creep requires multiple specimens to ascertain the response under different values of stress and temperature. However, the use of indentation-creep experiments under vacuum conditions can resolve this problem.

Impression test using a flat ended cylindrical punch to study creep was first proposed by Chu and Li [135].

It has been shown through some earlier studies that self-similar indentation can be used to extract material properties like power-law creep exponents and activation energy for creep equivalent to the ones obtained from conventional uniaxial creep tests [136]. The self-similar impression creep test can evaluate the creep response using a small volume of the material. In these kinds of tests, a conical or cylindrical indenter is pressed on the surface of a specimen at high ambient temperature and the depth penetrated by the indenter increases with time and is monitored to extract the high temperature mechanical properties. The uniaxial creep response of metals comprises of three regimes that are primary, secondary and tertiary creep. However, the impression creep response of metals consists of just the first 2 stages and the accelerating stage of tertiary creep is not present since the deformation is stable to the last (Fig 6-2).

Careful experiments can be designed to ascertain the creep response of nano-twinned copper. For this indentation at different values of stresses and temperature can be done. The rate of penetration of the indenter in the secondary stage is almost constant and has been found to be related to the plastic strain rate in uniaxial creep tests. These tests would give us an idea of the effect of twin density on then activation energy of creep and also the power law creep exponents.

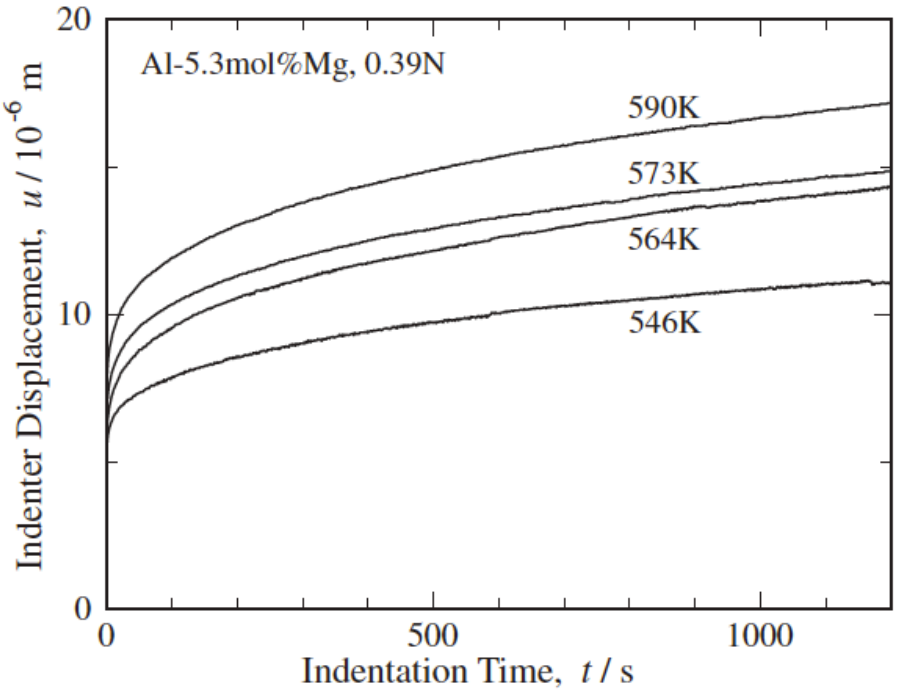

Figure 6-2: Indentation creep response of an Al-Mg alloy [136].

Appendix A :

Elasto plastic parameters used in the current study for the FEM computations

E(GPa)	σ_y (MPa)
10	100
10	300
50	200
50	1000
90	500
90	3000
130	1000
130	3000
170	300
170	3000
210	300
210	3000

Bibliography

[1] Siegel RW, Fougere GE. Mechanical properties of nanophase metals. Nanostructured Materials 1995; 6(1-4):205-216.

[2] Sanders PG, Eastman JA, Weertman JR. Elastic and tensile behavior of nanocrystalline copper and palladium. Acta Materialia 1997; 45(10):4019-4025.

[3] Gleiter H. Nanostructured materials: Basic concepts and microstructure. Acta Materialia 2000; 48(1):1-29.

[4] Wang YM, Chen MW, Zhou FH, Ma E. High tensile ductility in a nanostructured metal. Nature 2002; 419(6910):912-915.

[5] Kumar KS, Van Swygenhoven H, Suresh S. Mechanical behavior of nanocrystalline metals and alloys. Acta Materialia 2003; 51(19):5743-5774.

[6] Dao M, Lu L, Asaro RJ, De Hosson JTM, Ma E. Toward a quantitative understanding of mechanical behavior of nanocrystalline metals. Acta Materialia 2007; 55(12):4041-4065.

[7] Schuh CA, Nieh TG, Yamasaki T. Hall-Petch breakdown manifested in abrasive wear resistance of nanocrystalline nickel. Scripta Materialia 2002; 46(10):735-740.

[8] Mishra R, Balasubramaniam R. Effect of nanocrystalline grain size on the electrochemical and corrosion behavior of nickel. Corrosion Science 2004; 46(12):3019-3029.

[9] Hanlon T, Chokshi AH, Manoharan M, Suresh S. Effects of grain refinement and strength on friction and damage evolution under repeated sliding contact in nanostructured metals. International Journal of Fatigue 2005; 27(10-12):1159-1163.

[10] Birringer R, Gleiter H, Klein HP, Marquardt P. Nanocrystalline Materials an Approach to a Novel Solid Structure with Gas-Like Disorder. Physics Letters A 1984; 102(8):365-369.

[11] J.R.Groza. Non-equilibrium Processing of Materials. Oxford: Pergamon Press, 1999.

[12] Erb U, A.M.El-Sherik, G.Palumbo, K.T.Aust. Synthesis, structure and properties of electroplated nanocrystalline materials. Nanostructured Materials 1993; 2:383.

[13] K.Lu. Nanocrystalline metals crystallized from amorphous solids : nanocrystallization , structure and properties Materials Science and Engineering 1996; 16(4):161-221.
[14] Valiev RZ, Korznikov AV, Mulyukov RR. Structure and Properties of Ultrafine-Grained Materials Produced by Severe Plastic-Deformation. Materials Science and Engineering a-Structural Materials Properties Microstructure and Processing 1993; 168(2):141-148.
[15] Iwahashi Y, Wang JT, Horita Z, Nemoto M, Langdon TG. Principle of equal-channel angular pressing for the processing of ultra-fine grained materials. Scripta Materialia 1996; 35(2):143-146.
[16] Zhilyaev AP, Lee S, Nurislamova GV, Valiev RZ, Langdon TG. Microhardness and microstructural evolution in pure nickel during high-pressure torsion. Scripta Materialia 2001; 44(12):2753-2758.
[17] Hansen N. New discoveries in deformed metals. Metallurgical and Materials Transactions a-Physical Metallurgy and Materials Science 2001; 32(12):2917-2935.
[18] Ueji R, Tsuji N, Minamino Y, Koizumi Y. Ultragrain refinement of plain low carbon steel by cold-rolling and annealing of martensite. Acta Materialia 2002; 50(16):4177-4189.
[19] Bay B, Hansen N, Hughes DA, Kuhlmannwilsdorf D. Overview No-96 - Evolution of Fcc Deformation Structures in Polyslip. Acta Metallurgica Et Materialia 1992; 40(2):205-219.
[20] Van Swygenhoven H, Derlet PM, Hasnaoui A. Atomic mechanism for dislocation emission from nanosized grain boundaries. Physical Review B 2002; 66(2).
[21] Derlet PM, Van Swygenhoven H, Hasnaoui A. Atomistic simulation of dislocation emission in nanosized grain boundaries. Philosophical Magazine 2003; 83(31-34):3569-3575.
[22] Schuh CA, Nieh TG, Iwasaki H. The effect of solid solution W additions on the mechanical properties of nanocrystalline Ni. Acta Materialia 2003; 51(2):431-443.
[23] Jeong DH, Erb U, Aust KT, Palumbo G. The relationship between hardness and abrasive wear resistance of electrodeposited nanocrystalline Ni-P coatings. Scripta Materialia 2003; 48(8):1067-1072.

[24] Chokshi AH, Rosen A, Karch J, Gleiter H. On the Validity of the Hall-Petch Relationship in Nanocrystalline Materials. Scripta Metallurgica 1989; 23(10):1679-1683.
[25] Masumura RA, Hazzledine PM, Pande CS. Yield stress of fine grained materials. Acta Materialia 1998; 46(13):4527-4534.
[26] Suresh S. Fatigue of Materials. . Second edition. Cambridge: Cambridge University Press, 1998.
[27] Hanlon T, Kwon YN, Suresh S. Grain size effects on the fatigue response of nanocrystalline metals. Scripta Materialia 2003; 49(7):675-680.
[28] Hanlon T, Tabachnikova ED, Suresh S. Fatigue behavior of nanocrystalline metals and alloys. International Journal of Fatigue 2005; 27(10-12):1147-1158.
[29] Schwaiger R, Moser B, Dao M, Chollacoop N, Suresh S. Some critical experiments on the strain-rate sensitivity of nanocrystalline nickel. Acta Materialia 2003; 51(17):5159-5172.
[30] Suresh S, Li J. Deformation of the ultra-strong. Nature 2008; 456(7223):716-717.
[31] Mirshams RA, Mao CH, Whang SH, Yin WM. R-curve characterization of the fracture toughness of nanocrystalline nickel thin sheets. Materials Science and Engineering A 2001; 315(1-2):21-27.
[32] Gertsman VY, Birringer R. On the Room-Temperature Grain-Growth in Nanocrystalline Copper. Scripta Metallurgica Et Materialia 1994; 30(5):577-581.
[33] Zhang K, Weertman JR, Eastman JA. The influence of time, temperature, and grain size on indentation creep in high-purity nanocrystalline and ultrafine grain copper. Applied Physics Letters 2004; 85(22):5197-5199.
[34] Zhang K, Weertman JR, Eastman JA. Rapid stress-driven grain coarsening in nanocrystalline Cu at ambient and cryogenic temperatures. Applied Physics Letters 2005; 87(6).
[35] Jin M, Minor AM, Stach EA, Morris JW. Direct observation of deformation-induced grain growth during the nanoindentation of ultrafine-grained Al at room temperature. Acta Materialia 2004; 52(18):5381-5387.
[36] Gianola DS, Van Petegem S, Legros M, Brandstetter S, Van Swygenhoven H, Hemker KJ. Stress-assisted discontinuous grain growth and its effect on the

deformation behavior of nanocrystalline aluminum thin films. Acta Materialia 2006; 54(8):2253-2263.

[37] Fan GJ, Wang YD, Fu LF, Choo H, Liaw PK, Ren Y, Browning ND. Orientation-dependent grain growth in a bulk nanocrystalline alloy during the uniaxial compressive deformation. Applied Physics Letters 2006; 88.

[38] Liao XZ, Kilmametov AR, Valiev RZ, Gao HS, Li XD, Mukherjee AK, Bingert JF, Zhu YT. High-pressure torsion-induced grain growth in electrodeposited nanocrystalline Ni. Applied Physics Letters 2006; 88(2).

[39] Callister Jr. WD. Materials Science and Engineering, An Introduction. Fifth Edition. New York: Wiley, 2000.

[40] Brandes EA, Brook GB. Smithells Metals Reference Book. Seventh Edition. Oxford: Butterworth-Heinemann, 1998.

[41] Andrews PV, West MB, Robeson CR. The Effect of Grain Boundaries on the Electrical Resistivity of Polycrystalline Copper and Aluminium. Philosophical Magazine 1969; 19(161):887-898.

[42] Pry RH, Hennig RW. On the Use of Electrical Resistivity as a Measure of Plastic Deformation in Copper. Acta Metallurgica 1954; 2(2):318-321.

[43] Freund LB, Suresh S. Thin Film Materials. New York: Cambridge University Press, 2003.

[44] Lu L, Schwaiger R, Shan ZW, Dao M, Lu K, Suresh S. Nano-sized twins induce high rate sensitivity of flow stress in pure copper. Acta Materialia 2005; 53(7):2169-2179.

[45] Dao M, Lu L, Shen YF, Suresh S. Strength, strain-rate sensitivity and ductility of copper with nanoscale twins. Acta Materialia 2006; 54(20):5421-5432.

[46] Lu K, Lu L, Suresh S. Strengthening Materials by Engineering Coherent Internal Boundaries at the Nanoscale. Science 2009; 324(5925):349-352.

[47] Shen YF, Lu L, Dao M, Suresh S. Strain rate sensitivity of Cu with nanoscale twins. Scripta Materialia 2006; 55(4):319-322.

[48] Lu L, Zhu T, Shen YF, Dao M, Lu K, Suresh S. Stress relaxation and the structure size-dependence of plastic deformation in nanotwinned copper. Acta Materialia 2009; 57(17):5165-5173.

[49] Christian JW, Mahajan S. Deformation Twinning. Progress in Materials Science 1995; 39(1-2):1-157.

[50] Lu L, Dao M, Zhu T, Li J. Size dependence of rate-controlling deformation mechanisms in nanotwinned copper. Scripta Materialia 2009; 60(12):1062-1066.

[51] Zhang X, Misra A, Wang H, Nastasi M, Embury JD, Mitchell TE, Hoagland RG, Hirth JP. Nanoscale-twinning-induced strengthening in austenitic stainless steel thin films. Applied Physics Letters 2004; 84(7):1096-1098.

[52] Zhang X, Misra A, Wang H, Shen TD, Nastasi M, Mitchell TE, Hirth JP, Hoagland RG, Embury JD. Enhanced ardening in Cu/330 stainless steel multilayers by nanoscale twinning. Acta Materialia 2004; 52(4):995-1002.

[53] Shen YF, Lu L, Lu QH, Jin ZH, Lu K. Tensile properties of copper with nano-scale twins. Scripta Materialia 2005; 52(10):989-994.

[54] Lu L, Shen YF, Chen XH, Qian LH, Lu K. Ultrahigh strength and high electrical conductivity in copper. Science 2004; 304(5669):422-426.

[55] Sutton AP, Ballufi RW. Interfaces in Crystalline Materials Clarendon: Oxford University Press, 1995.

[56] Zhang Y, Tao NR, Lu K. Mechanical properties and rolling behaviors of nano-grained copper with embedded nano-twin bundles. Acta Materialia 2008; 56(11):2429-2440.

[57] Ma E, Wang YM, Lu QH, Sui ML, Lu L, Lu K. Strain hardening and large tensile elongation in ultrahigh-strength nano-twinned copper. Applied Physics Letters 2004; 85(21):4932-4934.

[58] Zhao WS, Tao NR, Guo JY, Lu QH, Lu K. High density nano-scale twins in Cu induced by dynamic plastic deformation. Scripta Materialia 2005; 53(6):745-749.

[59] Li YS, Tao NR, Lu K. Microstructural evolution and nanostructure formation in copper during dynamic plastic deformation at cryogenic temperatures. Acta Materialia 2008; 56(2):230-241.

[60] Zhang Y, Li YS, Tao NR, Lu K. High strength and high electrical conductivity in bulk nanograined Cu embedded with nanoscale twins. Applied Physics Letters 2007; 91(21).

[61] Hong CS, Tao NR, Lu K, Huang X. Grain orientation dependence of deformation twinning in pure Cu subjected to dynamic plastic deformation. Scripta Materialia 2009; 61(3):289-292.
[62] Qin EW, Lu L, Tao NR, Tan J, Lu K. Enhanced fracture toughness and strength in bulk nanocrystalline Cu with nanoscale twin bundles. Acta Materialia 2009; 57(20):6215-6225.
[63] Agnew SR, Vinogradov AY, Hashimoto S, Weertman JR. Overview of fatigue performance of Cu processed by severe plastic deformation. Journal of Electronic Materials 1999; 28(9):1038-1044.
[64] Agnew SR, Weertman JR. Cyclic softening of ultrafine grain copper. Materials Science and Engineering a-Structural Materials Properties Microstructure and Processing 1998; 244(2):145-153.
[65] Feltner CE, Laird C. Cyclic Stress-Strain Response of Fcc Metals and Alloys .1. Phenomenological Experiments. Acta Metallurgica 1967; 15(10):1621-&.
[66] Feltner CE, Laird C. Cyclic Stress-Strain Response of Fcc Metals and Alloys .2. Dislocation Structures and Mechanisms. Acta Metallurgica 1967; 15(10):1633-&.
[67] Forsyth P. A two stage process of fatigue crack growth. Crack Propagation. Proceedings of Cranfield Symposium, 1962. p.76-94.
[68] AK Vasudevan KS, N Louat. A review of crack closure , fatigue crack threshold and related phenomena Materials Science and Engineering a-Structural Materials Properties Microstructure and Processing 1994; A188:1-22.
[69] Suresh S. Fatigue Crack Deflection and Fracture Surface-Contact - Micromechanical Models. Metallurgical Transactions a-Physical Metallurgy and Materials Science 1985; 16(2):249-260.
[70] ASTM. E399: Standard Test Method for Linear-Elastic Plane-Strain Fracture Toughness K_{IC} of Metallic Materials. West Conshohocken, PA : ASTM International, 2009.
[71] Witney AB, Sanders PG, Weertman JR, Eastman JA. Fatigue of Nanocrystalline Copper. Scripta Metallurgica Et Materialia 1995; 33(12):2025-2030.

[72] Mughrabi H, Höppel HW. Cyclic deformation and fatigue properties of ultra fine grain size materials: current status and some criteria for improvement of the fatigue resistance. Materials Research Society Symposium, vol. 634 2001. p.B2.1.1-B2.1.12.

[73] Hoppel HW, Zhou ZM, Mughrabi H, Valiev RZ. Microstructural study of the parameters governing coarsening and cyclic softening in fatigued ultrafine-grained copper. Philosophical Magazine a-Physics of Condensed Matter Structure Defects and Mechanical Properties 2002; 82(9):1781-1794.

[74] Moser B, Hanlon T, Kumar KS, Suresh S. Cyclic strain hardening of nanocrystalline nickel. Scripta Materialia 2006; 54(6):1151-1155.

[75] Fan GJ, Fu LF, Wang GY, Choo H, Liaw PK, Browning ND. Mechanical behavior of a bulk nanocrystalline Ni-Fe alloy. Journal of Alloys and Compounds 2007; 434:298-300.

[76] Yang Y, Imasogie B, Fan GJ, Liaw PK, Soboyejo WO. Fatigue and fracture of a bulk nanocrystalline NiFe alloy. Metallurgical and Materials Transactions a-Physical Metallurgy and Materials Science 2008; 39A(5):1145-1156.

[77] Farkas D, Van Petegem S, Derlet PM, Van Swygenhoven H. Dislocation activity and nano-void formation near crack tips in nanocrystalline Ni. Acta Materialia 2005; 53(11):3115-3123.

[78] Xie JJ, Wu XL, Hong YS. Study on fatigue crack nucleation of electrode posited nanocrystalline nickel, edited by: Yang W, Geni M, Wang TJ, Zhuang Z. Advances in Fracture and Materials Behavior, Pts 1 and 2, vol. 33-37. 2008. p.925-930.

[79] Trusov LT, Gryaznov VG. Growth of Crystals, p.55. New York and London: Consultants Bureau, 1991.

[80] Karimpoor AA, Erb U. Mechanical properties of nanocrystalline cobalt. Physica Status Solidi a-Applications and Materials Science 2006; 203(6):1265-1270.

[81] Ovid'ko IA, Sheinerman AG. Ductile vs. brittle behavior of pre-cracked nanocrystalline and ultrafine-grained materials. Acta Materialia 2010; 58(16):5286-5294.

[82] Shute CJ, Myers BD, Xie S, Barbee TW, Hodge AM, Weertman JR. Microstructural stability during cyclic loading of multilayer copper/copper samples with nanoscale twinning. Scripta Materialia 2009; 60(12):1073-1077.

[83] Tang L, Lu L. Effect of Twin Lamellar Thichkness on the Fatigue Properties of Nano-Twinned Cu. Acta Metallurgica Sinica 2009; 45(7):808-814.
[84] Cheng S, Zhao YH, Wang YM, Li Y, Wang XL, Liaw PK, Lavernia EJ. Structure Modulation Driven by Cyclic Deformation in Nanocrystalline NiFe. Phys Rev Lett 2010; 104(25):255501.
[85] Zhou HF, Qu SX, Yang W. Toughening by nano-scaled twin boundaries in nanocrystals. Modelling and Simulation in Materials Science and Engineering 2010; 18(6):065002.
[86] Zhou HF, Qu SX. The effect of nanoscale twin boundaries on fracture toughness in nanocrystalline Ni. Nanotechnology 2010; 21(3):035706.
[87] Rabinowicz E. Friction and Wear of Materials, 2nd Edition, Chap.1. New York: Wiley-Interscience, 1995.
[88] Benjamin P, Weaver C. Adhesion of Metal Films to Glass. Proceedings of the Royal Society of London Series a-Mathematical and Physical Sciences 1960; 254(1277):177-&.
[89] Hirth JP, Rigney DA. Crystal Plasticity and Delamination Theory of Wear. Wear 1976; 39(1):133-141.
[90] Bhargava RK, Moteff J, Swindeman RW. Dislocation Substructures, Carbides and Deformation Mechanism Map for AISI 303 Stainless-Steel. Metallurgical Transactions a-Physical Metallurgy and Materials Science 1977; 8(5):799-800.
[91] Rigney DA, Glaeser WA. Significance of near-Surface Microstructure in Wear Process. Wear 1978; 46(1):241-250.
[92] Emge A, Karthikeyan S, Rigney DA. The effects of sliding velocity and sliding time on nanocrystalline tribolayer development and properties in copper. Wear 2009; 267(1-4):562-567.
[93] Rigney DA, Naylor MGS, Divakar R, Ives LK. Low-Energy Dislocation-Structures Caused by Sliding and by Particle Impact. Materials Science and Engineering 1986; 81(1-2):409-425.
[94] Li J, Elmadagli A, Gertsman VY, Lo J, Alpas AT. FIB and TEM characterization of subsurfaces of an Al-Si alloy (A390) subjected to sliding wear. Materials Science and

Engineering a-Structural Materials Properties Microstructure and Processing 2006; 421(1-2):317-327.

[95] Rigney DA, Hammerberg JE. Unlubricated sliding behavior of metals. Mrs Bulletin 1998; 23(6):32-36.

[96] Hughes DA, Dawson DB, Korellis JS, Weingarten LI. A Microstructurally Based Method for Stress Estimates. Wear 1995; 181:458-468.

[97] Rigney DA, Chen LH, Naylor MGS, Rosenfield AR. Wear Processes in Sliding Systems. Wear 1984; 100(1-3):195-219.

[98] Singh JB, Cai W, Bellon P. Dry sliding of Cu-15 wt%Ni-8 wt%Sn bronze: Wear behaviour and micro structures. Wear 2007; 263:830-841.

[99] Singh JB, Wen JG, Bellon P. Nanoscale characterization of the transfer layer formed during dry sliding of Cu-15 wt.% Ni-8 wt.% Sn bronze alloy. Acta Materialia 2008; 56(13):3053-3064.

[100] Hughes DA, Dawson DB, Korellis JS, Weingarten LI. Near-Surface Microstructures Developing under Large Sliding Loads. Journal of Materials Engineering and Performance 1994; 3(4):459-475.

[101] Jiang JR, Stott FH, Stack MM. A Mathematical Model for Sliding Wear of Metals at Elevated Temperatures. Wear 1995; 181:20-31.

[102] Subramanian C. On Mechanical Mixing During Dry Sliding of Aluminium-12.3 Wt Percent Silicon Alloy Against Copper. . Wear 1993; 161(1-2):53-60.

[103] N.R.Tao, L.Lu, M.Dao, S.Suresh. Unpublished results. 2010.

[104] Rupert TJ, Schuh CA. Sliding wear of nanocrystalline Ni-W: Structural evolution and the apparent breakdown of Archard scaling. Acta Materialia; 58(12):4137-4148.

[105] Farhat ZN, Ding Y, Northwood DO, Alpas AT. Effect of grain size on friction and wear of nanocrystalline aluminum. Materials Science and Engineering a-Structural Materials Properties Microstructure and Processing 1996; 206(2):302-313.

[106] Lee KH, Chang D, Kwon SC. Properties of electrodeposited nanocrystalline Ni-B alloy films. Electrochimica Acta 2005; 50(23):4538-4543.

[107] Lv XR, Wang SG, Liu Y, Long K, Li S, Zhang ZD. Effect of nanocrystallization on tribological behaviors of ingot iron. Wear 2008; 264(7-8):535-541.

[108] Zhang YS, Han Z, Wang K, Lu K. Friction and wear behaviors of nanocrystalline surface layer of pure copper. Wear 2006; 260(9-10):942-948.
[109] A.Singh, L.Tang, M.Dao, L.Lu, S.Suresh. Fracture Toughness and fatigue crack growth characteristics of nanotwinned copper. Acta Materialia 2011; 59:2437-2446.
[110] T.L.Anderson. Fracture Mechanics: Fundamentals and Applications. Second Edition: CRC Press, 1994.
[111] Hertzberg RW. Deformation and Fracture Mechanics of Engineering Materials: Fourth edition. John Wiley & Sons, Inc., 1996.
[112] Chaudhri MM. Subsurface strain distribution around Vickers hardness indentations in annealed polycrystalline copper. Acta Materialia 1998; 46(9):3047-3056.
[113] Dao M, Chollacoop N, Van Vliet KJ, Venkatesh TA, Suresh S. Computational modeling of the forward and reverse problems in instrumented sharp indentation. Acta Materialia 2001; 49(19):3899-3918.
[114] Gouldstone A, Chollacoop N, Dao M, Li J, Minor AM, Shen YL. Indentation across size scales and disciplines: Recent developments in experimentation and modeling. Acta Materialia 2007; 55(12):4015-4039.
[115] Cheng YT, Cheng CM. Relationships between hardness, elastic modulus, and the work of indentation. Applied Physics Letters 1998; 73(5):614-616.
[116] Cheng YT, Cheng CM. Scaling approach to conical indentation in elastic-plastic solids with work hardening. Journal of Applied Physics 1998; 84(3):1284-1291.
[117] Shih CF. Relationships between the J-Integral and the Crack Opening Displacement for Stationary and Extending Cracks. Journal of the Mechanics and Physics of Solids 1981; 29(4):305-326.
[118] Donahue RJ, Clark HM, Atanmo P, Kumble R, McEvily AJ. Crack Opening Displacement and Rate of Fatigue Crack Growth. International Journal of Fracture Mechanics 1972; 8(2):209-219.
[119] Yoder GR, Cooley LA, Crooker TW. Quantitative-Analysis of Microstructural Effects on Fatigue Crack Growth in Widmanstatten Ti-6al-4v and Ti-8al-1mo-1v. Engineering Fracture Mechanics 1979; 11(4):805-&.

[120] Sadananda K, Shahinian P. Prediction of Threshold Stress Intensity for Fatigue Crack Growth Using a Dislocation Model. International Journal of Fracture 1977; 13(5):585-594.
[121] Kitsunai H, Kato K, Hokkirigawa K, Inoue H. The Transitions between Microscopic Wear Modes During Repeated Sliding Friction Observed by a Scanning Electron-Microscope Tribosystem. Wear 1990; 135(2):237-249.
[122] Gee MG. Low load multiple scratch tests of ceramics and hard metals. Wear 2001; 250:264-281.
[123] Bellemare S, Dao M, Suresh S. The frictional sliding response of elasto-plastic materials in contact with a conical indenter. International Journal of Solids and Structures 2007; 44(6):1970-1989.
[124] Liu Q, Jensen DJ, Hansen N. Effect of grain orientation on deformation structure in cold-rolled polycrystalline aluminium. Acta Materialia 1998; 46(16):5819-5838.
[125] Wang YB, Liao XZ, Zhu YT. Grain refinement and growth induced by severe plastic deformation. International Journal of Materials Research 2009; 100(12):1632-1637.
[126] Ungar T, Gubicza J, Ribarik G, Borbely A. Crystallite size distribution and dislocation structure determined by diffraction profile analysis: principles and practical application to cubic and hexagonal crystals. Journal of Applied Crystallography 2001; 34:298-310.
[127] Wang K, Tao NR, Liu G, Lu J, Lu K. Plastic strain-induced grain refinement at the nanometer scale in copper. Acta Materialia 2006; 54(19):5281-5291.
[128] Shabib I, Miller RE. A molecular dynamics study of twin width, grain size and temperature effects on the toughness of 2D-columnar nanotwinned copper. Modelling and Simulation in Materials Science and Engineering 2009; 17(5).
[129] Wang YB, Liao XZ, Zhao YH, Lavernia EJ, Ringer SP, Horita Z, Langdon TG, Zhu YT. The role of stacking faults and twin boundaries in grain refinement of a Cu-Zn alloy processed by high-pressure torsion. Materials Science and Engineering a-Structural Materials Properties Microstructure and Processing; 527(18-19):4959-4966.
[130] Wang YB, Wu B, Sui ML. Dynamical dislocation emission processes from twin boundaries. Applied Physics Letters 2008; 93(4).

[131] Ke M, Hackney SA, Milligan WW, Aifantis EC. Observation and Measurement of Grain Rotation and Plastic Strain in Nanostructured Metal Thin-Films. Nanostructured Materials 1995; 5(6):689-697.
[132] Wang YB, Li BQ, Sui ML, Mao SX. Deformation-induced grain rotation and growth in nanocrystalline Ni. Applied Physics Letters 2008; 92(1).
[133] Cheng S, Ma E, Wang YM, Kecskes LJ, Youssef KM, Koch CC, Trociewitz UP, Han K. Tensile properties of in situ consolidated nanocrystalline Cu. Acta Materialia 2005; 53(5):1521-1533.
[134] Bellemare SC, Dao M, Suresh S. Effects of mechanical properties and surface friction on elasto-plastic sliding contact. Mechanics of Materials 2008; 40(4-5):206-219.
[135] Chu SNG, Li JCM. Impression creep; a new creep test. Journal of Materials Science 1977; 12:2200-2208.
[136] Takagi H, Dao M, Fujiwara M, Otsuka M. Creep Characterization of Aluminium-Magnesium Solid-Solution alloy through Self-Similar Microindentation. Materials Transactions 2006; 47(8):2006-2014.